2016

Exploring Conditions for the Enhancement of Acene Semiconductors Through the Use of the Diels-Alder Reaction

Brittni Qualizza Qualizza
Loyola University Chicago

LOYOLA UNIVERSITY CHICAGO

EXPLORING CONDITIONS FOR THE ENHANCEMENT OF ACENE SEMICONDUCTORS THROUGH THE USE OF THE DIELS-ALDER REACTION

A DISSERTATION SUBMITTED TO

THE FACULTY OF THE GRADUATE SCHOOL

IN CANDIDACY FOR THE DEGREE OF

DOCTOR OF PHILOSOPHY

PROGRAM IN CHEMISTRY

BY

BRITTNI A. QUALIZZA

CHICAGO, IL

DECEMBER 2016

ACKNOWLEDGMENTS

I would like to thank all the remarkable teachers and professors I have had, all the way back to kindergarten, that encouraged and inspired me to follow my passions with strength and fervor. In addition to the education I received, the mentors I have encountered over the years have each given me something special to incorporate into the woman I am becoming. Dr. Toni Lee Owen Barstis, Dr. Dorothy M. Feigl and Dr. Christopher Dunlap from the Department of Chemistry and Physics at my alma mater – thank you for the patience and guidance it took to populate my brain with fundamental chemical knowledge and stimulation to continue into graduate studies. Dr. Jan Florian, Dr. Daniel Becker, and Dr. Dave Crumrine of my PhD committee – thank you so much for the inspiring and often therapeutic discussions as well as the extra hours spent with me for PCMs, reference letters and celebrations. Also, I can't forget Dr. Dave French, Dr. Dan Killilea, Dr. Duarte Freitas, Dr. Rick Holz, and Dr. Chad Eichman for a plethora of knowledge, including support and guidance in my undertakings.

This entire graduate education was unlike anything else, including the supervision and inspiration I have received from Dr. Jacob W. Ciszek. He is an award winning, scientifically charismatic man, whom I worked diligently to satisfy and impress over the years. He has been an incredible scientist to pursue excellence with, and I feel forever indebted to him for the skills he patiently and meticulously instilled in me over the past 6 years. If it weren't for his extremely prestigious Young Investigator's award,

granted by the NSF, I would not have been able to run the hundreds of expensive experiments. Additionally, I would like to thank the staff of the Department of Chemistry and Biochemistry at Loyola University Chicago for their provision of resources, from tuition costs to counseling. The community here is nurturing of collegiality and mentorship; this palpable feeling is something I will promote to others in future academic endeavors. This also includes an amazing group of Deans in the Graduate School, Dr. Jessica Horowitz, Dr. Patricia Mooney-Melvin and Dr. Sam Attoh., of which I have had the privilege of interacting with in their research mentoring program and other graduate student experiences. In my last year of the dissertation process, I was honored to receive funding as a fellowship from the Arthur J. Schmitt Foundation and would like to gratefully thank all the board members for choosing me.

Finally, I want to thank my friends and family. Scientific excellence feels like nothing without friends in your community, so thank you to the lab colleagues and fellow graduate students I have worked with over the years – you all know who you are. I hope everyone knows how special and meaningful our interactions have been and I wish the best to everyone continuing their journey at Loyola University Chicago. To my true love, Clifford Oneal, for all his patience and support while dealing with me throughout (especially) my last year of graduate school. My mother, Susan, gave me more than just life, but the desire, perseverance, and heart to be the best person I can. Words cannot express how much she has influenced my career as a scientist. She also blessed me with three siblings, of whom I draw strength to provide for them an expressive mentor. Dana, Heather and Bradley – you are my future.

This work is dedicated to Dr. David French and Mrs. Beth Hagerman.

You give up your narcissism, your egotism. That's how you achieve chemistry.

—Nick Nolte

TABLE OF CONTENTS

LIST OF TABLES

LIST OF FIGURES

CHAPTER ONE

AN INTRODUCTION TO THE ENHANCEMENT OF SEMICONDUCTOR PROPERTIES IN ORGANIC MATERIALS

The development of materials for electronic devices has progressed to include the use of *organic compounds* in applications such as organic light emitting diodes (OLEDs),[1] organic field effect transistors (OFETs)[2,3] and organic photovoltaics.[4] The use of organic materials in electronics offers a variety of valuable traits, such as their processability, potentially lower cost of production, and flexibility.[5] Currently, there are several organic electronic devices available as cell phone displays, which include the Galaxy S series (Figure 1a) and the flexible LG Chem prototype (Figure 1b). The organic semiconductor class of materials includes a diverse range of polymers and small molecules, including phthalocyanines, poly-thiophenes, and pentacene and its derivatives.[6–8] Each has different utilities. Devices comprised of phthalocyanine and pentacene are formed by deposition of organic molecules through evaporation or spin-coating, making them useful in OLEDs and OFETs. Poly-thiophenes are usually processed from solution, making them popular in ink-jet deposition on a flexible substrate. This work primarily focuses on a category consisting of highly aromatic, fused, ring systems called acenes. These have been used primarily in transistors, but also in diodes[9] and flexible circuits.[10]

Figure 1. Samsung and LG organic electronic devices currently on the market. (a) The Samsung Galaxy S7 edge mobile phone. The organic components of this device are included in the display, making a more vibrant screen using OLEDs. Image was taken directly from reference 11. (b) The LG Chem prototype. Flexible plastics and semiconductors are used to produce a thin sheet of material, capable of being curved without destruction of the device integrity. Image was taken directly from reference 12.

a  b 

Organic materials still have several limitations which prevent them from realizing their full potential. This includes their low charge carrier mobility in comparison to their inorganic counterparts,[13] as well as their propensity to degrade in air due to issues with oxidation and humidity.[14] This is not unusual as inorganic semiconductors share many of these weaknesses. The difference is that with inorganic systems, many undesirable traits have been remedied via the addition of self-assembled monolayers (SAMs) to the surface of the bulk.[15–17] A SAM, as depicted in Figure 2, is a layer of organized molecules, one molecule thick. It forms through spontaneous adsorption of an end of a molecule to the surface of a substrate. Commonly this adsorption is a chemical reaction between the head group of the solution phase (and less commonly gas phase) molecule with a surface site, and over time, the entire surface is filled with the molecule.[18] SAMs' properties are influenced by their molecular structure, specifically the tail group which provides an especially effective means to tailor the properties of the surface.[19–21] It is by this means that organic semiconductor properties could be possibly improved.

Figure 2. Self-assembly of solution molecules onto a substrate and the formation of Self-Assembled Monolayers (SAMs). Self-assembly will occur when a substrate is immersed in any SAM solution. Within minutes, the formation of a closely-packed SAM occurs due to a chemisorption of the head-group and, over time, the order of the film nominally increases. Molecular interactions between the alkyl groups, as well as the group at the interface of the SAM and air, direct the self-assembly and the properties of the SAM coated substrate.

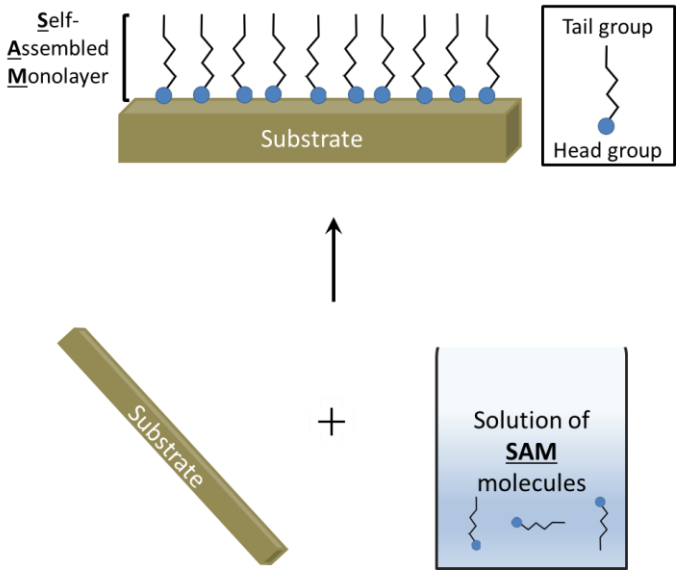

An example of minimizing undesirable traits via monolayers utilized *n*-alkanethiol SAMs on gold for corrosion prevention.[16] In the presence of normally corroding solutions of halide salts, the rate of gold corrosion was suppressed when, in particular, COOH- and OH-terminated SAMs were appended to the surface (via an S-Au covalent bond). Also interesting was that in comparison to CH_3- terminated monolayers, COOH- and OH- terminated monolayers prevented corrosion of gold with more strength. This phenomenon was thought to have occurred due to interaction of the group terminal on the monolayer with the gold surface (as seen in Figure 3B) after initial etching began (Figure 3A). This study demonstrated the significance of the group terminal on the monolayer as a means of preventing corrosion.

Figure 3. Corrosion resistance on gold (Au) by SAMs of varying terminations. The formation of pits in the surface of a COOH- or OH- terminated SAM coated on a gold surface when in the presence of bromide ions (halide salt solution). A SAM defect begins the corrosion, by allowing a bromide ion to reach the gold surface. As the gold is etched, COOH- and OH- terminated monolayers begin to lay on the exposed gold surface, protecting it from additional etching. This image was directly taken from reference 16.

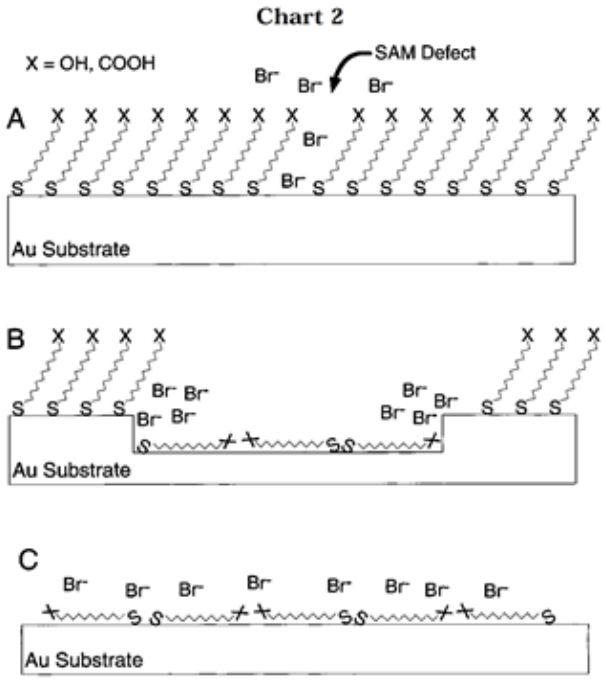

Furthermore, a variety of molecules which have been shown to chemisorb to the surface of silicon has been abundantly explored. Molecules like alkanes, highly fluorinated species and even more complex substituents like ferrocene, can be appended to the surface of Si(111) and Si(100) using radical initiators, heat, and other photochemical processes (Figure 4). Not only have SAMs reduced the oxidation of silicon, but have also been shown to protect against dissolution in extreme acidic, basic, or fluoride conditions.[22] In addition, they provide a foundation for subsequent reactions, providing for a range of functionalization possibilities.[15]

Figure 4. Examples of molecules adsorbed to silicon substrates as SAMs. The monolayer prevents oxidation, corrosion and etching of silicon as well as providing a foundation for subsequent reactions to append molecules and alter functionality. Figure taken directly from reference 15.

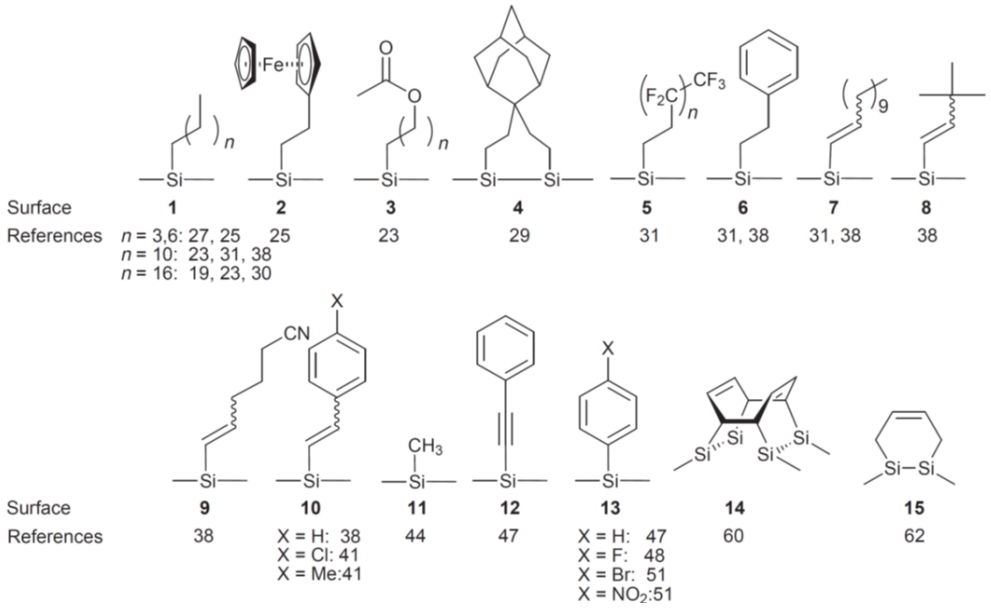

In another example, SAMs were used to improve the efficiency of electron/hole injection from a metal contact. In electronic devices, there is substantial contact resistance between the metal and the organic material resulting in poor conductivity. As seen in Figure 5, SAMs were used to coat a TiO_2 surface in an organic solar cell, thereby increasing the capacity for conduction between the interfaces of the inorganic TiO_2 with the organic P3HT/PCBM bulk material. This improved the device performance of the organic polymer solar cells of interest by 35% when the SAM applied consisted of C_{60} molecules.[17]

Figure 5. Application of a SAM on a solar cell device for lower contact resistance and increased efficiency. The structure of a solar cell device made from an organic polymer mixture of P3HT/PCBM. The addition of SAMs on the TiO_2 layer decreased the contact resistance and increased efficiency by 35% in the case of the C_{60} SAM. Figure taken directly from reference 17.

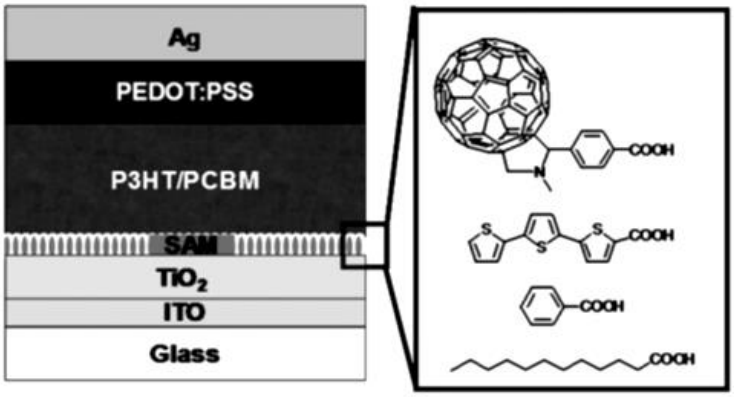

These data are but a handful of examples that lend to the hypothesis that the application of SAMs to the surface of organic materials, if realized, could improve traits of the material, such as stability in air and electronic capabilities. Interestingly, there are two reports that suggest this approach should be applicable to organic materials. In one theoretical investigation, completed by Tsetseris et al., the creation/destruction of carrier traps on the surface of a rubrene single crystal is suspected to be the manner by which conductivity is influenced.[23] These carrier traps are thought to be made by the presence of impurities, such as water or oxygen. If these trap states could be created or destroyed via the addition of a SAM, they may provide for better conductivity and enhancement of the electronic properties of these materials.

The second is a report where the conductivity of rubrene single crystals is changed, by roughly three orders of magnitude, via the addition of a complex thin film. Calhoun et al. attached a highly fluorinated analog of octadecylsilane (OTS), called FTS,

to the surface of rubrene (Figure 6).[24] As they show, an increase in conductivity could be correlated to the formation of films. The irreversible adsorption of these FTS molecules suggested a chemically bonded film as the likely suspect for influencing the conductivity of the bulk organic. The *nature* of the chemical bonds in the film formation, although not exactly known, was thought to happen between silane head groups with oxidized pockets of acene on the surface.[24] Incremental measurements of the surface using atomic force microscopy were completed for FTS exposure times up to 8 hours.

Figure 6. Changes in conductivity measured for rubrene and tetracene single crystals due to trichloro- and triethoxy- monolayers. (a) The addition of an FTS SAM on the surface of a rubrene single crystal increased the conductivity in the crystal from nearly 0 to nearly 0.3 mA over the course of 8 h. (b) Conductivity in tetracene and rubrene single crystals increased by roughly three orders of magnitude when the monolayer consisted of FTS molecules. The effect was suggested to occur due to a polar effect on the surface once the formation of the SAM occurred. For monolayers of triethoxy- and trichloro-silanes, a significantly smaller increase in conductivity occurred. Figure taken directly from reference 24.

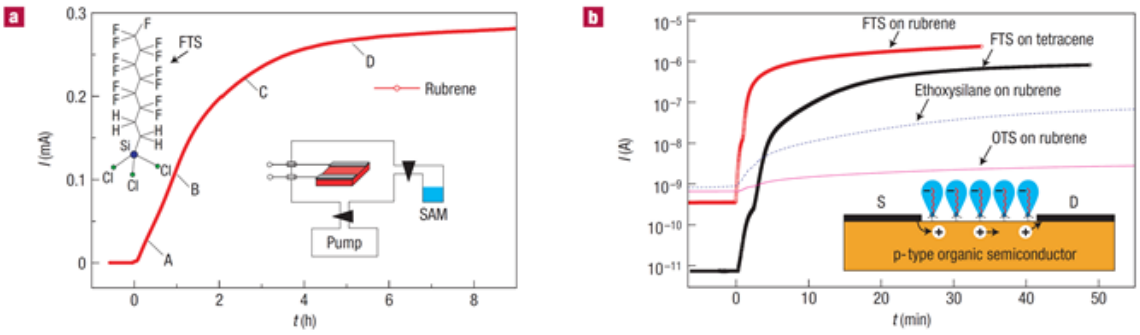

If the work described by Calhoun et al.[24] was extended to a highly defined and perhaps milder reaction, a wider variety of functional groups could be appended to an organic surface with the eventual hopes of manipulating the material's properties. Since the use of SAMs on surfaces has demonstrated the ability to influence tribology,[25–27] adhesion,[28–31] biocompatibility,[32–34] corrosion resistance,[35] catalysis,[36] and even

electronic properties,[37–40] it seems probable that reaction of the surfaces of *organic* semiconductors would diversify properties of these materials. To improve upon the ability to functionalize organic semiconductors, the goal of this dissertation became to use the Diels-Alder reaction to modify the surface of organic semiconductors in the acene family, with greater control over density and location of the influential SAM.

For 85 years, the Diels-Alder reaction has provided chemists with the ability to form C-C bonds and has continuously evolved to match modern scientists' needs and interests. These interests include a remarkably regio-selective reaction within aqueous molecular hosts exhibiting enzymatic behavior,[41] a versatile means for linking functionalizable organic molecules directly to semiconductor surfaces like silicon,[42,43] or acting as the model reaction in deciphering RNA catalyzed C-C bond formation *in vitro*,[44] with each example providing a new facet for this classic reaction. This thesis contains a new embodiment, where the reaction is applied to the *surface* of tetracene and rubrene single crystals via vapor dosing of the dienophiles.[45]

The Diels-Alder reaction was chosen because of its prevalence in literature, and because of the ability to append a wide variety of functional groups with little or no by-products. The reaction occurs between a diene, an unsaturated hydrocarbon with two double bonds between carbon atoms, with a dienophile, a "lover" of dienes containing one double bond. The 4+2 cycloaddition is believed to be concerted and results in the addition of diene and dienophile to form the Diels-Alder adduct. In this thesis, acenes like tetracene, pentacene and rubrene (in various crystalline forms) act as the dienes. The pool of dienophiles range in reactivity. Both the accepted mechanism and a variety of reactive

dienophiles are displayed in Figure 7. One may notice that several dienophiles are tagged with halogens, such as the doubly chlorinated maleic anhydride and the fluorine saturated benzoquinone. These are particularly interesting for surface studies, due to their utility in surface spectroscopy, a preference which will be elaborated on later in chapter three of this dissertation. Other dienophiles, like the *N*-maleimides and triazoline diones, were interesting as potentially biocompatible SAMs.

Figure 7. The Diels-Alder reaction mechanism presented between tetracene and a generic dienophile, and a collection of many commercially available dienophiles. The Diels-Alder reaction, a [4+2] cycloaddition, is proposed as a means of appending dienophile SAMs to the surface of diene acenes. (a) The reaction mechanism between tetracene and a generic dienophile. For tetracene, the reaction occurs exclusively at the 5,12-position yielding the cycloadduct. (b) Several types of dienophiles commonly used in the Diels-Alder reaction literature. Majority of these dienophiles are commercially available and have literature precedence to undergo the Diels-Alder reaction with dienes.

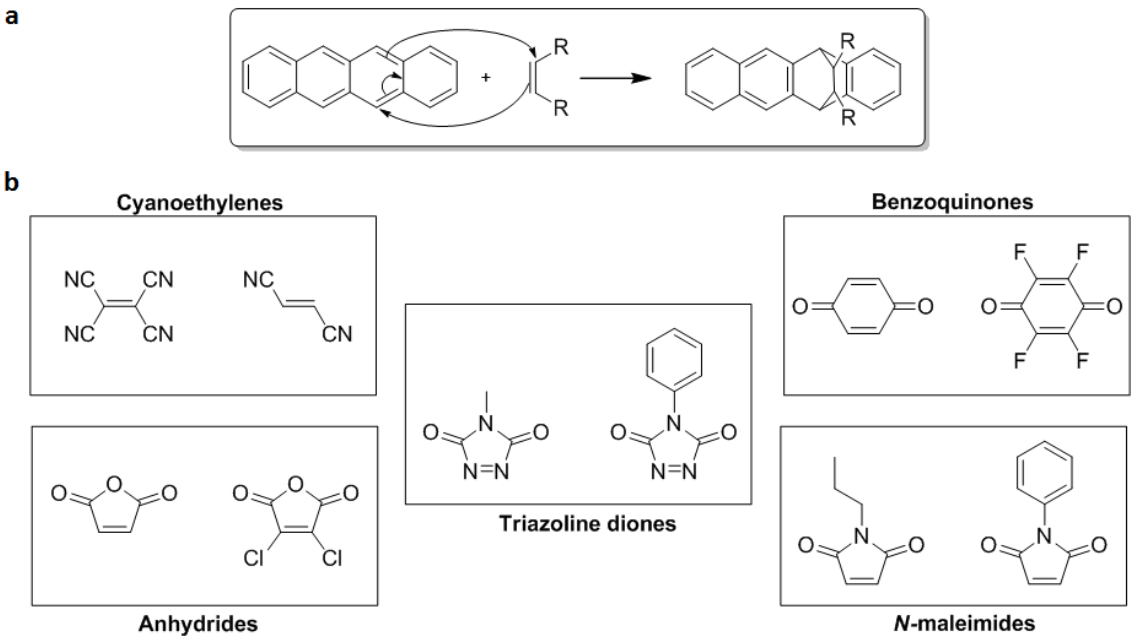

To begin the project, our system of choice for diene was single crystals of acenes. In contrast to thin-film organic materials, where various crystalline domains inhibit study of well-defined chemical reactions, organic single crystals have very low defect densities [46] and regular packing. Single crystals are those in which the crystal lattice is completely continuous and free of grain boundaries, allowing for experimental reproducibility and, more interestingly, site defined chemical reactivity. The molecules which comprise the crystals (acenes) are a class of polycyclic aromatic hydrocarbons with linearly fused benzene rings. They have grown in popularity as potential organic semiconductors and span a range of size and reactivity. In Figure 8, the acenes are listed in order of literature precedence as popular organic semiconductors (from left to right).

Figure 8. Acene type organics utilized within this thesis for their literature precedence in Diels-Alder reactions or their popularity as semiconductor materials. From left to right: anthracene, tetracene, pentacene, and rubrene. Tetracene consists of four linearly fused benzene rings and makes up the backbone of rubrene, the acene with phenyl substituents on the central rings, and the most promising semiconductor.

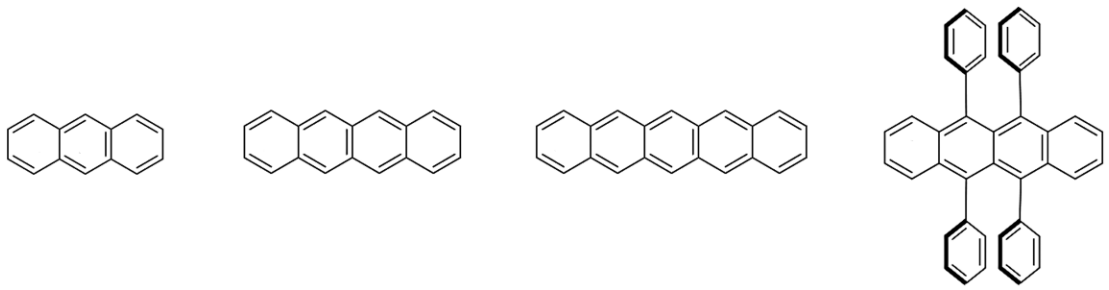

Tetracene has four linearly fused rings and makes up the backbone of the most popular semiconductor choice, rubrene, which has additional phenyl substituents on the central rings. Rubrene has a reported conductivity of 15 $cm^2\ V^{-1}s^{-1}$ in its single crystal form, which is an additional seven times greater than in amorphous silicon thin-film

transistor.[47] Because of the more interesting semiconductor properties of rubrene, it has become a popular choice for potential use in organic electronic devices.

This dissertation demonstrates the application of SAMs to the surface of acene crystals, specifically of tetracene and rubrene, using the Diels-Alder reaction. The second chapter details preliminary reaction results and two analytical methods which were employed to confirm adsorption of the dienophile on the surface of single crystals, tetracene and rubrene. These were mass spectrometry and X-ray photoelectron spectroscopy (XPS). Mass spectrometry experiments distinguish the chemical identity of adduct on the crystals and it discerned chemi- and physisorbed molecules from one another. XPS was used to prove face selectivity of the reaction by the detection of dichloromaleic anhydride.

From a mechanistic standpoint, this system demonstrated unusual steric effects: the reaction of one face of the tetracene crystal was virtually inert, while another face was facile. The dienophiles' steric bulk was also expected to play critical role for these confined systems, however analysis of surface data was hindered by the relative lack of corresponding solution kinetic data. While the rate of anthracene's reaction has been studied extensively with a range of dienophiles[48–51] and tetracene/pentacene has been studied theoretically[52,53] (with limited experimental reports),[54] an expansive report was generated to aid in future interpretations of acene systems. These results constitute chapter three.

Work within this thesis has been disseminated via two publications in

Chemical Communications,[32] and the Journal of Physical Organic Chemistry.[55] Additionally the method for surface-modified organic semiconductors resulted in a patent.[56] The response to this work at meetings has been well received and several other members of the group are now involved in discerning aspects of fabricating electronic devices, the reaction of the large face at elevated temperatures, acene film morphologies, surface kinetics and secondary reactions.

CHAPTER TWO

EVIDENCE OF SELECTIVE FACIAL REACTIVITY FOR SINGLE CRYSTALS OF TETRACENE AND RUBRENE

As detailed in chapter one, the addition of a SAM to the surface of organic acenes has the potential to modify properties of the material. Some of these changes could include the alleviation of oxidation/corrosion inherent in these organic acenes, and feasibly enhance their electronic properties.[57] Calhoun et al. describes the boost of conductivity in reacted single crystals of rubrene to be caused by an increase in surface carriers.[24] However, in order to study the effects of films on organic surfaces, film formation needs to be well controlled and regular. Using the site-specific Diels–Alder reaction and a series of vapor phase dienophiles, this dissertation sought to provide the organic electronic community with a reaction to amend poor traits and enhance conductivity in organic materials.

This second chapter presents the initial demonstration of surface Diels-Alder reactivity via X-ray photoelectron spectroscopy (XPS) and mass spectrometry experiments. The methods were used to confirm adsorption of dienophiles on single crystals of acenes and demonstrate the reaction's applicability to a range of dienophiles, respectively. Mass spectrometry experiments were completed in collaboration with M. Paul Chiarelli and included herein are details of a series of dienophiles for which the Diels-Alder adducts were observed. Furthermore, XPS results indicated facial selective reaction for single crystals of tetracene, a result which is predicted on the crystal lattice

structure. The molecules used as the crystal surface, tetracene (**1**) and rubrene (**2**), are shown in Figure 9 as well as adsorbates (**3**–**7**), which were used to change these surfaces.

To begin the project, single crystals of tetracene and rubrene were grown by physical-vapor transport under a stream of argon and in a horizontal tube furnace (a modified version of Laudise et al.).[58] Single crystals for use in XPS and MS were taken from collection zone and if not used immediately, were placed in a vacuum chamber in the dark. For experiments, crystals were either grown directly on slides or collected off the furnace walls as free materials, both substrate types are displayed in Figure 10. Microscale crystal substrates specifically for XPS analysis consisted of small single crystals of the organic semiconductor grown on gold coated glass slides (Figure 10a) which were placed/removed in/from the growth zone of the furnace. All other conditions were identical. In our hands, we found that runs containing the substrates for microcrystal growth also yielded larger single crystals in the collection tubes (Figure 10b)

Figure 9. The Diels–Alder reaction occurring between the surface of single crystal acenes (the Diels–Alder dienes, 1, 2) and commercially available dienophiles (3–7). (top) In the case of tetracene (1), the reaction preferentially occurs at the 5,12 position. (bottom left) In the case of rubrene (2), the reaction is predominately at the unsubstituted 1,4 position.

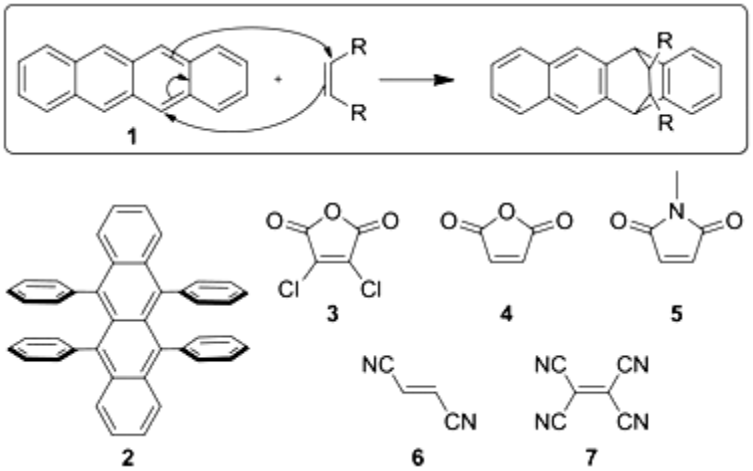

Figure 10. Single crystals of tetracene generated via physical vapor transport in a horizontal tube furnace. (a) A gold coated glass substrate with hundreds of micro-single crystals (b) Free single crystals nearly 1 cm 1 cm in size.

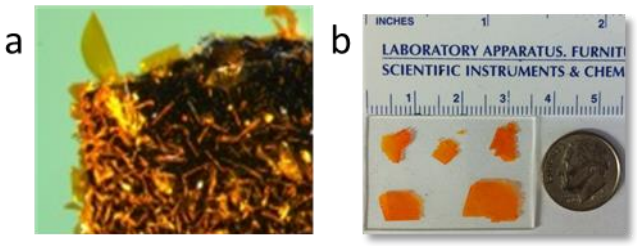

The furnace was comprised of quartz tubes, which were purchased from National Scientific Co. or MTI Corp, and a thermal gradient was produced using windings of resistive type K thermocouple wire. Wrappings were between two tubes, the dimensions of which were one of 27×30 mm and the other of 37×40 mm in diameter, and both 50.8 cm in length. The thermal gradient for rubrene can be seen below in Figure 11 (the same gradient was used with tetracene but at a lower temperature setting). Five 17×19 mm diameter, 7.62 cm length tubes were used as the source/collection tubes and placed within a long reactor tube having 25 mm OD × 21 mm ID and a length of 60.96 cm.

Figure 11**.** The thermal gradient for the rubrene crystal tube furnace.

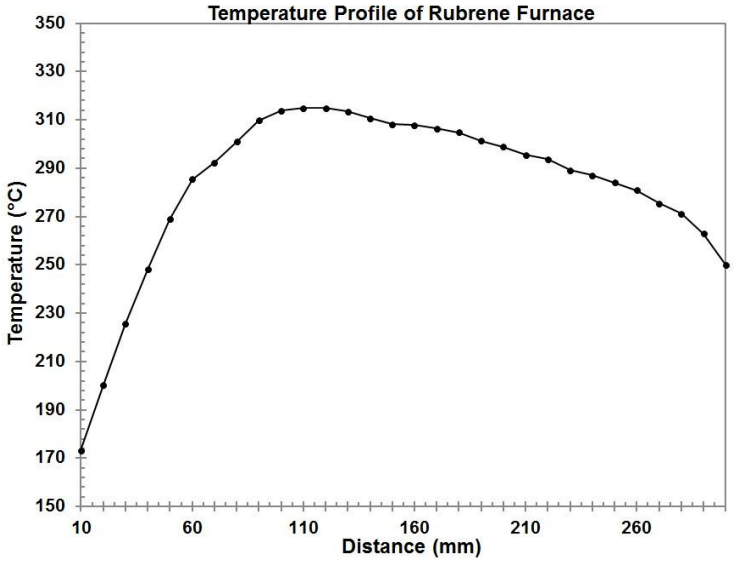

Prior to use, the reactor tube and the inner growth tubes were cleaned with acetone wetted Kimwipes. Upon air drying, the reactor tube was placed into the furnace tubes followed by the five-inner source/collection tubes (the first of which contained amorphous sublimed grade source material, 99.99% Sigma). Both ends of the long tube were sealed using vacuum accessories (O-ring flange). Prior to use, the system was flushed with argon at 80 mL/min for at least 1 h. Growth occurred over 16-24 h in the dark at atmospheric pressure with an argon flow rate of 40-45 mL/min.

For a typical reaction, a single crystal was placed in a Schlenk round bottom flask equipped with a glass hollow stopper containing a dienophile and the crystal was placed approximately 8 cm away. The pressure in the flask was reduced 3 times (10^{-1} Torr) to remove residual volatiles and replaced with N_2 then heated to 85 °C (where all dienophiles display a vapor pressure of at least 0.27 Torr).[59] Reactions were allowed to proceed for up to 3 days to ensure substantial coverage. If crystals were removed more than an hour before analysis, they were stored in a nitrogen filled glovebox or a vacuum chamber in the dark. Reacted substrates remained crystalline as determined by X-ray diffraction.

First we probed a reacted tetracene crystal surface for the presence of dienophile adsorbates. To provide a diagnostic XPS signal, which was not obscured by the elements present on a pristine surface, 2,3-dichloromaleic anhydride (**3**) was chosen as the dienophile. The lack of Cl 2p signal for an unreacted crystal can be seen in Figure 12 (dotted line). In the reacted crystal, the characteristic Cl $2p^{3/2}$ and $2p^{1/2}$ signals are clearly seen. When necessary, these solid–vapor Diels–Alder reactions were compared to

solution generated equivalents (sealed tube, toluene, 0.1–0.3 M, 120–150 1C, 8–72 h) so that the known adduct, once characterized, could be used as a standard. Such samples are referred to as the standard adduct throughout this dissertation and their characterization data, NMRs and IRs, are included in Appendix A.

Importantly, the Cl 2p signal in Figure 12a (solid line) (201.3, 202.9 eV) has a similar binding energy to that of the standard adduct (Figure 12b) which was analyzed as a powder. Indirectly, these same data can also be used as an indication of chemisorption of the species: the low pressure (10^{-8} Torr) and ambient temperature of the XPS chamber suggest against physisorption in the case of our sample.[60,61] Similar results were observed for rubrene, though the data here are suggestive of two distinct adsorbed species (Figure 13).

Figure 12. The XPS studies of the Cl 2p core electrons from the Diels-Alder adduct of tetracene with 2,3-dichloromaleic anhydride. (a) The Cl 2p core electrons for tetracene single crystals grown directly on gold slides demonstrating adsorption of 2,3-dichloromaleic anhydride (black line). Unreacted single crystals grown directly on gold slides (dotted line) demonstrated no Cl 2p signal. (b) The Cl 2p core electrons for standard adduct of tetracene with 2,3-dichloromaleic anhydride analyzed as a powder. Signal binding energies were referenced to the C 1s signal occurring at 284.5 eV.

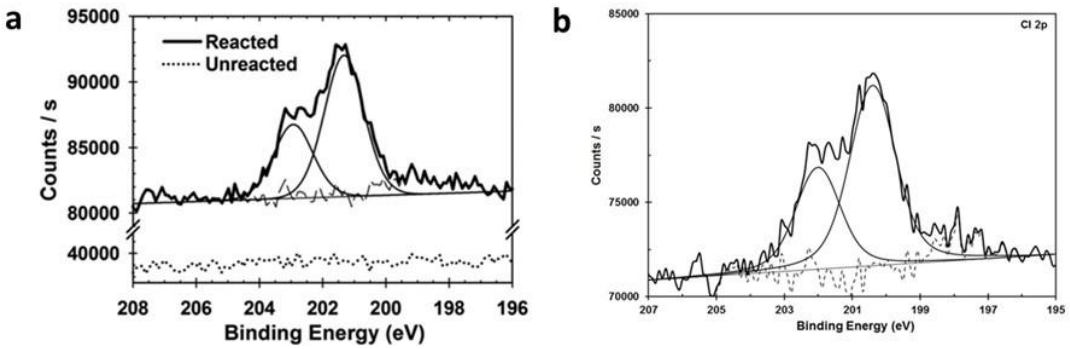

Figure 13. The XPS studies of the Cl 2p core electrons from the adduct of rubrene with 2,3-dichloromaleic anhydride. The sample consisted of single crystals grown directly on gold slides demonstrating adsorption of 2,3-dichloromaleic anhydride. Signal binding energies were referenced to the C 1s signal occurring at 284.5 eV.

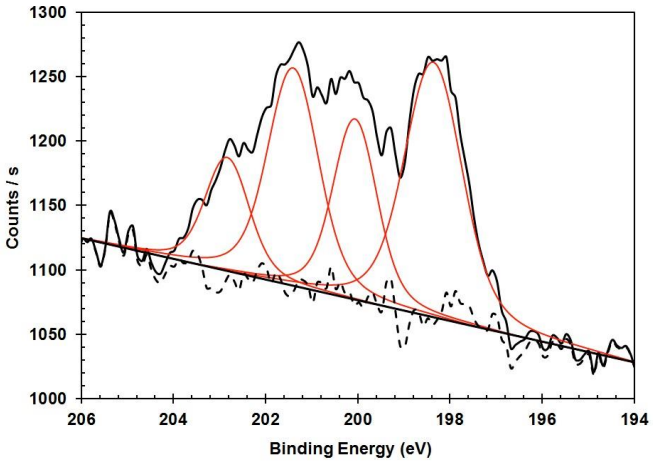

To confirm the (chemisorbed) nature of the adsorbed species, mass spectrometry was used to identify the maleic anhydride adduct at the crystal surface. Here, a crystal exposed to maleic anhydride (**4**) was directly vaporized at 10^{-8} Torr via a thermal probe. Molecular ions and fragmentation patterns for the single crystal are identical to those of the standard adduct (Figure 14). Thermal experiments also allow us to conclude that the majority species is chemisorbed (Figure 15, right), based on a small but observable signal for physisorbed material, distinct from the prominent adduct signal. This was observed in only one diene/dienophile combination. With chemical adsorption of the dienophile established, MS was also used to screen several tetracene–dienophile reactions for adduct formation. Figures 15, 16, and 17 confirm the adduct of tetracene single crystals reacted in the presence of *N*-methylmaleimide (**5**), fumarodinitrile (**6**), and tetracyanoethylene (**7**).

Figure 14**.** Electron impact ionization mass spectra of the tetracene with maleic anhydride adduct generated both in solution and on a single crystal. Electron impact ionization mass spectra of the tetracene-maleic anhydride reaction product formed in solution, on the left, and formed by gas phase reaction on a tetracene crystal, on the right.

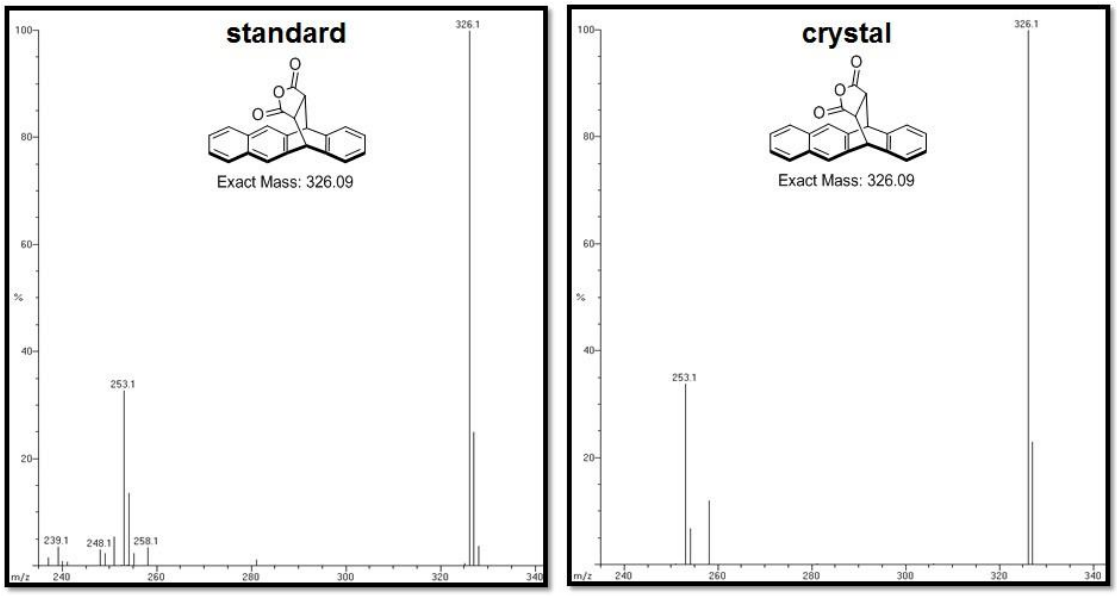

Figure 15. Electron impact ionization mass spectra of the tetracene with fumarodinitrile adduct generated on a single crystal. (Left) Electron impact ionization mass spectra of the tetracene-fumarodinitrile reaction product formed by gas phase reaction on a tetracene crystal (HRMS: theoretical m/z 306.11570, measured m/z 306.11573, 1.2 ppm error). (Right) Plots of ion current versus time for the analysis of the fumarodinitrile adduct formed on the surface of the tetracene crystal. (top) m/z 306.1 (adduct). (middle) m/z 78 (fumarodinitrile; first represents physisorbed material, the second is a fragment from adduct). (bottom) Probe temperature as a function of time.

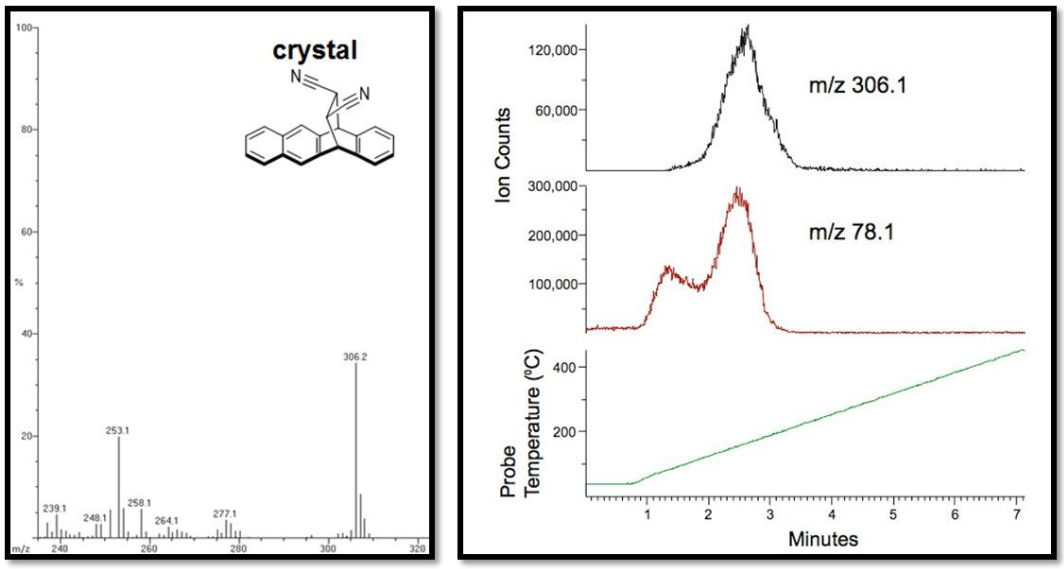

Figure 16. Electron impact ionization mass spectra of the tetracene with *N*-methylmaleimide reaction formed by gas phase reaction on a single crystal (HRMS theoretical m/z 339.12593, measured m/z 339.12737, 4.2 ppm error).

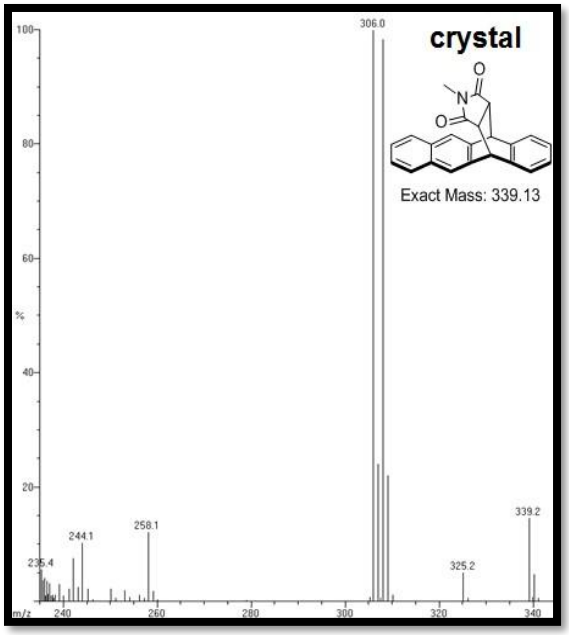

Figure 17. Electron impact ionization mass spectra of the tetracene with tetracyanoethylene reaction product formed by gas phase reaction on a single crystal (HRMS: theoretical m/z 356.10620, measured m/z 356.10519, 2.8 ppm error).

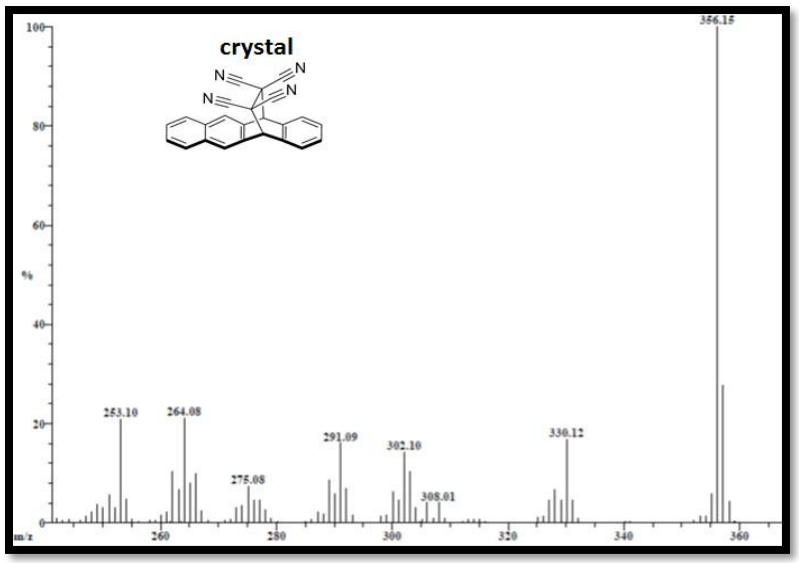

The previous mass spectrometry results also allow us to comment on the potential applicability of the Diels–Alder reaction to other reactants. Dienophiles (**3–7**) were

chosen in order to cover a range of reactivity from highly activated olefins (**7**), to intermediate (**3, 4, 5**), to mild (**6**).[52] The presence of an adduct for fumarodinitrile (**6**) is worth noting due to its low activity. We assume that a successful reaction is a consequence, in part, of the tetracene; a rather reactive diene. This acene core displays reaction rates with maleic anhydride more than 10 times as much as 1,3 butadiene, a standard diene. Other typical acene organic semiconductors (pentacene, rubrene) have been shown to be even more active toward dienophiles.[54] This activity is important as we expect that the reaction must occur in a sterically demanding environment.

Theoretically, the fixed orientation of the reactive diene moiety within the single crystal could induce confinement effects,[62] limiting the kinetics and possibly the thermodynamic stability of the system. Such effects should be predictable based on the crystallographic density of the acene core and its orientation with respect to the exposed surface and its nearest neighbors (Figure 18). Crystallographic data of tetracene[63] show that the largest face, the *ab* face (Figure 18b), is primarily composed of a staggered herringbone structure with a nearest adjacent molecule approximately 5 Å apart. Tetracene molecules are in the same plane and the hydrogen on the adjacent molecules is approximately 3 Å distant from the neighboring acene core, presumably impeding the reaction. Instead, the other faces of the crystal, including the *bc* and *ac*, are expected to react with greater ease, based on a more exposed acene core (Figure 18).

Figure 18. The crystal packing of tetracene and its arrangement relative to exposed crystal faces. (a) A simple unit cell for tetracene including crystallographic axes. Bond distances and molecular orientation can be found in ref. 82. (b–d) The unit cell shown with an overlaid macroscopic crystal face highlighting the portions of the molecules associated with the (*ab*) (*ac*) and (*bc*) faces of the unit cell.

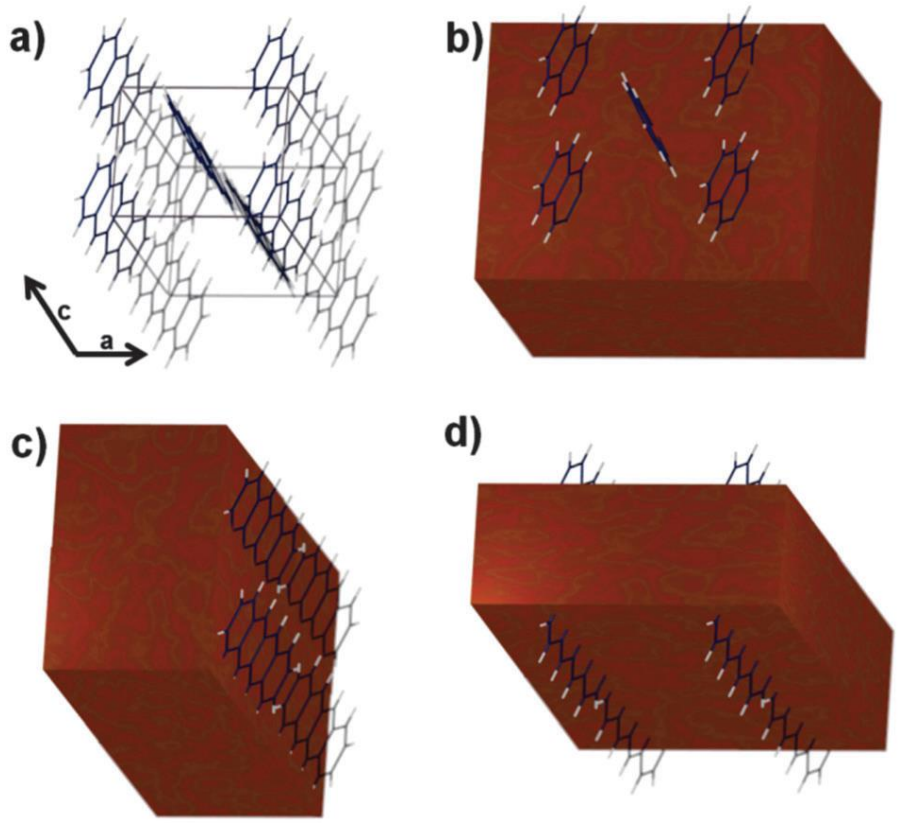

Evidence of the predicted differences in reactivity was observed when examining single crystal tetracene crystals which have been reacted with 2,3-dicholoromaleic anhydride (**2**). Figure 19a shows an optical microscopy image of a single crystal of tetracene with the ab face in the plane of the image. As can be seen in the Cl 2p region of the XPS spectrum (inset) no discernible chlorine signal can be seen. When a crystal is examined on its side (where a combination of other faces exists) a significant chlorine signal is observed. While this does not rule out reaction on the ab face, it does suggest that the rates for the various faces are different by orders of magnitude, much higher than reports of Diels–Alder reactions at sites with limited accessibility.[64] It also indicates the

potential for face selective reactions. Further study of this phenomenon is clearly warranted.

Figure 19. Optical images of the tetracene single crystals and their corresponding Cl 2p XPS spectra as insets. (a) The large face of a tetracene single crystal (scale bar is 1 mm) displays little/no reaction as determined by the lack of chlorine signal. (b) A single crystal placed on its side to expose the edge shows the presence of chlorine. Binding energies were referenced to the C 1s signal occurring at 284.5 eV and signals have been normalized to the area of the sample within the focal point of the beam.

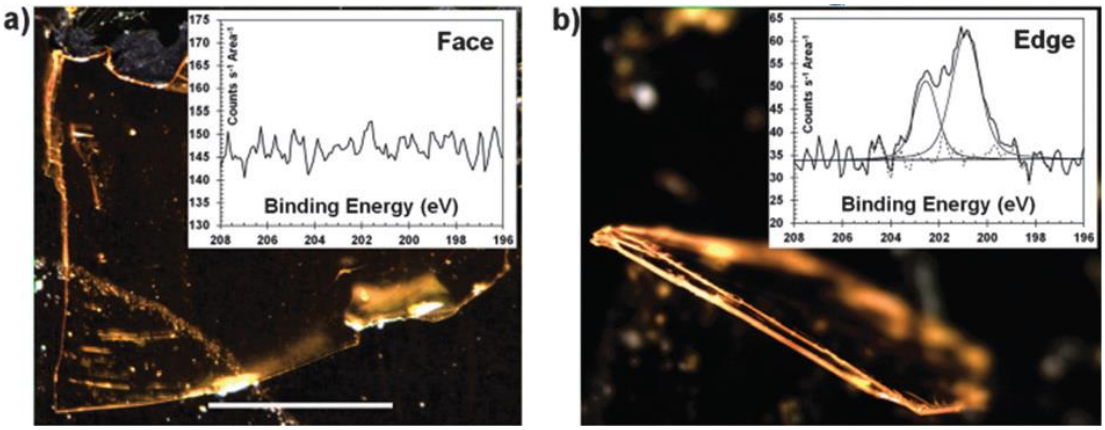

In summary, I have demonstrated that it is possible to dose adsorbates onto single crystals of tetracene and rubrene using the Diels–Alder reaction. A wide range of adsorbates containing functional groups such as imides, anhydrides, and cyano- groups were applied, demonstrating this chemistry to functionalize crystals of the acene class. While much exploration remains (e.g. rates of reaction and explicit surface coverage), potential exists for this chemistry to generate a defined, regular, and reproducible surface chemistry. Understanding these further properties and harnessing the capability to tailor the adlayer will surely lead to stimulating advancements in the theoretical and the experimental domain of organic materials, particularly at their surfaces. To deduce which dienophile molecules were best suited for swift reactivity with acenes, solution phase

kinetic experiments were surveyed; the data of which is contained in next chapter, chapter three, of this dissertation.

CHAPTER THREE

A SURVEY OF ACENE DIELS-ALDER REACTIONS FOR DERIVING SOLUTION PHASE KINETICS

In chapter two, the viability of creating an organized chemisorbed layer on the surface of semiconductor acenes was realized using the Diels-Alder reaction.[45] Both free single crystals and those grown on gold substrates displayed reactivity with a series of vapor phase dienophiles. This reactivity was proven using XPS and MS studies, which showed the presence of Diels-Alder adduct for several dienophiles and even displayed differences in reactivity based on the crystallographic face of tetracene. In the hopes of eventually using the Diels-Alder adduct monolayers to influence the properties of acene materials, it was necessary to flesh out information on the kinetics of these vapor/solid reactions.

To make the study of a complex system such as the Diels-Alder reaction between vapor dienophiles and solid acene surfaces more facile, solution phase experiments were carried out first. This chapter contains the second-order rate constants which were gathered for solution Diels-Alder reactions of substituted and unsubstituted acenes. These data were gathered with the intention of ascertaining ideal diene-dienophile combinations. Particular focus was placed on the larger ring systems namely tetracene, pentacene and rubrene. The rate constants between the acenes ranged roughly six orders of magnitude, from the slowest reacting diene, rubrene, to the fastest diene, pentacene. The utilized dienophiles covered a large range of reactivity from 2,3-dichloromaleic anhydride to tetracyanoethylene.

To aid in the interpretation of acene reactivity, constants were compared to the extensive body of Diels-Alder literature with well-studied dienes such as anthracene and *trans*-1-methoxy-1,3-butadiene serving as points of reference. Complex reaction kinetics for the addition of MeTAD and rubrene was found: initial fast consumption generated an intermediate, followed by dramatically slower product formation. The kinetic data creates a foundation for the analysis of prior and future reactions between organic semiconductor acene materials with volatized dienophiles, a surface functionalization technique for enhancing these electronic materials. The kinetic data herein is for rubrene, tetracene, and pentacene with common dienophiles (*N*-methylmaleimide, fumarodinitrile, 4-methyl-1,2,4-triazoline-3,5-dione, tetracyanoethylene, and maleic anhydride) and specialized molecules used in surface reactions (2,3-dichloromaleic anhydride, *p*-benzoquinone, and tetrafluoro-1,4-benzoquinone), Figure 20. The molecules selected for these experiments were chosen to encompass a range of reactivity and expand the data library of acene/dienophile pairs, but an even greater priority was placed on the applicability of these molecules to later use for vapor/solid reaction on organic semiconductor surfaces. For example, several of the halogenated dienophiles were picked as they provide ideal diagnostic signals for surface analysis, like XPS, ToF-SIMS or mass spectrometry. We compare these systems with the well-studied *trans*-1-methoxy-1,3-butadiene and anthracene, which serves as a point of reference for systems of interest.

Figure 20. The reaction pathway of an acene type diene with generic $R_{1\text{-}4}$ substituted dienophiles for kinetic experiments performed in solution. Acene systems for these experiments consist of three or more linearly fused benzene rings: anthracene, tetracene, pentacene and rubrene. Dienophiles spanned a range of reactivity and consisted of

substituted anhydrides, MeTAD, a substituted maleimide, quinones and cyano substituted olefins. Structures of dienophiles and acenes are also listed in Figure 22.

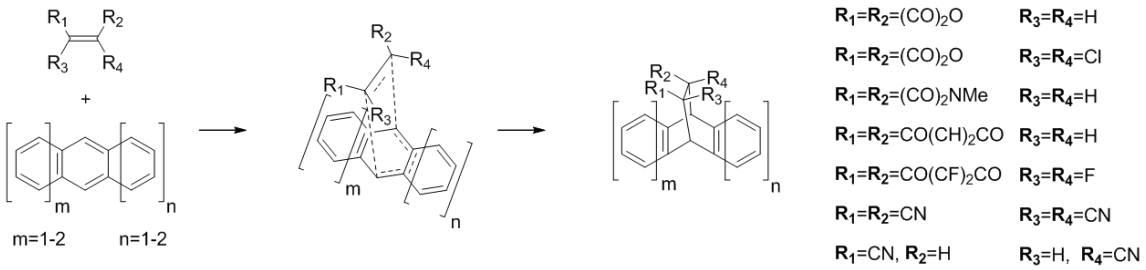

Determination of second-order rate constants

General kinetic experiments were performed at 85 °C in toluene-d_8 and monitored directly via ^{1}H NMR. Dienes were prepared as a stock solution of deuterated toluene at a concentration of approximately 2 mM with the internal standard, 1,2,4,5-tetramethylbenzene, added at 10 times the concentration of the diene. Neat dienophile was added directly to the NMR tube (already at 85 °C), with the concentration at a 10-fold excess relative to the diene, and outside of initial hand agitation, no stirring was used and reactions were kept in the dark. Consumption of the diene was monitored as a function of time to determine the pseudo-first order rate constant, k_1', and these values were periodically checked with the values for product formation to ensure starting material was not being oxidized, degraded, precipitated, etc.

From these general procedures, several nuances must be reported. The long reaction time for rubrene required that air free techniques be utilized (glove box, Schlenk flask) with aliquots removed periodically. Similarly, the sensitivity of *trans*-1-methoxy-1,3-butadiene meant that samples were prepared in the glove box. Additionally,

rubrene's characteristic signals could not be used to monitor the rate of reaction. Thus, production formation was used to determine kinetics rather than starting material consumption.

The extent of reaction was monitored over time for a period of anywhere from 20 min to >35 days. In the case of reactions completing in less than 30 min, measurements were initially taken every 30 s, then every minute after t=5 min and then every 2 min after t=10 min. Transient acquisition took approximately 16 s (2 transients) and triplicate measurements of starting materials gave integrations within ±3%. For reactions reaching completion in more than an hour but less than a day, measurements were taken every five minutes until t=30 min, then every 10- 60 min thereafter (~60 s acquisition time, 8 transients). For slower reactions, taking 24 to 72 h, the initial data point was acquired within the first hour of the reaction initiation and was acquired thereafter every 4 to 16 h (~103 s acquisition time, 16 transients). The rubrene kinetic run was taken approximately every 7 days and displayed nearly equimolar formation of oxidized rubrene and adduct. In every other instance, no discernible side products were seen in the final spectra, and when examined, consumed starting material directly correlated to product formation. Raw NMR data files (FID) can be found as a separate data file in the Supporting Information at onlinelibrary.wiley.com-doi/10.1002.[55]

The final class of reactions is those demonstrating rapid kinetics. Due to their rate, reactions were performed at room temperature, at 10 to 100-fold lower concentrations, and with a UV-vis. These reactions extended anywhere from 1 s to 24 h.

For the fast reactions between tetracene and tetracyanoethylene or 4-methyl-1,2,4-triazoline-3,5-dione, a stopped-flow UV-vis was used to acquire the data at a rapid rate. Additionally, for these reactions, chloroform was used as the solvent because of a charge transfer complex between tetracyanoethylene and toluene.[65] As pentacene has been reported to readily oxidize, reaction solutions were degassed before analysis.[66,67] As a manner of consistency, all other UV-vis samples were prepared in a similar manner. Diene concentration was monitored by using absorbance of the lowest energy band, and analysis was performed in a manner analogous to the NMR experiments. To facilitate comparison of the kinetics at elevated and room temperature, the reaction between tetracene and *N*-methylmaleimide was performed at both temperatures utilizing the respective instrumentation. Data plots for UV-vis experiments can be found in Chapter 5 (HPLC and stopped flow) and Appendix B (kinetic experiments).

All reactions, except for the reaction between *trans*-1-methoxy-1,3-butadiene with maleic anhydride and rubrene with 4-methyl-1,2,4-triazoline-3,5-dione, took place cleanly and gave linear ln[acene] vs. time plots. Reactions were treated as pseudo-first-order and known dienophile concentrations allowed determination of the second-order rate constant, k_2 ($M^{-1}s^{-1}$). Rate constants from data collected at 85 °C and room temperature, are listed in Tables 1 and 2 respectively (as $1000 \times k_2$). To associate the rate constant obtained at 85 °C to the room temperature measurement, data on tetracene's reaction with *N*-methylmaleimide was collected at both temperatures. This produced one second-order constant at 85 °C (1.2×10^{-1} $M^{-1}s^{-1}$) and another at room temperature (1.5 ×

10^{-2} $M^{-1}s^{-1}$). Furthermore, the rate constant for the tetracene/maleic anhydride reaction was measured three times, producing rate constant values within a 17% agreement of one another (standard deviation) and the errors were assumed to be of similar magnitude for the other reactions. Tetracene, pentacene and rubrene generate more than one diastereoisomer, termed *endo* and *exo*,[68] for each reaction ring because of the asymmetry produced in the adducts. However, these isomers are relatively consistent between acenes (generally about 1:2) and do not display unusual kinetics, so the two are combined here.

Established Theory of Diels-Alder Reactivity

In this section I aim to introduce much of the experimental or theoretical precedence of the Diels-Alder on acenes and highlight how our data contributes to this area. Each subsequent paragraph within this section first describes consensus in literature and concludes with data and analysis. To begin, unsubstituted acenes are reasonably facile partners in the Diels-Alder reaction as the fused aromatic core provides several electron rich dienes, all of which are a viable site for the reaction. Of these dienes, the center most ring is primarily attacked during reaction (Figure 21); here the loss of aromaticity in the product is less substantial than for reaction at outlying rings.[69] Theoretical calculations, of reaction between acenes and acetylene, predict 100% reactivity on the B rings for anthracene and the B rings of tetracene. When examined experimentally using ^{1}H NMR spectra, these systems contain splitting patterns which would allow us to distinguish these structural isomers. In all instances, the data supports the adduct formation exclusively on the inner most ring of anthracene and tetracene.

Figure 21. The labeling of the rings in the acenes studied in this work. Acene systems consisted of anthracene, tetracene, pentacene, and rubrene, respectively, shown above. Substantial difference in reactivity exists between rings in the same acene: electronically, A is the least reactive and C is the most.

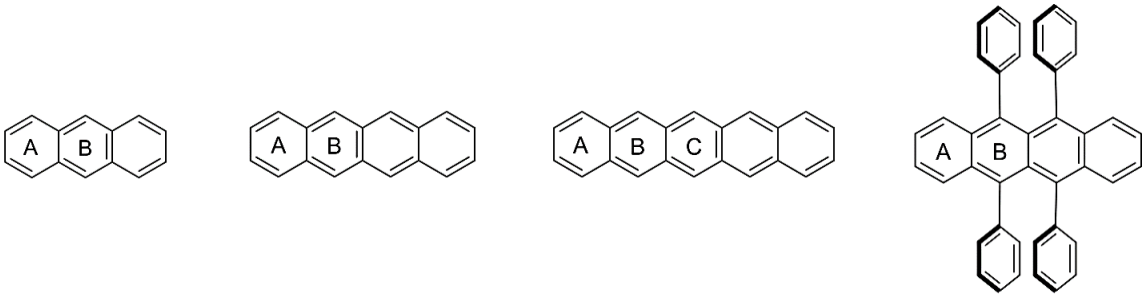

In contrast to tetracene and anthracene, pentacene should be the exception, with a mere 6.7 kJ per mole difference between the activation energies on the C and B rings which corresponds to a roughly 6:1 ratio of products (when one considers the duplicity of reaction sites for the B ring).[69] In the experiments, multiple products were present in the reaction mixture having chemical shifts commensurate of bridgehead protons (4.92-4.68 ppm) suggesting both B and C ring reaction. These components were separated via HPLC, and UV detection was used to distinguish the anthracene moiety of the B ring isomer from the naphthalene moieties of the major C ring isomer. According to ^{1}H NMR, the ratio of C to B isomers was nearly equivalent to the proposed 6:1 ratio (when a 1:1 pentacene:*N*-methylmaleimide mixture was heated to 110 °C for several minutes, an 8.5:1 ratio occurred). Additional experimental details and results are contained in Chapter 5, including HPLC chromatograms, NMR integrations, and a UV spectrum of the two separated components from the reaction mixture.

The data above also allows brief commenting on the applicability of aromaticity surrogates, such as NICS (nucleus-independent chemical shifts). NICS is one of the most widely employed indicators of aromaticity and was proposed by Schleyer *et al*. to be used as an assessment of reactivity based on the magnetic properties of a structure.[70] As a qualitative means of examining ring reactivity in polyacene systems, more negative NICS values are used to predict the location of reaction (i.e. reaction will occur on the given ring where a more negative NICS value exists). When examining the structural isomer data, NICS values (more precisely the NICS(0)π values given by Schleyer)[69] having a difference of 3 or more generated only the central ring isomer. For example, anthracene and tetracene differ in NICS values between their B and A rings by 3.1. In the case of pentacene, the difference between C and A is 4.5 (no detectable amount of A ring isomers were generated in our experiments). Additionally, small differences in NICS(0)π values (the difference between the C and B ring in pentacene is only 0.9) generated the aforementioned mixture of structural isomers. It would be interesting to study a more extended system in the future, such as hexacene, where the NICS(0)π difference is 1.5.

Theory also predicts[69] that each successive linear addition of a benzene ring to an acene system causes an increase in reactivity, a result borne out in previous experiments.[54] If the observed trend is described using the aromaticity of the central ring, opposite rates of reaction would be expected, however, such assessment neglects the nature of the formed product and its substantial contribution to the reaction pathway and rate.[69] In this data the trend along the acenes is similar (Figure 22): when *N*-

methylmaleimide reacts with tetracene as opposed to anthracene, the observed rate constant increased by 68 times (Table 1). This is consistent with theoretical calculations which predict rate differences of 38 times from anthracene to tetracene with acetylene,[69] and is comparable to experimental results on similar systems.[54] This trend continued with pentacene as the reaction with *N*-methylmaleimide was seven times faster compared to the same reaction with tetracene (Table 2).

Literature precedence also provides a predicted trend in dienophile reactivity, one expected to carry over to our acene systems. The reactants commonly utilized in Diels-Alder reactions (tetracyanoethylene, 4-methyl-1,2,4-triazoline-3,5-dione, *N*-methylmaleimide, maleic anhydride and fumarodinitrile; listed in order of reactivity) thus provide a reference point which will allow the relative kinetics of the second, surface specific, group to be referenced to a greater body of literature. For the established group, the trend in this data matched that which was anticipated, e.g. tetracyanoethylene displayed the fastest reaction time, 4-methyl-1,2,4-triazoline-3,5-dione was more facile than the anhydride, while lower reactivity was observed with fumarodinitrile.[71] Experimental rate constant data reported by Biermann and Schmidt, for reaction between tetracene and maleic anhydride (trichlorobenzene, 91.5 °C), differs by just a factor of five which is easily attributed to the slight difference in solvent and temperature.

Figure 22. Dienophiles and dienes listed in order of reactivity as determined by kinetic experiments.

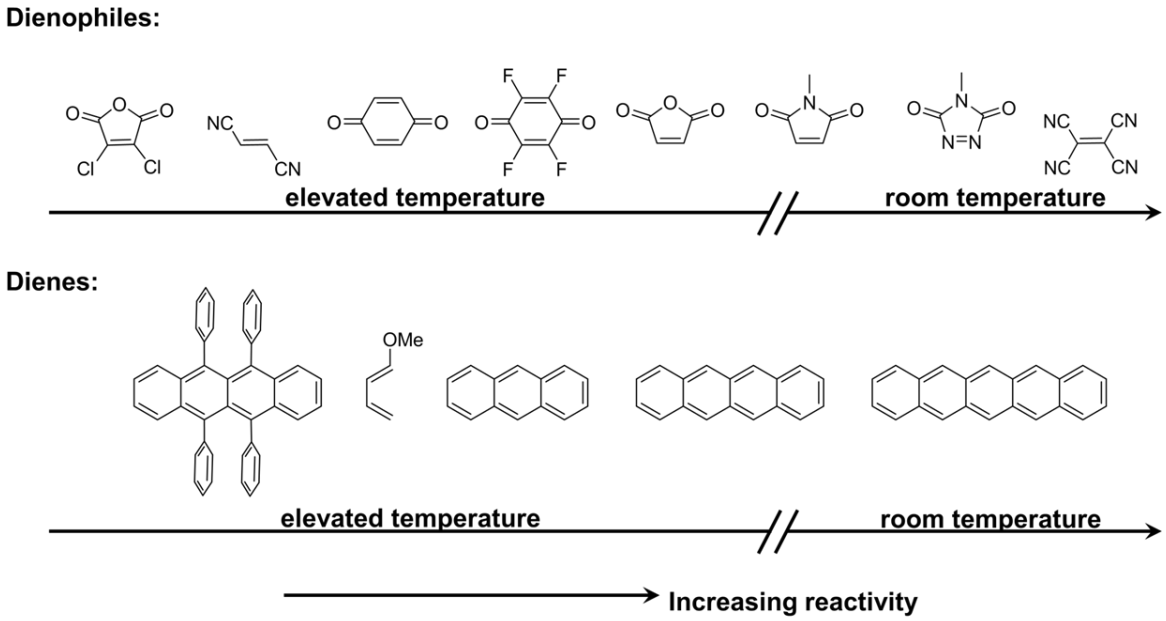

Of further interest was the impressive similarity in literature rate constants of *N*-methylmaleimide and maleic anhydride with dienes spanning reactivity of over a million fold.[72] It was because of this trend that comparable reactivity between these dienophiles with the acenes was anticipated. My results do deviate from this slightly. When the two are reacted with *trans*-1-methoxy-1,3-butadiene, maleic anhydride occurred 4.5 times faster than with *N*-methylmaleimide, notably outside the 0.5-2 range reported.[72] This ordering is inverted for the acenes, where the reaction of maleic anhydride occurred at a rate 0.1 and 0.17 times that of *N*-methylmaleimide for both anthracene and tetracene. Although slightly different from reported results, this trend was not investigated further with the other diene-dienophile pairings.

Incorporation of Halogens for XPS Measurements

The primary motivation for this work is to provide reference data for reactions promising for study on surfaces. Measurement at surfaces often needs tagged molecules, whereby the addition of halide(s) is convenient. Typically, halogens are not found as contaminants either inherently in the organic acenes or within common atmospheric adsorbates, making them an appropriate group for proving definite reactivity. Furthermore, many halogen substituted dienophiles are readily available for purchase, and give the potential to tag many of the other compounds listed in Figure 22. Molecules like 2,3-dichloromaleic anhydride, a doubly chlorinated maleic anhydride derivative, and tetrafluoro-1,4-benzoquinone, a per fluorinated benzoquinone, are expected to participate in the Diels-Alder reaction and have sufficient volatility, making them surface/vapor reaction viable.[45] I sought not to only understand their base reactivity in comparison to their unsubstituted versions, but to tease out information on electronic and steric effects using the slight variance in halogen electronegativity, halogen size and ring size.

Chemical intuition suggests that, based purely on electronic effects, electron withdrawing halogen substituents should higher reactivity in the Diels-Alder reaction. This is supported by theory which predicts these substituents result in a stabilized $LUMO_{dienophile}$ allowing for a more overlap with the $HOMO_{diene}$.[73] Detailed analysis of almost one hundred diene/dienophile combinations allowed Kiselev and Konovalov[52] to develop an empirical model of the energy of the system based on three thermodynamic factors. The first two are extent of frontier orbital interaction: the HOMO/LUMO energy

difference and the interatomic distance between the diene's reactive carbons (C_1, C_4) which have a strong influence on the overlap coefficients.[74] In addition they add a factor pertaining to the energy of bond cleavage/formation. Interestingly though, their discerned relationship (much like chemical intuition) predicts faster reactivity for halogenated dienophiles, but experimental evidence (including that same work) shows *reduced* reaction rates when the substitution is on the double bond in the dienophile.

In fact, virtually all instances of Diels-Alder reactions show inhibited reaction for chloro- or bromo- substituted dienophiles, signifying substantial effects brought on by size of the substituent which counters its ability to withdraw electron density.[51,75] In a report by Andrews and Keefer, a single chlorine substitution caused a decrease in rate of 2-8 times and the decelerating effect was considered to be caused by more double bond character existing in the C-Cl bond of the dienophile, thereby reducing the C-C double bond character. The exception to this are fluorinated species, which have been reported to accelerate Diels-Alder reactions.[76] This thesis found analogous reactivity in the halogenated species: the addition of fluorine to benzoquinone *sped up* the reaction 6-fold, while the addition of chlorine to maleic anhydride caused a 65-fold *decrease* in the rate constant. It would be interesting to see if this effect is amplified at the surface where access to the diene is dramatically more hindered than in solution. This will be reexamined once surface kinetic experiments are determined.

Encumbered Rubrene Substrates and Surface Viable Reactions

Rubrene is one of the most attention-grabbing materials currently being tested for organic electronics because of its high carrier mobility and increased device performance when functionalized.[57] Interestingly, exhaustive literature searches for Diels-Alder reactions of rubrene show only one report of an adduct (formed with *N*-methylmaleimide)[77] and no reports of the kinetic aspect of this reaction. This is most likely due to the fact that the promising device behavior is rather recent.[78]

Overall, results for rubrene were quite interesting. Tetracyanoethylene (TCNE), one of the fastest dienophiles in literature,[52] showed no reactivity towards rubrene at room temperature (24 h). In fact even when heating the reaction to 125 °C for 13 days, no appreciable signal was found in the region from 6.5 to 3.5 ppm, which is normally associated with these adducts.[45] For these measurements, the smallest resolvable signal in this region corresponded to 0.5% of the starting material, and this signal cannot be conclusively assigned this to product. This is in contrast with the reaction of *N*-methylmaleimide (a dramatically slower dienophile) which was complete 4% complete at this time, even at lower temperatures.

Table 1. Rate constants for all elevated temperature reactions (85 °C).

Diene	**Dienophile**	**$k_s \times 1000$ ($M^{-1}s^{-1}$)**
Rubrene	*N*-Methylmaleimide	0.004

trans-1-Methoxy-1,3-butadiene	*N*-Methylmaleimide	1.4
trans-1-Methoxy-1,3-butadiene	Maleic anhydride	6.4
Anthracene	*N*-Methylmaleimide	1.7
Anthracene	Maleic anhydride	0.21
Tetracene	*N*-Methylmaleimide	120
Tetracene	Maleic anhydride	19
Tetracene	Tetrafluoro-1,4-benzoquinone	5.6
Tetracene	*ρ*-Benzoquinone	0.91
Tetracene	Fumarodinitrile	0.35
Tetracene	2,3-Dichloromaleic anhydride	0.29

Table 2. Rate constants for all room temperature reactions (20-25 °C).

Diene	**Dienophile**	**k_s × 1000 ($M^{-1}s^{-1}$)**
Tetracene	Tetracyanoethylene	5,000,000
Tetracene	4-Methyl-1,2,4-triazoline-3,5-dione	690,000

Tetracene	*N*-Methylmaleimide	15
Pentacene	*N*-Methylmaleimide	110
Rubrene	Tetracyanoethylene	-
Rubrene	4-Methyl-1,2,4-triazoline-3,5-dione	k_1 ($M^{-1}s^{-1}$) = 22 $k_2 \times 1000$ ($M\,s^{-1}$) = 0.019

The TCNE rubrene reaction contrasts nicely with our other fast dienophile, 4-methyl-1,2,4-triazoline-3,5-dione (MeTAD), which although generally slower than tetracyanoethylene in the acene Diels-Alder reactions (Table 2),[79] reacted completely with rubrene in ~1 h time. This result is not entirely surprising; the large phenyl substituents on the central rubrene are expected to make this substrate particularly sensitive to the sterics of the dienophile. TCNE's substitution on both ends of the olefin makes it particularly slow in this regard, while the 1,2 positions of MeTAD are unsubstituted rendering the reaction more facile.

It was also interesting that in the case of rubrene with MeTAD, the reaction occurred but did not follow pseudo-first-order reactivity. Within 40 s of reacting, the rubrene concentration appeared to decrease by half (from 0.2 mM to ~0.1 mM) followed by dramatically slower kinetics. To confirm the influence of two distinct rates, the reaction was monitored via stopped flow UV-vis. Figure 23 shows an absorbance vs. time plot over the course of 1000 s, where rubrene was monitored at 432 nm. Visibly

different rates of reaction occur, neither of which follow pseudo-first-order reactivity. Many mechanisms common to Diels-Alder reaction of TADs could provide justification for a non-pseudo-first-order rate (zwitterion -,+ or aziridinium ion, AI, or precomplex formation),[80,81] and all mechanisms imply that the starting material is consumed *rapidly* to form intermediates before slowing, as equilibrium becomes important. Such kinetics should follow equation 1.

$$\text{RUB} + \text{MeTAD} \underset{k_{-1}}{\overset{k_1}{\rightleftharpoons}} \text{I} \xrightarrow{k_2} \text{Diels-Alder Adduct} \qquad (1)$$

To confirm the presence of an intermediate in this reaction ^{1}H NMR spectroscopy was utilized. Proton spectra indicated that within the first 15-20 min of reaction, rubrene was consumed (~50% consumption), but no product was present. Specifically, the adduct protons at 2.9 ppm (corresponding to the *N*-methyl protons) and 5.4 ppm (corresponding to the bridgehead protons) were absent. Formation of an intermediate could be suggested by the transient peak at 2.6 ppm, which after 40 hours no longer persists in the ^{1}H NMR spectrum but is replaced by the presence of peaks from the isolated adduct. For this reaction, two rates are reported. The first, k_1 equal to 22 $M^{-1}s^{-1}$, was calculated assuming pseudo-first-order reactivity in the initial rate (1.2 s of data, Figure 23 inset) before k_{-1} becomes significant. The rapid kinetics leads to a standard deviation of 22% for this value. It was also interesting that the data for k_2 appeared to correspond to zero order reactivity (Figure 23) and its value was equal to 1.9×10^{-5} M s^{-1}.

Figure 23. UV-vis stopped flow experiment of rubrene with MeTAD. UV-vis stopped-flow was used to monitor the reaction between Rubrene and MeTAD at 432 nm for nearly 17 min. The inset displays the natural log of the data points in the first 1.2 s of

reaction versus time, with a linear fit used to calculate the pseudo-first-order rate constant.

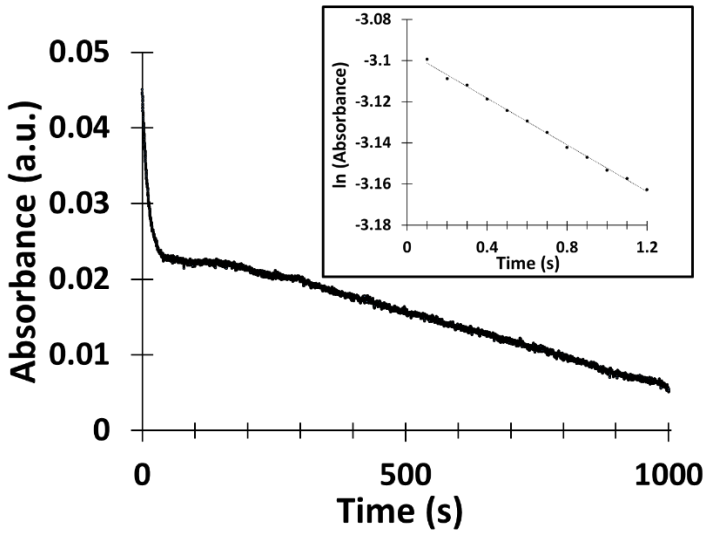

In addition to displaying interesting kinetics, rubrene also allows commenting on the relative reactivity of each ring in tetracene. From a reactivity standpoint, rubrene should behave as a substituted version of tetracene with phenyl groups on the reactive B rings (Figure 21). Based off of assignments of products in the kinetic run, any reactivity of the B rings in rubrene with *N*-methylmaleimide is well below the detection limit of the experiment, leaving only the A rings to participate in cycloaddition. Unsurprisingly, the rate of rubrene was very slow, taking 5 weeks to generate 10% product adduct (exclusively one diastereomer). As previously mentioned, this reduced rate constant for the A ring is due to a decrease in the enthalpy of reaction and increase in activation barrier, in comparison to the B ring. More importantly, the gathered rate constant data for the reaction between *N*-methylmaleimide and rubrene gave the ability to comment on

reactivity of the hindered diene relative to the reactivity of its unhindered counterpart, tetracene.

Similar electron distribution between the A rings of tetracene and rubrene allow for predictions on the reactivity of rubrene. Based on this assumption, we can infer that the A ring of rubrene should have the similar reactivity to the A ring of tetracene. Theoretical calculations examining approximate differences in reaction rate between the A and B rings of tetracene with acetylene (at 85 °C), predict a 9,060-fold difference, in favor of reactivity at the B ring (calculations are without consideration of the prefactor).[69] Naively it would be expected that the reactivity of rubrene would be slower than tetracene by roughly this amount, as it is electronically similar to tetracene but is sterically forced to react at the A ring as opposed to the B ring. If substantial differences in the calculated and theoretical rate constants between tetracene and rubrene exist, it would suggest substantial steric effects induced by the presence of phenyl rings on the reactivity *of the A ring*. Rate constant data supports slight steric influence by the introduction of phenyl substituents to tetracene, as rubrene was approximately 30,000 times slower.

These same discussions also play a heavy role in reanalyzing surface data for tetracene (as well as rubrene). Surface experiments from the same setup described in chapter two[10] showed incomplete reaction at 24 hours between maleic anhydride and tetracene, a result that seems at odds with the observation of adduct for the dramatically slower rubrene. The fact that tetracene and rubrene crystals reacted in such similar

amounts of time would make more sense if the reaction was occurring on same deactivated A ring in both cases. Indeed the crowded environment of a crystal surface could lead to sterically demanding reaction, possibly allowing primarily the exposure of the A rings. This would not be without precedence, confinement effects have limited the reactivity in a similar system. Kwon reported that moving a monolayer immobilized dienophile from the surface to subsurface reduced reactivity by a factor of 8 and when recessed by an additional ~ 2Å the rate declined by an additional factor of 3.5.[64] Thus this explanation seems plausible, but obtaining experimental proof is challenging as this would require assignment of the crystallographic faces of the single crystal surfaces.[82] These challenging experiments, along with rate data on the various faces, would allow for definitive comment.

In closing, these data provide an expansive set of Diels-Alder acene-dienophile pairs and allows for comparison of reactivity between acene type dienes with surface-relevant dienophiles. Observed kinetics are consistent with general notions of the Diels-Alder; both the size and electronic nature of the dienophiles influenced rate of reaction. It was also observed that the central ring was primarily attacked for reaction in each system, that the reactivity of the acenes was influenced by the number of linearly fused benzene rings (larger being faster), and the kinetics for rubrene were reported for the first time. Of most importance, the data has given an ability to loosely predict crystal substrate reactivity for in progress solid state kinetic experiments. Faster reacting dienophiles like tetracyanoethylene or tetrafluoro-1,4-benzoquinone, are good targets for

studying crystal reactivity, and in addition to their speed they have the potential to provide spectroscopically interesting signals. Other molecules like *N*-methylmaleimide and *p*-benzoquinone are nominally biologically interesting surface addendums, producing films with the ability for further functionalization. Overall this work provides precedence for a range of surface specific studies.

CHAPTER FOUR

CONCLUSIONS

This thesis demonstrates that it is possible to dose adsorbates onto single crystals of tetracene using the Diels–Alder reaction and that a wide range of adsorbates can be appended. Functional groups such as imides, anhydrides, and cyano- groups have been applied, demonstrating this chemistry as a manner to functionalize crystals of the acene class. Currently the lab has ongoing experiments to determine rates of reaction and explicit surface coverage, providing a means to generate a defined, regular, and reproducible surface chemistry.

In addition to these surface data, the expansive set of Diels-Alder acene-dienophile pairs were examined in solution, allowing for comparison of reactivity between acene type dienes with surface-relevant dienophiles. All of the observed kinetics are consistent with general notions of the Diels-Alder reaction in solution. Furthermore, kinetics for rubrene were reported for the first time. Of most importance, the data has given an ability to loosely predict crystal substrate reactivity for future solid state kinetic experiments. Faster reacting dienophiles like tetracyanoethylene or tetrafluoro-1,4-benzoquinone, are good targets for studying crystal reactivity, and in addition to their speed they have the potential to provide spectroscopically interesting signals.

As a final point, I hope this work provides precedence for a range of surface specific studies in the future of acenes. If the realization of acenes as organic semiconductors could be better understood through the use of SAMs, perhaps organic electronic device complications could be alleviated.

CHAPTER FIVE

EXPERIMENTAL METHODS AND PENTACENE ISOMER CHARACTERIZATION

Reagent grade chloroform and toluene were degassed prior to use. All other reagents were used as shipped (Sigma-Aldrich). Tetracene used in solution reactions was >98% pure. Thin layer chromatography (TLC) was performed on silica gel 60 (F_{254}) with glass support. All column chromatography separations were carried out on silica gel 60 (230-400 mesh from EMD). ^{1}H and ^{13}C NMR spectra for characterizing synthesized compounds were recorded on a Varian 500 MHz spectrometer (except for the spectra of the adduct between rubrene with 4-methyl-1,2,4-triazoline-3,5-dione, which were recorded on a Varian 300 MHz spectrometer). All proton chemical shifts (δ) are downfield from tetramethylsilane and reported in ppm. All ^{13}C NMR spectra were referenced from $CDCl_3$ at 77.23 ppm. All IR spectra were obtained on a Bruker Tensor 37 equipped with a liquid nitrogen cooled MCT detector and samples were analyzed as KBr pellets or dropcasted.

For kinetic experiments ^{1}H NMR spectra were recorded on a Varian 500 MHz spectrometer at 85° C. Instrument temperature was equilibrated for two hours prior to any measurement. All proton chemical shifts (δ) are downfield from toluene-d_8 (δ 2.09) and reported in ppm. UV-vis spectra were recorded on a Shimadzu UV-2550, available in Appendix B, and an Applied Physics SX20 stopped-flow spectrometer, available in Chapter 3 as Figure 23.

General Procedure for All Vapor Dosed Reactions

A reaction chamber comprised of a Schlenk round bottomed flask fitted with a hollow ended stopper was used to dose the sample with dienophiles. Organic semiconductor samples were placed in the bottom of a flame dried round bottomed flask approximately 8 cm away from powder resting in the tip of the hollow stopper. When evacuated, the setup readily reaches 10^{-1} Torr, although the ultimate pressure is limited by the vapor pressure of the dienophile. The flask was then placed in an oven at ~ 85 °C, for three days. Upon removal from the oven, the tip of the stopper was cooled with liquid nitrogen or a dry ice/IPA bath to condense excess dienophile away from the sample. Vacuum on the system was released using an N_2 filled schlenk line.

General Procedure for X-ray Photoelectron Spectroscopy Experiments

For X-ray photoelectron spectroscopy (XPS) experiments tetracene and rubrene microscale crystal substrates, as well as tetracene single crystals, were reacted with 2,3-dichloromaleic anhydride according to the general vapor dosed reaction procedure at 85 °C. All X-ray photoelectron spectroscopy (XPS) measurements were acquired on a Thermo Scientific ESCALAB 250Xi XPS system at 3×10^{-7} mBar. A monochromatic Al X-ray source at 140 W was used with an analytical spot size of 200 μm and a 90º takeoff angle, with a pass energy of 50 eV. Surface samples were referenced against internal C 1s line at 284.5 eV.

General Procedure for Mass Spectrometry Experiments

Full scan mass spectra and accurate mass measurements were acquired with a JEOL GCmate II BE sector mass spectrometer (Tokyo, Japan) at the University of Illinois-Chicago's Research Resource Center using electron impact ionization (EI) in the positive ion mode. Standard adduct samples, synthesized in solution, were dissolved in a minimum of methanol and applied to a direct insertion solids probe for analysis (about 0.5 μg). Crystal samples prepared by solid:vapor phase reactions were applied to solids probe directly without any prior solvation (neat). The temperature of the solids was ramped at a rate of 64 ^{0}C per minute to a final temperature of 350 ^{0}C. The mass spectrometer was scanned from m/z 10 to m/z 800 at a rate of 530 ms per scan. Accurate mass measurements of molecular ions were carried out after the acquisition of full scans in unit mass resolution mode.

C vs. B ring Pentacene Isomer Characterization

The presence of both C and B ring isomers in the reaction mixture of pentacene with *N*-methylmaleimide was justified using two methods. ^{1}H NMR was used to quantify two distinct mixtures of the generated adduct, where one had been made more enriched in the presumed B ring isomer using column chromatography (3:7 ethyl acetate:hexane, R_f = 0.37). These same mixtures were also examined by HPLC to determine the retention times for the two main isomers. Adduct solutions were dissolved in 90/10 acetonitrile/THF, with roughly 1 mM concentrations. Using an HP1050 LabX, 10 μL injections via autosampler (200 μL/min) were run at a 1.0 mL/min flow rate through a

Zorbax SB-CN column of 4.6 mm ID/150 mm length, and with a 5 µm particle size. The UV detection ranged from 391-247 nm (recorded every 3 nm), in order to distinguish naphthalene versus anthracene absorption band in each of the C and B ring isomers, respectively. The majority species by NMR (14.6-14.7 min on HPLC) shows strong absorptions in regions typical of naphthalene and none indicative of anthracene,[7] and thus is assigned to the C ring adduct. The minor species by NMR (15.2-15.3 min on HPLC) absorbed well in excess of 350 nm and has been assigned as the B ring adduct. The method used for separation is outlined in the table below. A plot of the UV-vis data points, in mAU (taken from the peak heights), is also below followed by illustrative chromatograms at two wavelengths, 250 and 253 nm.

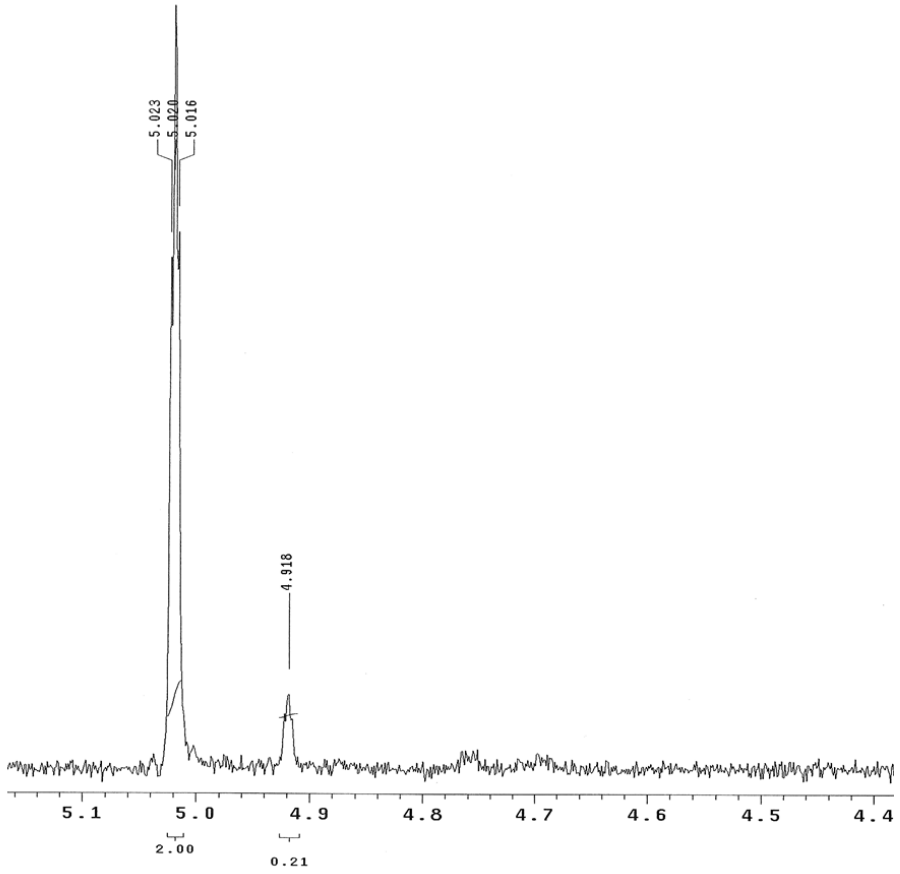

Above: ^{1}H NMR spectral region from 5.1 ppm-4.4 ppm for the reaction between pentacene with *N*-methylmaleimide depicting the two isomers. This region corresponds to the bridgehead protons. The major species at 5.02 ppm is the C ring isomer, followed by a chemical shift of 4.92 ppm pertaining to one of the B ring isomers. The ratio of isomers in this mixture is 8.5:1 and this mixture was used to determine HPLC retention times.

Method	% acetonitrile	% water
0 minutes	10	90
2.5 minutes	30	70
15 minutes	55	45
17.5 minutes	70	30
18.5 minutes	90	10
19 minutes	10	90
23 minutes	10	90

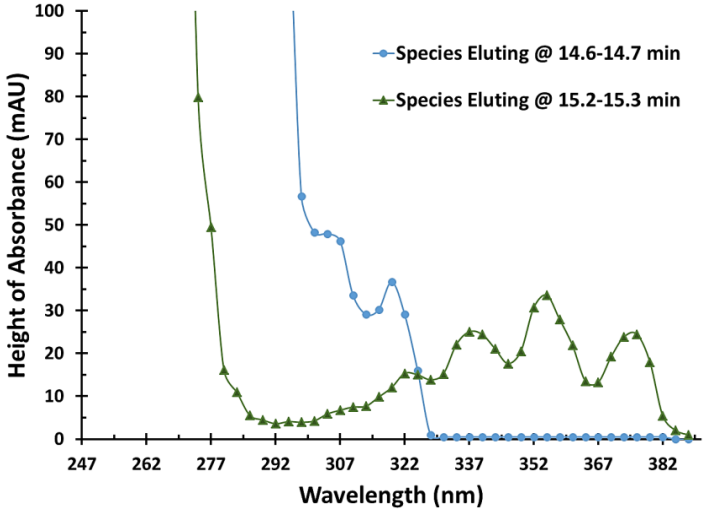

Above: A UV spectrum of the two eluting species at 14.6-14.7 min and 15.2-15.3 min. The species that eluted first (blue) was identified as the C ring isomer, since it lacks anthracene absorption bands in the 307-382 nm region. The species eluting second (green) was identified as the B ring isomer, since it has the previously reported anthracene absorption.

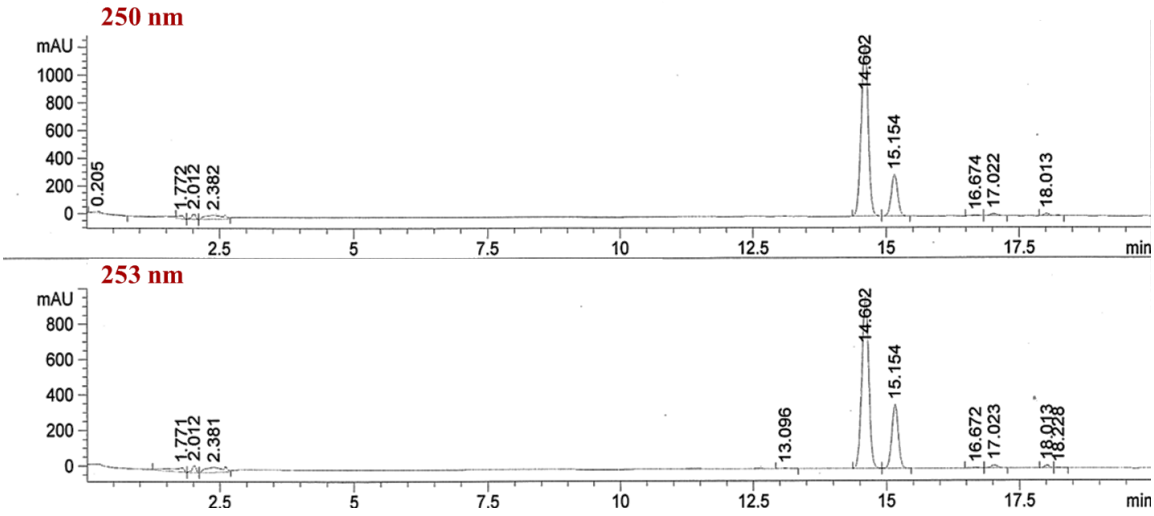

Above: HPLC traces observed at 250 nm and 253 nm detection for the dissolved reaction product of the pentacene with *N*-methylmaleimide. Two species eluted, one occurring at 14.6-14.7 min and the other at 15.2-15.3 min. Each of the monitored wavelengths was contained in the naphthalene and anthracene absorption region (from 391-247 nm), and their heights were plotted to give a UV spectrum pertaining to the isolated compounds.

General Procedure for Standard Diels-Alder Adduct Formation and Purification

For the production of standard Diels-Alder adducts, sealed tubes containing diene and dienophile were first evacuated and filled with nitrogen three times prior to addition of solvent. In the case of methoxybutadiene, the reaction was set up in the glovebox, and then transferred to a hood for heating. Degassed toluene was added via syringe while stirring. The tube was sealed and the reaction was stirred for 12-19 h at 120-125 °C in the dark, except for the reaction of 4-methyl-1,2,4-triazoline-3,5-dione with tetracene, which was reacted at room temperature, and of *N*-methylmaleimide with rubrene, which was refluxed in xylenes for 2 weeks. Afterwards, the reaction mixture was cooled to 4 °C

overnight before additional techniques were applied to the solution in order to isolate and identify major and minor isomers.

Although most reactions yielded a precipitate when cooling, in two instances (tetracene with tetrafluorobenzoquinone and with *N*-methylmaleimide) this material was comprised of only one stereoisomer (though it was not pure from unreacted tetracene in the former). For all reactions the filtrate was concentrated via rotary evaporation and combined with the precipitate. The combined materials were purified from remaining starting materials via column chromatography. In all cases stereoisomers were inseparable by column chromatography, but chromatography was useful in that the *endo* or *exo* isomers were enriched in the various fractions allowing for identification of the major and minor isomer.

All of the following Diels-Alder adducts were previously reported in the literature. 3-Methoxy-*cis*-1,2,3,6-tetrahydrophthalic anhydride (***trans*-1-methoxy-1,3-butadiene with maleic anhydride adduct**).[83] 9,10-Dihydroanthracene-9,10-α,β-succinic acid anhydride (**anthracene with maleic anhydride adduct**).[84] 9,10-Dihydro-9,10-ethanoanthracene-11,12-dicarbonyl *N*-methylamide (**anthracene with *N*-methylmaleimide adduct**).[85] 5,12-dihydro-5,12-ethano-naphthacene-13,14-dicarboxylic acid anhydride (**tetracene with maleic anhydride adduct**), 5,12-dihydro-5,12-ethano-napthacene-13,14-dichlorodicarboxylic acid anhydride (**tetracene with 2,3-dichloromaleic anhydride adduct**), 13,13,14,14-tetracyano-5,12-dihydro-5,12-ethano-napthacene (**tetracene with tetracyanoethylene adduct**), 13,14-dicyano-5,12-dihydro-

5,12-ethano-napthacene **(tetracene with fumarodinitrile adduct**), 5,12-dihydro-5,12-ethano-napthacene-15-*N*-methylpyrrolidine-14,16-dione (**tetracene with *N*-methylmaleimide adduct**).[45] *N*-methyl ethano-1,4-dihydro-1,4-tetraphenyl-5,6,11,12-napthacene dicarboximide-13,14 (exo and endo) (**rubrene with *N*-methylmaleimide adduct**).[77] All others were generated and characterized according to the procedure above. Additionally, 4-methyl-1,2,4-triazoline-3,5-dione was made from the oxidation of 4-methyl urazole[86] (purchased from Enamine).

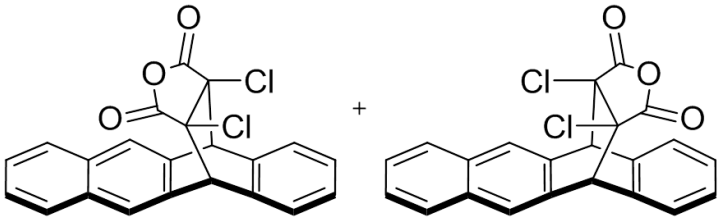

5,12-Dihydro-5,12-ethano-napthacene-13,14-dichlorodicarboxylic acid anhydride: Tetracene (0.151 g, 0.661 mmol), 2,3-dichloromaleic anhydride (0.122 g, 0.731 mmol) and toluene (4.0 mL) were placed in a sealed tube according to the general Diels-Alder procedure. The reaction mixture was stirred for 72 h at 120 °C. The Diels-Alder adduct (0.129 g, 0.326 mmol) was collected by simple filtration as a tan crystal in a 1:1.5 mixture of stereoisomers inseparable by silica gel chromatography, in a 50% yield. mp = 319-321 °C. Selected definitive ^{1}H NMR peaks were used for determination of stereoisomers. Major stereoisomer: ^{1}H NMR (500 MHz) δ 7.94 (s, 2H), 7.87 (dd, *J* = 6.2, 3.3 Hz, 2H), 7.55-7.51 (m, 2H), 7.39 (dd, J = 5.5, 3.2 Hz, 2H), 7.30 (dd, *J* = 5.5, 3.2 Hz, 2H), 4.98 (s, 2H). 13C NMR (125 MHz) δ 165.9, 136.1, 132.7, 132.4, 129.4, 128.0, 126.9, 126.24, 126.19, 71.4, 54.46. Minor stereoisomer: ^{1}H NMR (500 MHz) δ 7.81 (s,

2H), 7.79 (dd, *J* = 6.4, 3.4 Hz, 2H), 7.55-7.51 (m, 4H), 7.35 (dd, *J* = 5.6, 3.2 Hz, 2H), 4.99 (s, 2H). ^{13}C NMR (125 MHz) δ 165.8, 135.8, 133.0, 132.5, 128.3, 128.1, 127.4, 127.1, 125.5, 71.9, 54.52. IR (cm-1) 3053, 1868, 1798, 1608, 1504, 1480, 1462, 1403, 1350, 1262, 1216, 1139.

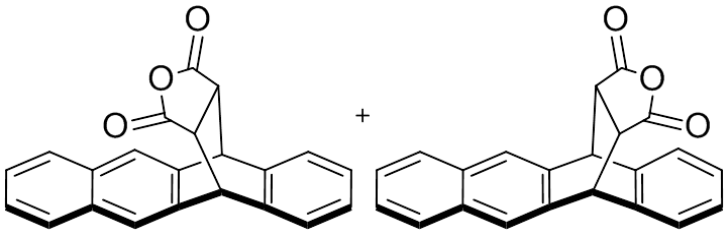

5,12-Dihydro-5,12-ethano-napthacene-13,14-dicarboxylic acid anhydride: Tetracene (0.073 g, 0.32 mmol), maleic anhydride (0.036 g, 0.36 mmol) and toluene (2.0 mL) were placed in a sealed tube according to the general Diels-Alder procedure. The reaction mixture was stirred for 8 h at 120 °C. The Diels-Alder adduct (0.061 g, 0.15 mmol) was collected by simple filtration as a tan crystal in a 1:2.5 mixture of stereoisomers inseparable by silica gel chromatography, in a 60% yield. mp = 276-280 °C. Selected definitive ^{1}H NMR peaks were used for determination of stereoisomers. Major stereoisomer: 1H NMR (500 MHz) δ 7.83 (s, 2H), 7.81-7.77 (m, 2H), 7.49-7.45 (m, 2H), 7.37 (dd, *J* = 5.4, 3.4 Hz, 2H), 7.23 (dd, *J* = 5.4, 3.2 Hz, 2H), 4.95-4.94 (m, 2H), 3.61 (dd, *J* = 2.2, 1.5 Hz, 2H). 13C NMR (125 MHz) δ 170.70, 138.0, 137.8, 132.6, 128.3, 128.0, 126.7, 125.6, 123.2, 48.0, 45.6. Minor stereoisomer: ^{1}H NMR (500 MHz) δ 7.79-7.77 (m, 4H), 7.49-7.45 (m, 2H), 7.42 (dd, *J* = 5.5, 3.3 Hz, 2H), 7.22 (dd, *J* = 5.6, 3.2 Hz, 2H), 4.94-4.93 (m, 2H), 3.62 (dd, *J* = 2.1, 1.3 Hz, 2H). ^{13}C NMR (125 MHz) δ

170.69, 140.6, 135.3, 132.8, 129.3, 128.5, 128.1, 124.8, 124.3, 48.3, 45.5. IR (cm-1) 3055, 3020, 2957, 1860, 1778, 1402, 1228, 1071, 923.

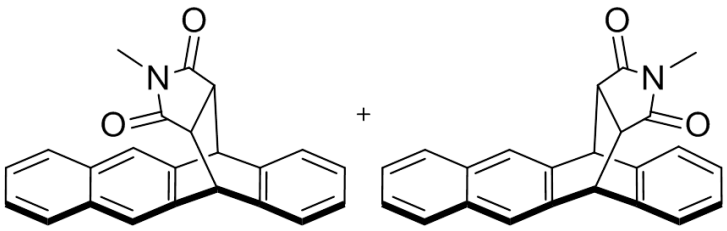

5,12-Dihydro-5,12-ethano-napthacene-15-*N*-methylpyrrolidine-14,16-dione: Tetracene (0.080 g, 0.35 mmol), *N*-methylmaleimide (0.043 g, 0.39 mmol) and toluene (2.0 mL) were placed in a sealed tube according to the general Diels-Alder procedure. The reaction mixture was stirred for 24 h at 120 °C. The Diels-Alder adduct (0.074 g, 0.22 mmol) was collected by filtration as a white and tan crystal in a 1:1.6 mixture of stereoisomers inseparable by silica gel chromatography, in a combined 62% yield. mp = 319-321 °C. Selected definitive ^{1}H NMR peaks were used for determination of stereoisomers. Major stereoisomer: ^{1}H NMR (500 MHz) δ 7.80-7.78 (m, 4H), 7.45 (dd, *J* = 6.2, 3.3 Hz, 2H), 7.29 (dd, J = 5.5, 3.3 Hz, 2H), 7.14 (dd, *J* = 5.4, 3.2 Hz, 2H), 4.91-4.90 (m, 2H), 3.30-3.28 (m, 2H), 2.54 (s, 3H). 13C NMR (125 MHz) δ 176.93, 138.7, 138.2, 132.40, 127.7, 127.3, 126.1, 125.0, 122.7, 46.9, 45.45, 24.36. Minor stereoisomer: ^{1}H NMR (500 MHz) δ 7.74 (dd, *J* = 6.1, 3.4 Hz, 2H), 7.70 (s, 2H), 7.43-7.39(m, 4H), 7.19 (dd, *J* = 5.6, 3.2 Hz, 2H), 4.90-4.88 (m, 2H), 3.31-3.30 (m, 2H), 2.43 (s, 3H). ^{13}C NMR (125 MHz) δ 176.97, 141.2, 135.9, 132.39, 127.8, 127.0, 126.0, 124.4, 123.5, 47.1, 45.36, 24.38. IR (cm-1) 3044, 2943, 1780, 1702, 1434, 1379, 1299, 1281, 1142.

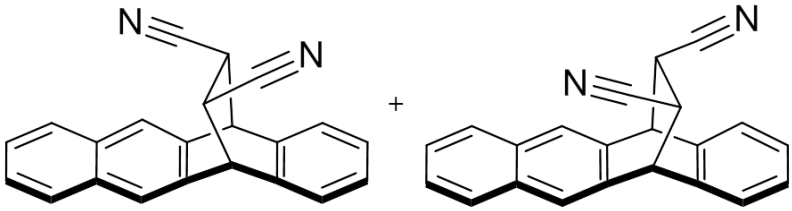

13, 14-Dicyano-5,12-dihydro-5,12-ethano-napthacene: Tetracene (0.076 g, 0.33 mmol), fumarodinitrile (0.027 g, 0.33 mmol) and toluene (1.5 mL) were placed in a sealed tube according to the general Diels-Alder procedure. The reaction mixture was stirred for 42 h at 150 °C. The Diels-Alder adduct (0.056 g, 0.18 mmol) was collected by simple filtration as a tan crystal in a 55% yield. mp = 240-244 °C. Stereoisomers are not distinguishable by NMR. ^{1}H NMR (500 MHz) δ 7.91 (s, 1H), 7.85-7.79 (m, 3H), 7.52-7.48 (m, 3H), 7.41-7.39 (m, 1H), 7.32-7.26 (m, 2H), 4.75 (d, *J* = 2.4 Hz, 1H), 4.74 (d, *J* = 2.4 Hz, 1H), 3.25 (dd, *J* = 5.1, 2.4 Hz, 1H), 3.24 (dd, *J* = 5.1, 2.4 Hz, 1H). ^{13}C NMR (125 MHz) δ 139.1, 137.1, 136.3, 134.1, 132.7, 132.6, 128.2, 128.14, 128.06, 127.8, 126.75, 126.68, 125.9, 124.8, 124.3, 123.0, 118.49, 118.47, 46.4, 46.3, 35.7, 35.6. IR (cm-1) 3057, 2941, 2245, 1501, 1477, 1461, 1400, 894.

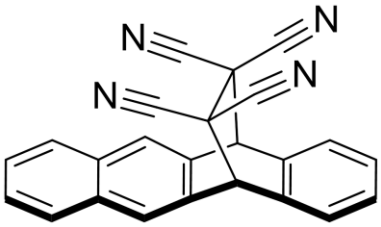

13, 13, 14, 14-Tetracyano-5,12-dihydro-5,12-ethano-napthacene: Tetracene (0.083

g, 0.36 mmol), tetracyanoethylene (0.054 g, 0.40 mmol) and toluene (2.0 mL) were placed in a sealed tube according to the general Diels-Alder procedure. The reaction mixture was stirred for 20 h at 120 °C. The Diels-Alder adduct (0.109 g, 0.31 mmol) was collected by simple filtration as a tan crystal in an 84% yield. mp > 282 °C (dec.) ^{1}H NMR (500 MHz) δ 8.04 (s, 2H), 7.91 (dd, *J* = 6.2, 3.3 Hz, 2H), 7.64-7.58 (m, 4H), 7.48 (dd, *J* = 5.4, 3.2 Hz, 2H), 5.16 (s, 2H). ^{13}C NMR (125 MHz) δ 134.1, 133.1, 130.2, 129.9, 128.4, 128.0, 126.8, 126.5, 110.76, 110.75, 53.1, 46.5. IR (cm-1) 3062, 3017, 2991, 2250, 1608, 1503, 1480, 1464, 1270, 881.

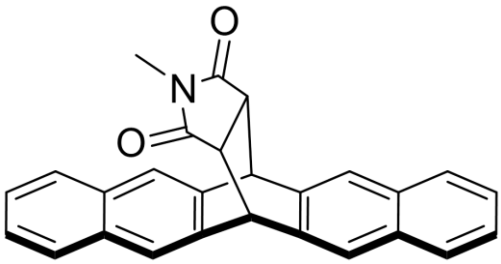

6,13-dihydro-6,13-ethano-pentacene-16-N-methylpyrrolidine-15,17-dione: Pentacene (0.106 g, 0.380 mmol), *N*-methylmaleimide (0.043 g, 0.39 mmol) and toluene (2 mL) were placed in a sealed tube according to the general Diels-Alder procedure. The heated reaction mixture was stirred for 19 h. The generated product was a mixture of adducts, though predominantly the regioisomer at the 6,13 carbons of pentacene. Inseparable regioisomers (0.056 g, 0.15 mmol), were purified via silica gel chromatography (3:7 ethyl acetate:hexane, R_f = 0.37) as an off-white crystal in a 38% yield. mp = 324-340 °C. Selected ^{1}H NMR peaks were only used for determination of the 6,13 adduct. Other

regioisomers were analyzed via high performance liquid chromatography outlined in the previous section (**C vs. B pentacene isomer characterization)**.

Major regioisomer: ^{1}H NMR (500 MHz) δ 7.84 (s, 2H), 7.80 (dd, *J* = 6.1, 3.2 Hz, 2H), 7.78-7.73 (m, 4H), 7.45 (dd, *J* = 6.3, 3.2 Hz, 2H), 7.42 (dd, *J* = 6.1, 3.2 Hz, 2H), 5.02 (s, 2H), 3.37 (s, 2H), 2.47 (s, 3H). ^{13}C NMR (125 MHz) δ 177.2, 138.7, 135.8, 132.8 (2C), 128.0, 127.9, 126.4, 126.2, 123.9, 123.1, 47.2, 45.5, 24.7. IR (cm^{-1}) 3050, 2962, 2949, 1775, 1699, 1437, 1399, 1383, 747.

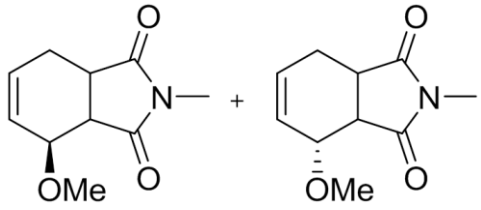

3-Methoxy-*N*-methyl-*cis*-1,2,3,6-tetrahydrophthalimide: *Trans*-1-methoxy-1,3-butadiene (38 µL, 0.032 g, 0.38 mmol), *N*-methylmaleimide (0.042 g, 0.38 mmol) and toluene (2 mL) were placed in a sealed tube according to the general Diels-Alder procedure. The heated reaction mixture was stirred for 19 h. The mixture (0.07:1) of adducts, inseparable by silica gel chromatography, was purified from starting materials by recrystallization from ether. The final compounds (0.056 g, 0.29 mmol) were isolated as a yellow solid in 77% yield. mp = 38-40 °C. Selective quantitative ^{13}C NMR peaks were used for determination of the ratio of stereoisomers. Quantitative ^{13}C NMR gave a ratio of isomers consistent with the mixtures observed in ^{1}H spectra.

Major stereoisomer: ^{1}H NMR (500 MHz) δ 6.14-6.08 (m, 2H), 4.21 (t, *J* = 5.6 Hz, 1H), 3.27 (s, 3H), 3.11-3.08 (m, 1H), 3.04-2.99 (m, 1H), 2.98 (s, 3H), 2.61-2.54 (m, 1H), 2.50-

2.44 (m, 1H). ^{13}C NMR (125 MHz) δ 180.1, 177.0, 131.5, 128.8, 72.0, 56.7, 45.0, 37.2, 24.8, 22.5. Minor stereoisomer: ^{1}H NMR (500 MHz) δ 6.14-6.08 (m, 2H), 4.21 (t, *J* = 5.6 Hz, 1H), 3.36 (s, 3H), 3.11-3.08 (m, 1H), 3.04-2.99 (m, 1H), 2.96 (s, 3H), 2.61-2.54 (m, 1H), 2.50-2.44 (m, 1H). ^{13}C NMR (125 MHz) δ 180.2, 177.7, 132.4, 128.2, 71.8, 56.5, 45.6, 37.4, 25.2, 23.4. IR (cm^{-1}) 3449, 2923, 2856, 2831, 1774, 1669, 1436, 1386, 1281, 1130, 1087.

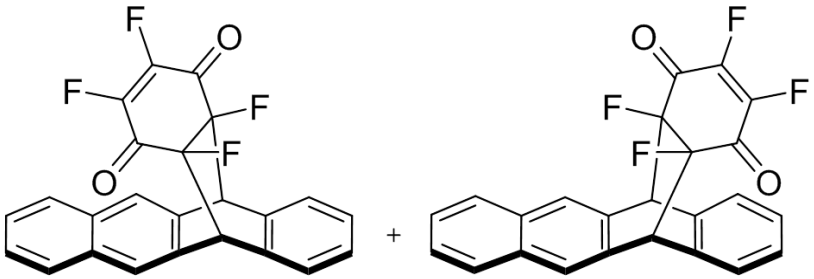

2,3,4a,5,12, 12a-Tetrafluoro-5,12-dihydro-5,12-o-benzeno-napthacene-1,4-dione: Tetracene (0.074 g, 0.32 mmol), tetrafluoro-1,4-benzoquinone (0.058 g, 0.32 mmol) and toluene (2 mL) were placed in a sealed tube according to the general Diels-Alder procedure. The heated reaction mixture was stirred for 12 h. The mixture (1.9:2) of adducts (0.063 g, 0.15 mmol), inseparable by silica gel chromatography, was isolated from starting material by column chromatography (1:1 ethyl acetate:hexane, R_f = 0.93) as a yellow crystal in a 48%. mp > 246 °C (dec.).

Major stereoisomer: ^{1}H NMR (500 MHz) δ 7.97 (s, 2H), 7.86 (dd, *J* = 6.2, 3.2 Hz, 2H), 7.51 (dd, *J* = 6.2, 3.2 Hz, 2H), 7.37-7.28 (m, 4H), 5.10 (t, *J* = 3.9 Hz, 2H). ^{1}C NMR (125 MHz) δ 184.5-184.0 (m), 149.5 (dd, *J* = 294.1, 7.3 Hz), 135.4, 133.3, 132.7, 129.7, 128.1, 126.94, 126.90, 126.1, 90.7 (dd, *J* = 220.7, 16.7 Hz), 52.6 (dd, *J* = 15.4, 9.5 Hz). Minor

stereoisomer: 7.76 (dd, *J* = 6.2, 3.2 Hz, 2H), 7.74 (s, 2H), 7.54 (dd, *J* = 5.6, 3.1 Hz, 2H), 7.51 (dd, *J* = 6.2, 3.2 Hz, 2H), 7.36 (dd, *J* = 5.6, 3.1 Hz, 2H), 5.11 (t, *J* = 4.2 Hz, 2H). ^{13}C NMR (125 MHz) δ 149.1 (dd, *J* = 293.4, 7.4 Hz), 135.8, 133.3, 131.6, 128.7, 128.2, 127.6, 126.9, 126.2, 91.0 (dd, *J* = 219.4, 15.6 Hz), 52.8-52.3 (m). The C=O could not be resolved due to low signal strength of the multiplet. IR (cm^{-1}) 3413, 2924, 2853, 1702, 1672, 1359, 1120, 1036, 917, 746.

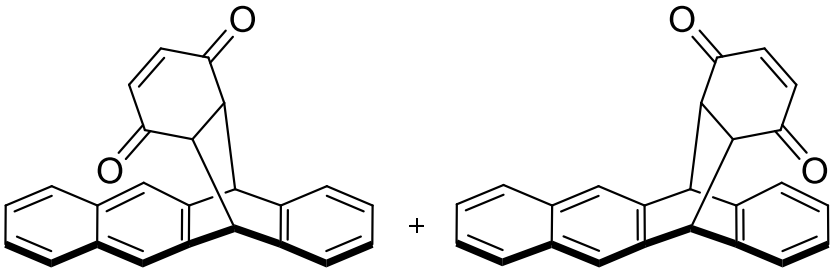

4a,5,12,12a-Tetrahydro-5,12-o-benzeno-napthacene-1,4-dione: Tetracene (0.074 g, 0.32 mmol), *p*-benzoquinone (0.352 g, 3.3 mmol) and toluene (2 mL) were placed in a sealed tube according to the general Diels-Alder procedure. The heated reaction mixture was stirred for 13 h. The mixture (0.3:2) of adducts (0.010 g, 0.030 mmol), inseparable by silica gel chromatography, was isolated from starting materials by column chromatography (6:4 dichloromethane:hexane, R_f = 0.21) as a pale yellow solid in an 8% yield. mp = 244-248 °C.

Major steroisomer: ^{1}H NMR (500 MHz) δ 7.83 (s, 2H), 7.80 (dd, *J* = 6.1, 3.4 Hz, 2H), 7.45 (dd, *J* = 6.2, 3.3 Hz, 2H), 7.23 (dd, *J* = 5.4, 3.2 Hz, 2H), 7.10 (dd, *J* = 5.4, 3.2 Hz, 2H), 6.37 (s, 2H), 5.00-4.99 (m, 2H , 3.25 (t, *J* = 1.3 Hz, 2H). ^{13}C NMR (125 MHz) δ 198.3, 141.1, 139.7, 139.3, 132.7, 127.9, 127.3, 126.2, 125.1, 122.5, 49.6, 49.0. Minor

stereoisomer: ^{1}H NMR (500 MHz) δ 7.72 (dd, *J* = 6.2, 3.3 Hz, 2H), 7.63 (s, 2H), 7.43-7.39 (m, 4H), 7.22-7.20 (m, 2H), 6.26 (s, 2H), 4.98-4.97 (m, 2H), 3.22 (t, *J* = 1.3 Hz, 2H). ^{13}C NMR (125 MHz) δ 198.7, 141.5, 140.9, 137.3, 132.5, 128.0, 127.2, 126.2, 124.3, 123.5, 49.2, 48.9. IR (cm^{-1}) 3433, 2957, 2924, 2853, 1673, 1608, 1265, 1099, 868, 766, 744.

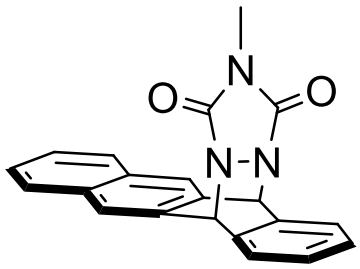

2-Methyl-4,11-dihydro-4,11-o-benzeno-napthacene-2,3a,11-triazolo-1,3-dione: Tetracene (0.036 g, 0.16 mmol), 4-methyl-1,2,4-triazoline-3,5-dione (0.0175 g, 0.16 mmol) and toluene (3 mL) were placed in a sealed tube according to the general Diels-Alder procedure. The heated reaction mixture was stirred for 12 h. The single adduct formed was isolated from starting material (0.031 g, 0.090 mmol) by column chromatography (2:3 ethyl acetate:hexane, R_f = 0.6) as a white solid in a 58% yield. mp = 262-264 °C. ^{1}H NMR (500 MHz) δ 7.86 (s, 2H), 7.82 (dd, *J* = 6.2, 3.3 Hz, 2H), 7.52 (dd, *J* = 6.2, 3.3 Hz, 2H), 7.48 (dd, *J* = 5.5, 3.2 Hz, 2H), 7.30 (dd, *J* = 5.5, 3.2 Hz, 2H), 6.33 (s, 2H), 2.84 (s, 3H). ^{13}C NMR (125 MHz) δ 157.5, 136.8, 133.5, 132.9, 128.8, 128.5, 127.3, 124.3, 123.3, 60.5, 25.8. IR (cm^{-1}) 3415, 3050, 2957, 1776, 1718, 1460, 1382, 1174, 1022, 890, 761. Since the Diels-Alder reaction has the potential to yield two

possible stereoisomers, *endo* or *exo*, the formation of only one isomer gives rise to ambiguity on our product's particular stereochemistry.

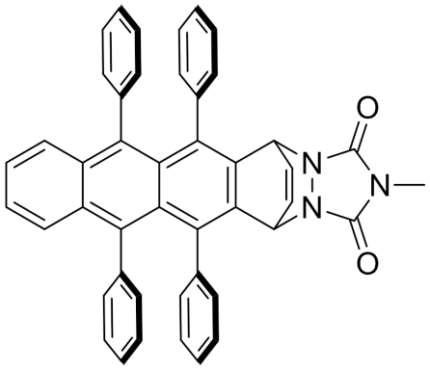

2-Methyl-4,11-dihydro-4,5,10,11-tetraphenyl-4,11-o-benzeno-napthacene-2,3a,11-triazolo-1,3-dione: Rubrene (0.014 g, 0.0026 mmol), 4-methyl-1,2,4-triazoline-3,5-dione (0.003 g, 0.0026 mmol) and toluene (2 mL) were placed in a sealed tube according to the general Diels-Alder procedure. The heated reaction mixture was stirred for 19 h. The single adduct formed was isolated from starting materials (0.013 g, 0.0019 mmol) by column chromatography (3:7 ethyl acetate:hexane, $R_f = 0.44$) as a light yellow solid in a 78% yield. mp >80 °C (dec.) ^{1}H NMR (300 MHz) δ 7.37 (dd, *J* = 6.9, 3.2 Hz, 2H), 7.24 (dd, *J* = 7.0, 3.3 Hz, 2H), 7.11-6.96 (m, 15H), 6.94-6.85 (m, 7H), 6.68-6.64 (m, 2H), 6.59 (dd, *J* = 4.2, 3.2 Hz, 2H), 5.41 (dd, *J* = 4.2, 3.2 Hz, 2H), 2.92 (s, 3H). ^{13}C NMR (75 MHz) δ 157.6, 140.7, 139.7, 138.8, 135.5, 133.3, 132.6, 132.4, 131.94, 131.90, 130.7, 130.4, 129.8, 128.2, 127.62, 127.59, 127.4, 126.8, 126.6, 126.5, 125.8, 54.7, 25.7. IR (cm^{-1}) 3057, 2925, 1775, 1714, 1444, 1394, 910, 733, 698.

APPENDIX A
^{1}H, ^{13}C NMR, AND IR SPECTROSCOPY OF SYNTHESIZED ADDUCTS

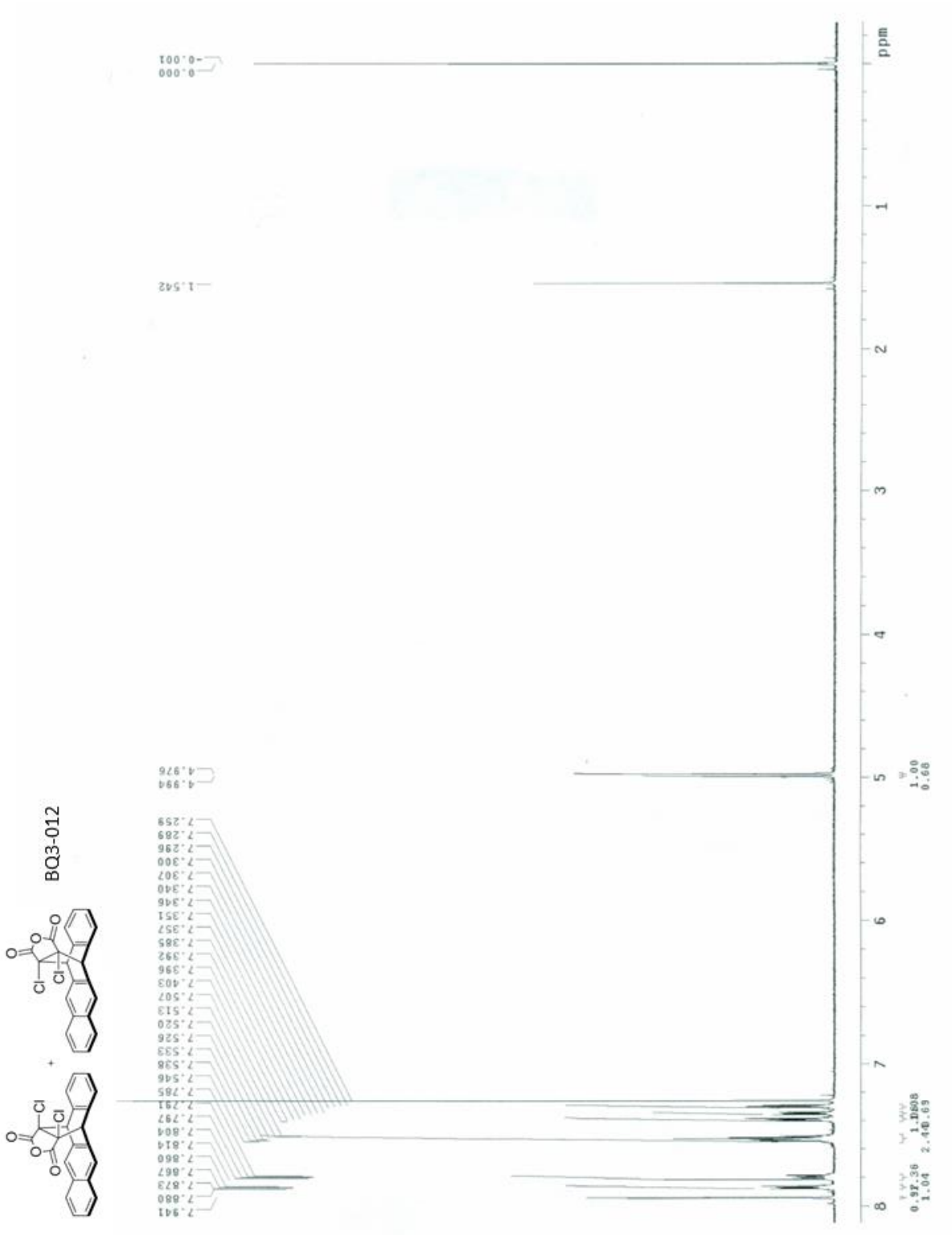
BQ3-012
Cl
Cl
O
O
O
+
Cl
Cl
O
O
O
-0.001
0.000
1.542
4.976
4.994
7.259
7.269
7.296
7.300
7.307
7.340
7.346
7.351
7.357
7.385
7.392
7.396
7.403
7.507
7.513
7.520
7.526
7.533
7.538
7.546
7.785
7.791
7.797
7.804
7.814
7.860
7.867
7.873
7.880
7.941
ppm
1
2
3
4
5
6
7
8
1.00
0.66
1.8808
2.4069
0.9736
1.04

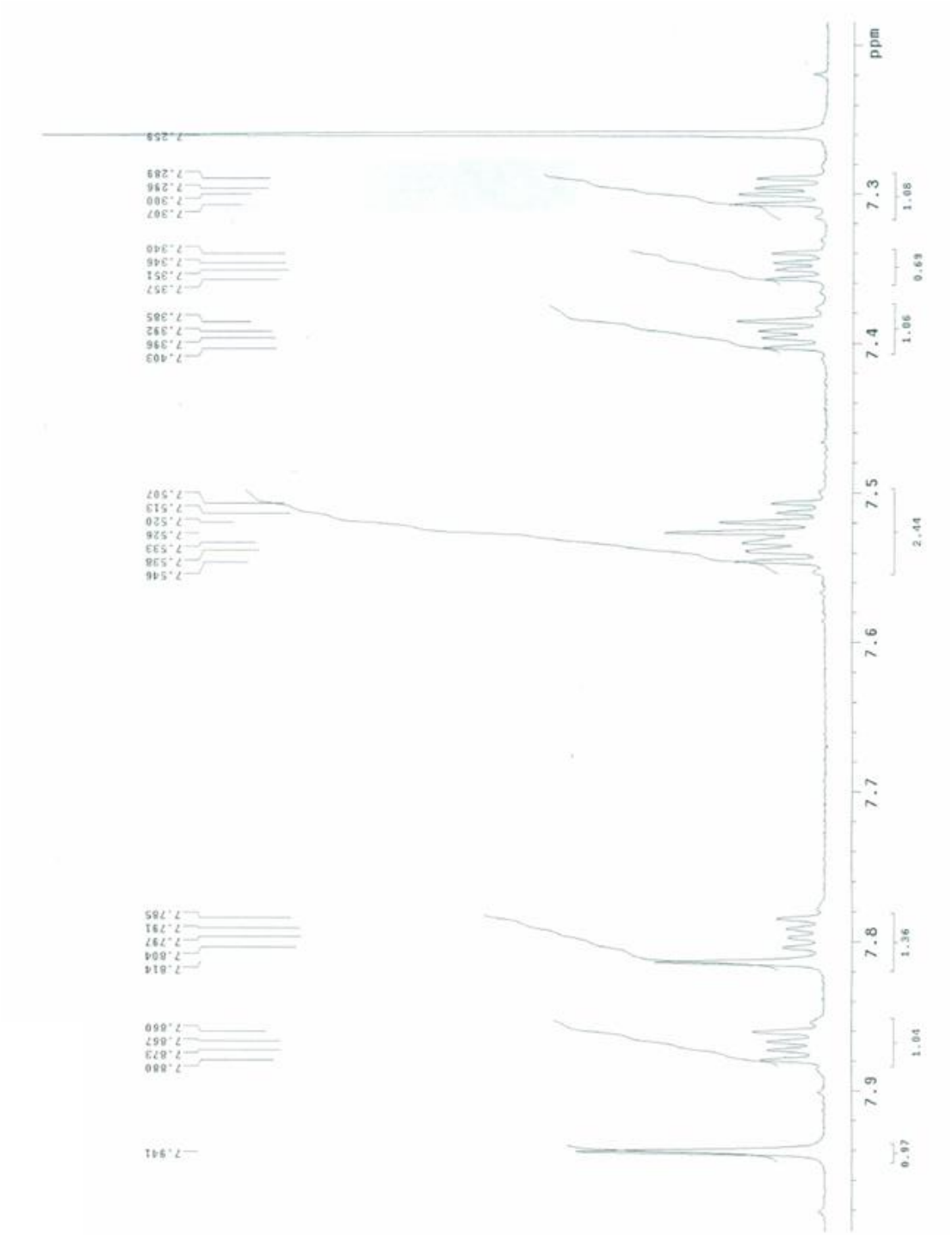
7.259
7.289
7.296
7.300
7.307
7.340
7.346
7.351
7.357
7.385
7.392
7.396
7.403
7.507
7.513
7.520
7.526
7.533
7.538
7.546
7.614
7.804
7.797
7.791
7.785
7.660
7.657
7.673
7.680
7.941
ppm
7.9
7.8
7.7
7.6
7.5
7.4
7.3
0.97
1.04
1.36
2.44
1.06
0.69
1.08

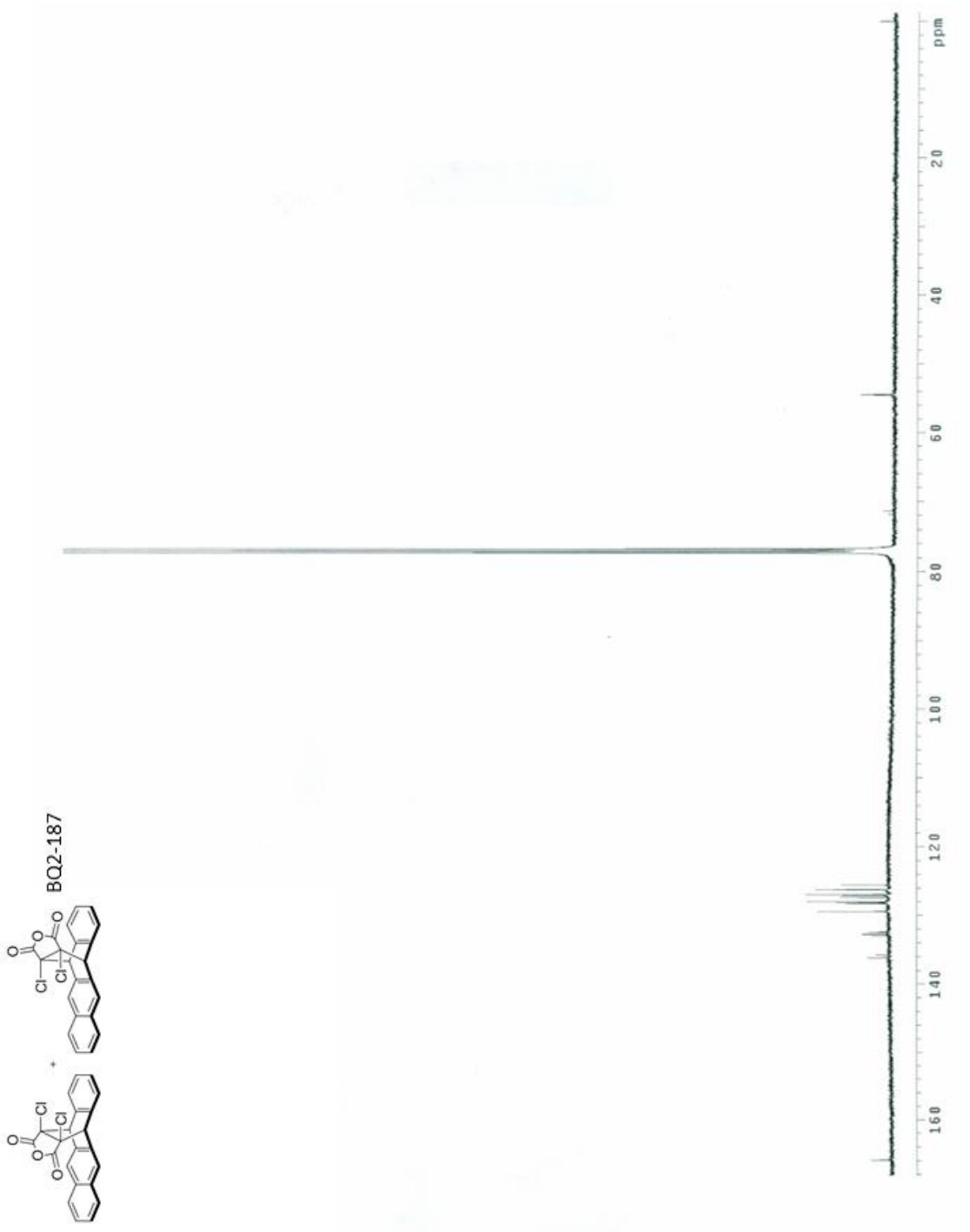
BQ2-187
ppm
20
40
60
80
100
120
140
160

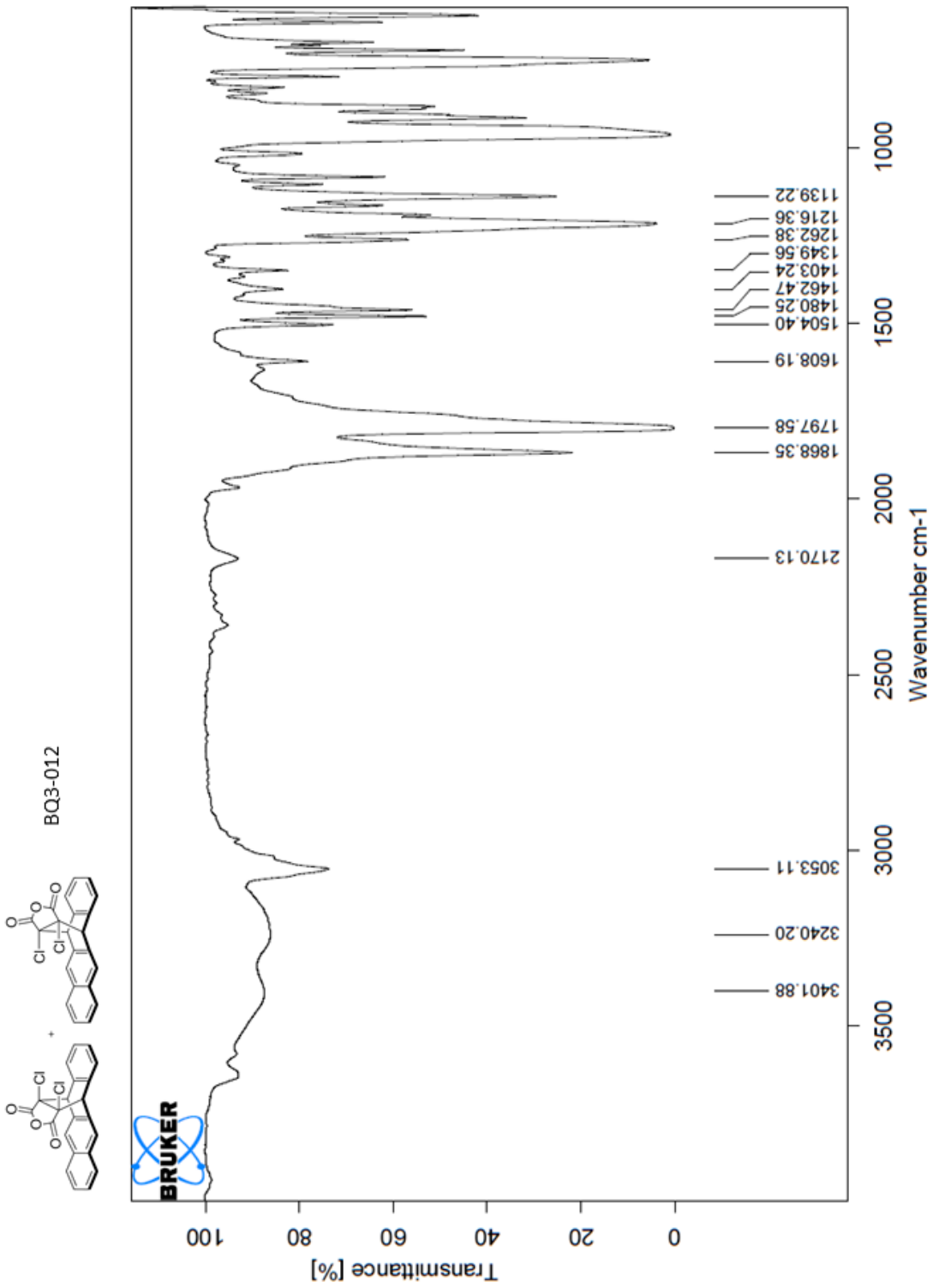
BQ3-012
BRUKER
Transmittance [%]
0
20
40
60
80
100
Wavenumber cm-1
3500
3000
2500
2000
1500
1000
3401.88
3240.20
3053.11
2170.13
1868.35
1797.58
1608.19
1504.40
1480.25
1462.47
1403.24
1349.56
1262.38
1216.36
1139.22

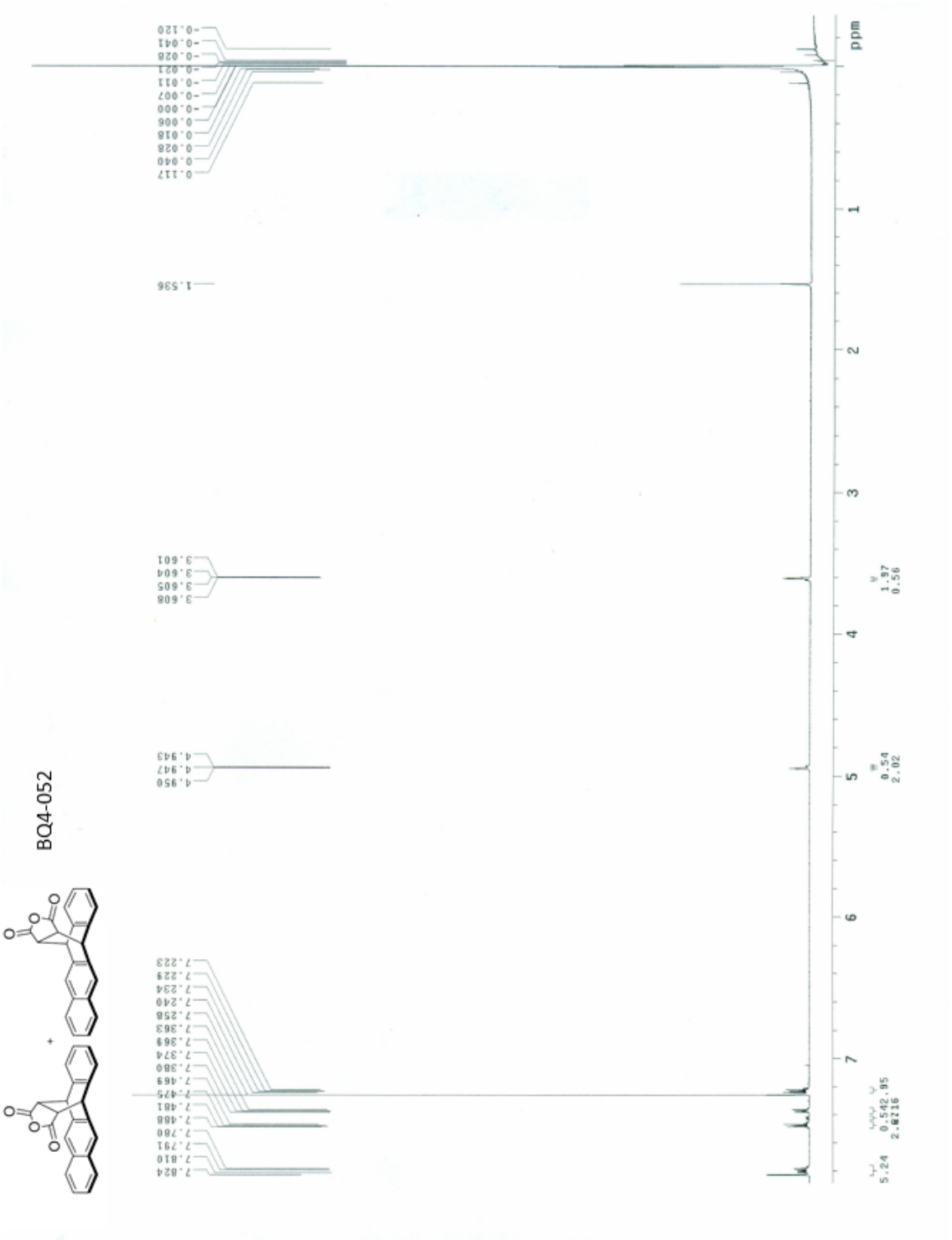
BQ4-052
ppm
1
2
3
4
5
6
7
1.37
0.56
0.54
2.02
0.542.95
2.6716
5.24
1.536
3.608
3.605
3.604
3.601
4.950
4.947
4.943
7.824
7.810
7.791
7.780
7.488
7.481
7.475
7.469
7.380
7.374
7.369
7.363
7.258
7.240
7.234
7.229
7.223
0.117
0.040
0.028
0.018
0.006
-0.000
-0.007
-0.011
-0.021
-0.028
-0.041
-0.120

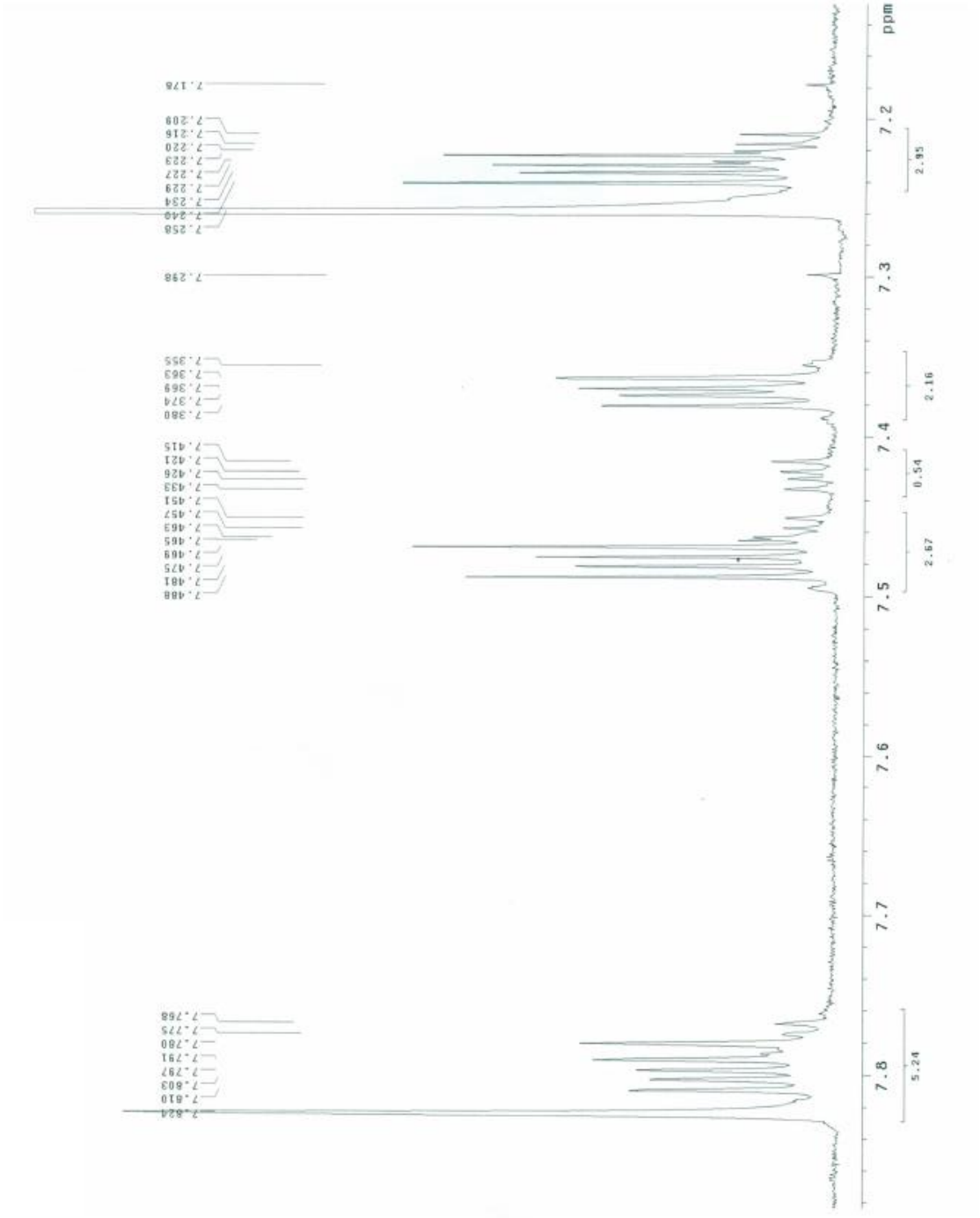
7.824
7.810
7.803
7.797
7.791
7.780
7.775
7.768
7.488
7.481
7.475
7.469
7.465
7.463
7.457
7.451
7.433
7.426
7.421
7.415
7.380
7.374
7.369
7.363
7.355
7.298
7.258
7.249
7.234
7.229
7.227
7.223
7.220
7.216
7.209
7.178
7.8
7.7
7.6
7.5
7.4
7.3
7.2
ppm
5.24
2.67
0.54
2.16
2.95

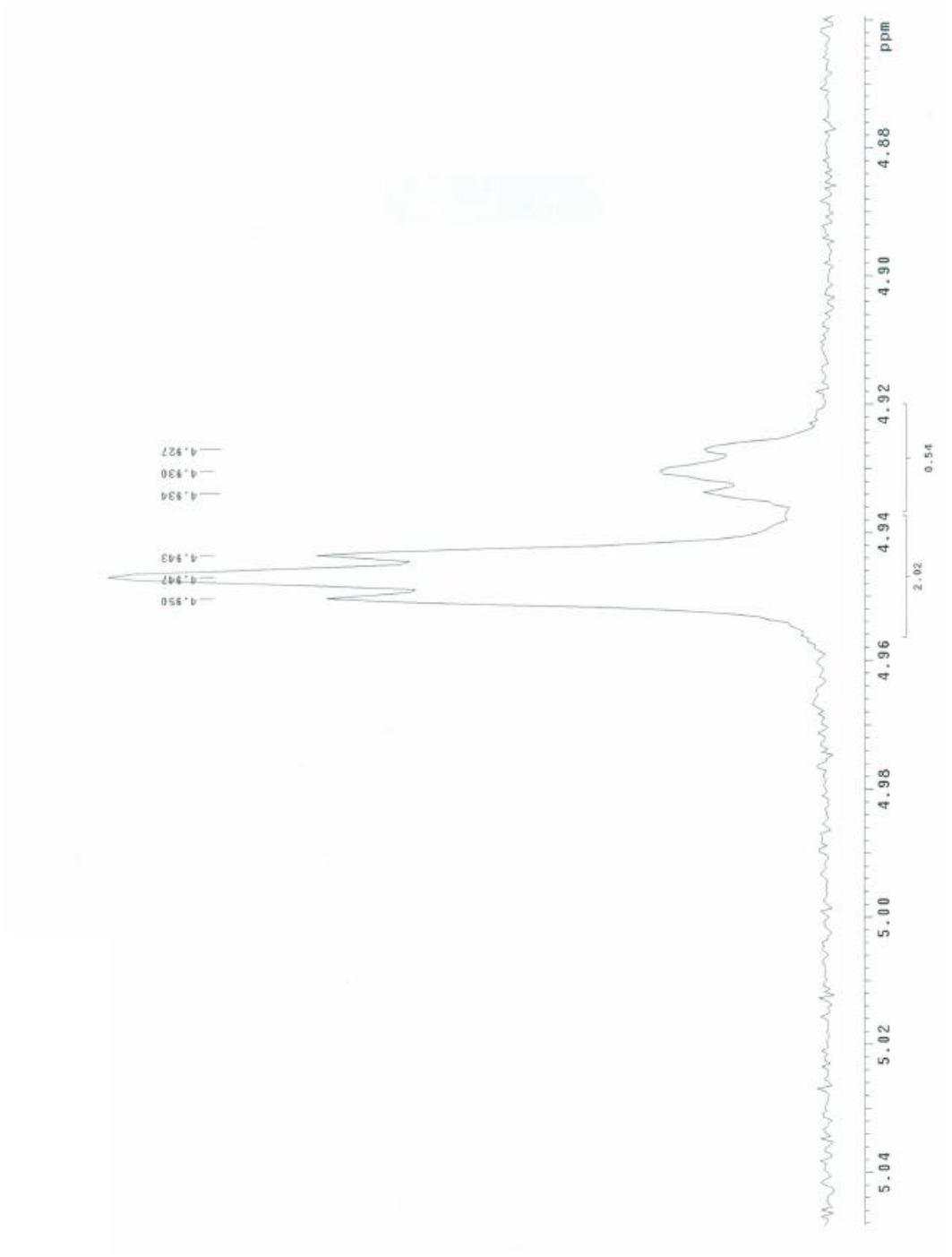
4.950
4.947
4.943
4.934
4.930
4.927
5.04
5.02
5.00
4.98
4.96
4.94
4.92
4.90
4.88
ppm
2.02
0.54

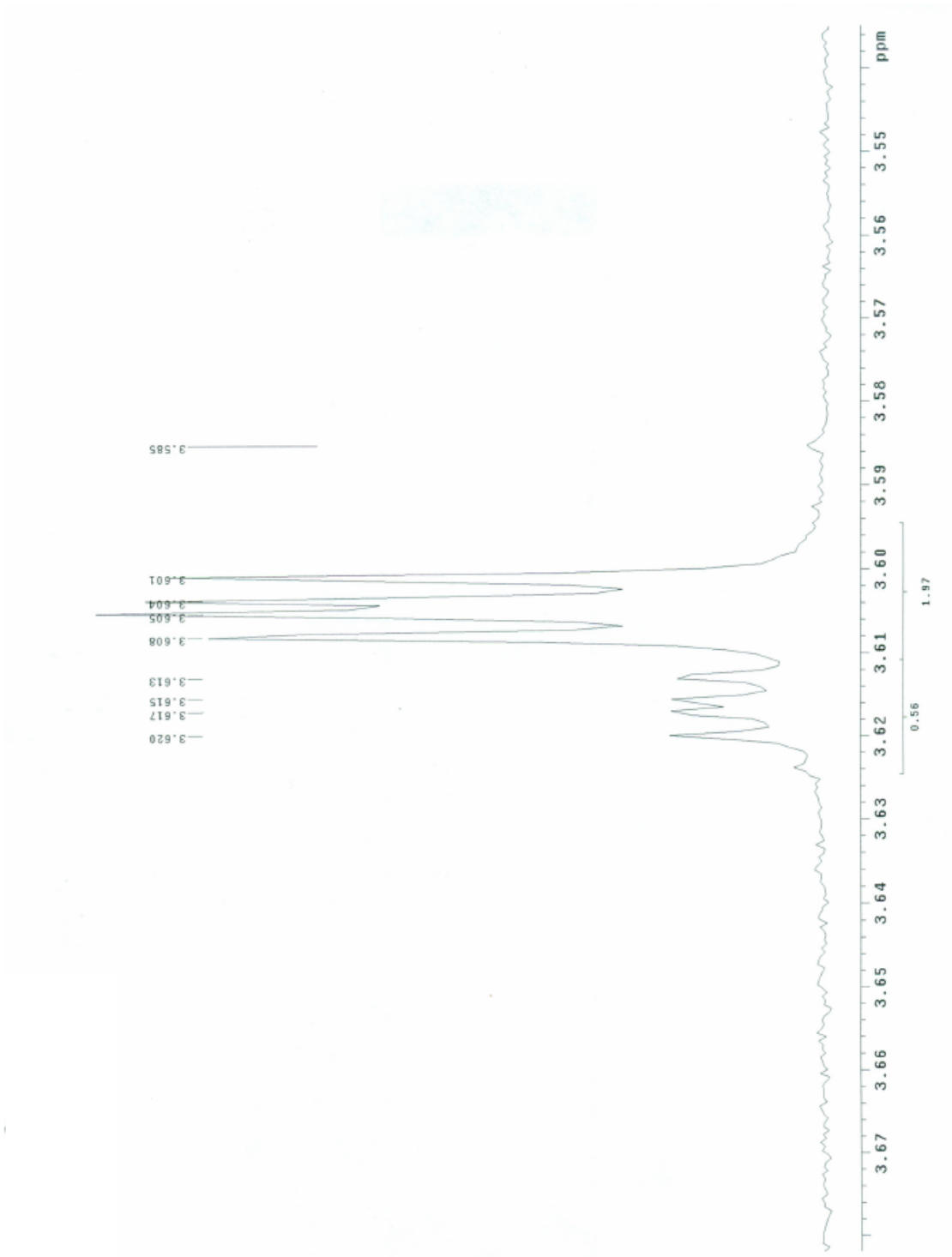
3.585
3.601
3.604
3.605
3.608
3.613
3.615
3.617
3.620
3.67
3.66
3.65
3.64
3.63
3.62
3.61
3.60
3.59
3.58
3.57
3.56
3.55
ppm
0.56
1.97

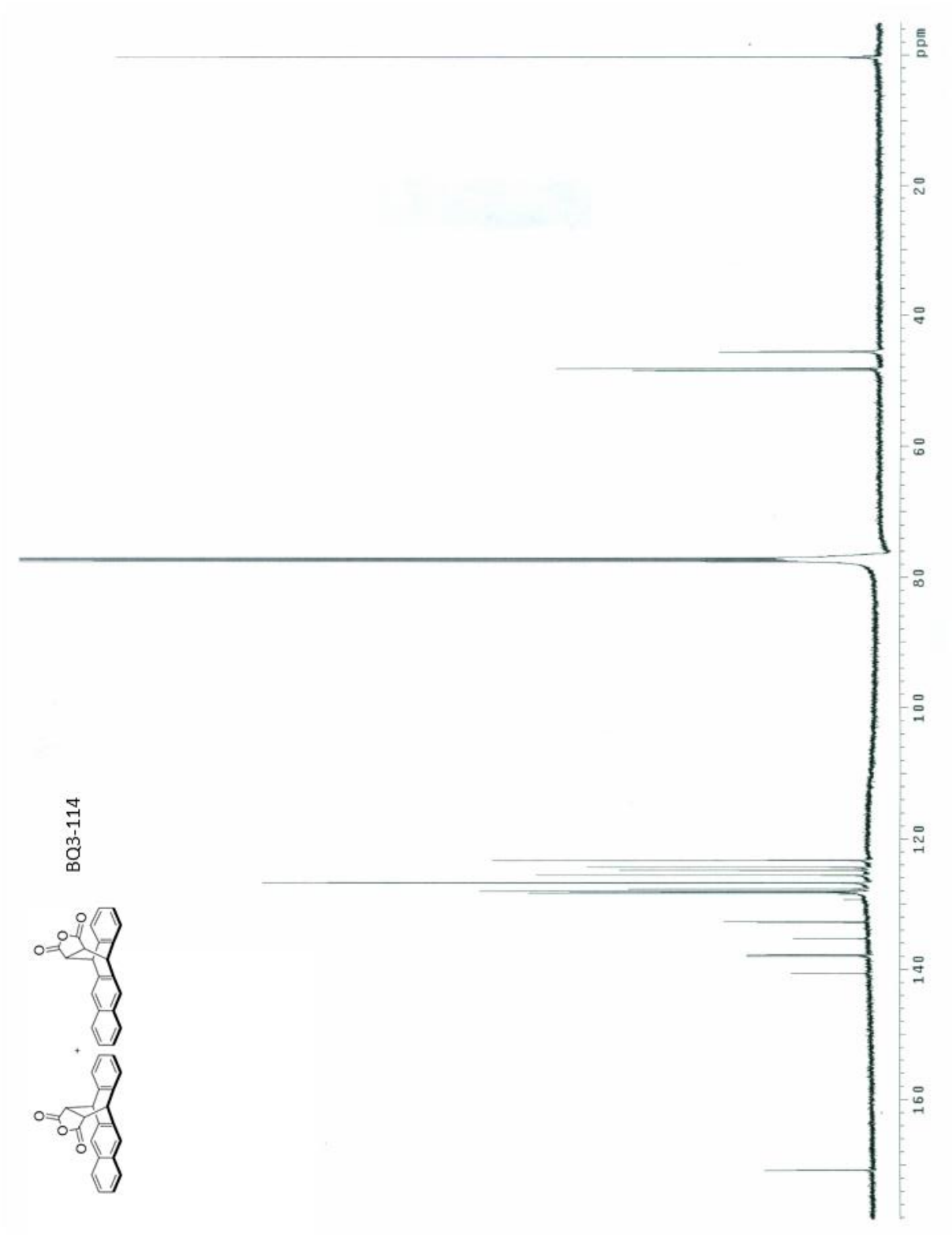
BQ3-114
ppm
20
40
60
80
100
120
140
160

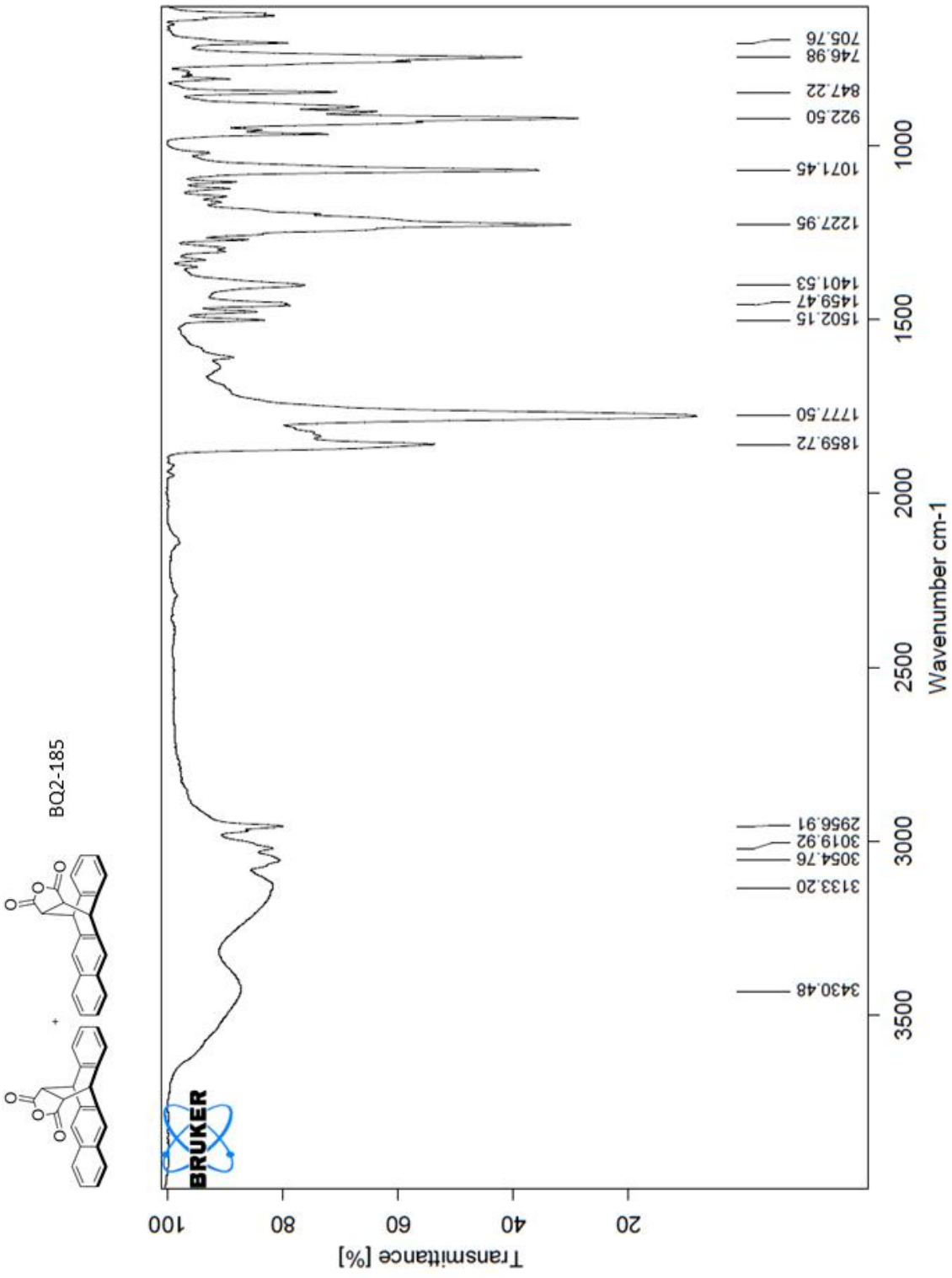
BQ2-185
BRUKER
Transmittance [%]
100
80
60
40
20
Wavenumber cm-1
3500
3000
2500
2000
1500
1000
3430.48
3133.20
3054.76
3019.92
2956.91
1859.72
1777.50
1502.15
1459.47
1401.53
1227.95
1071.45
922.50
847.22
746.98
705.76

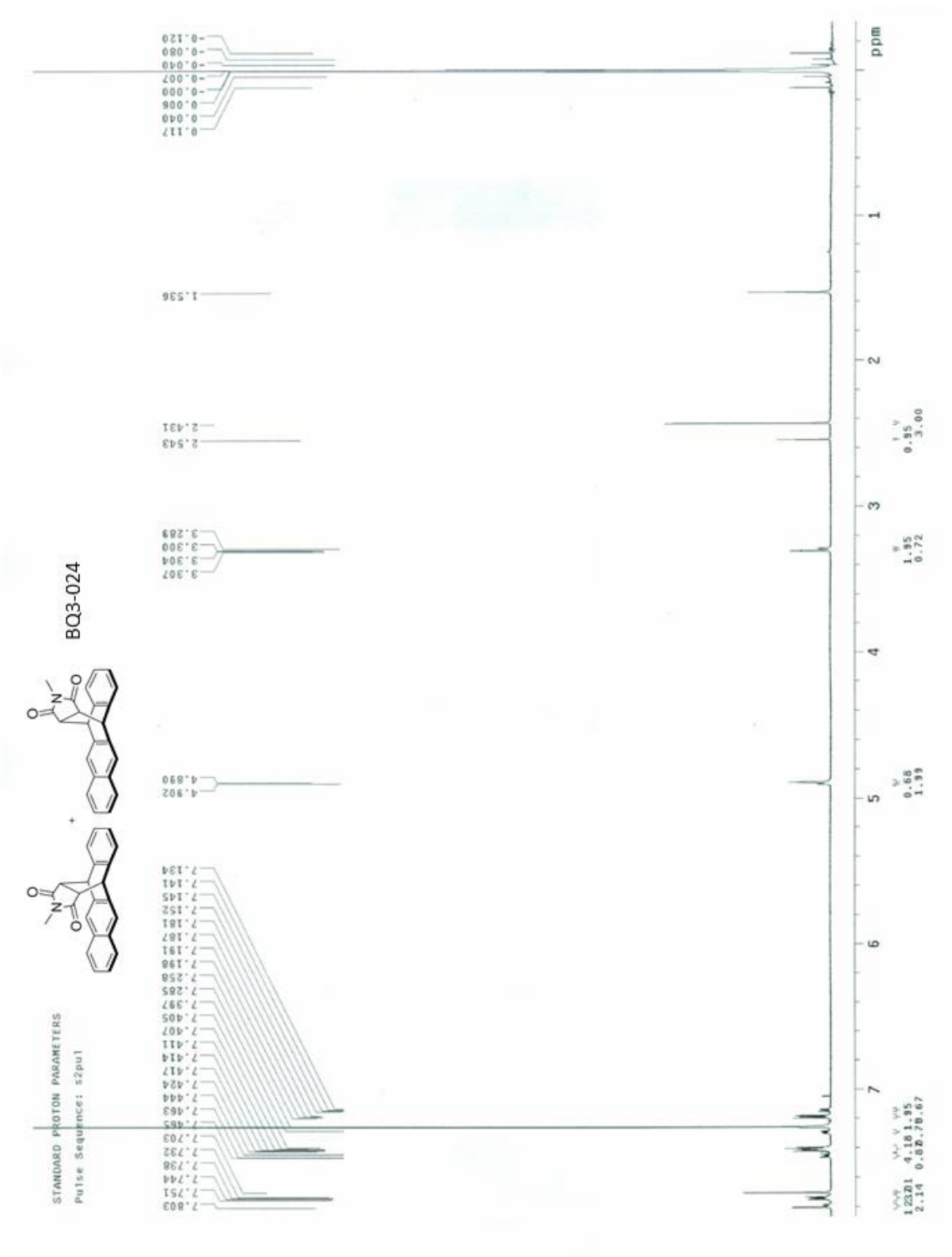
BQ3-024
STANDARD PROTON PARAMETERS
Pulse Sequence: s2pul
ppm

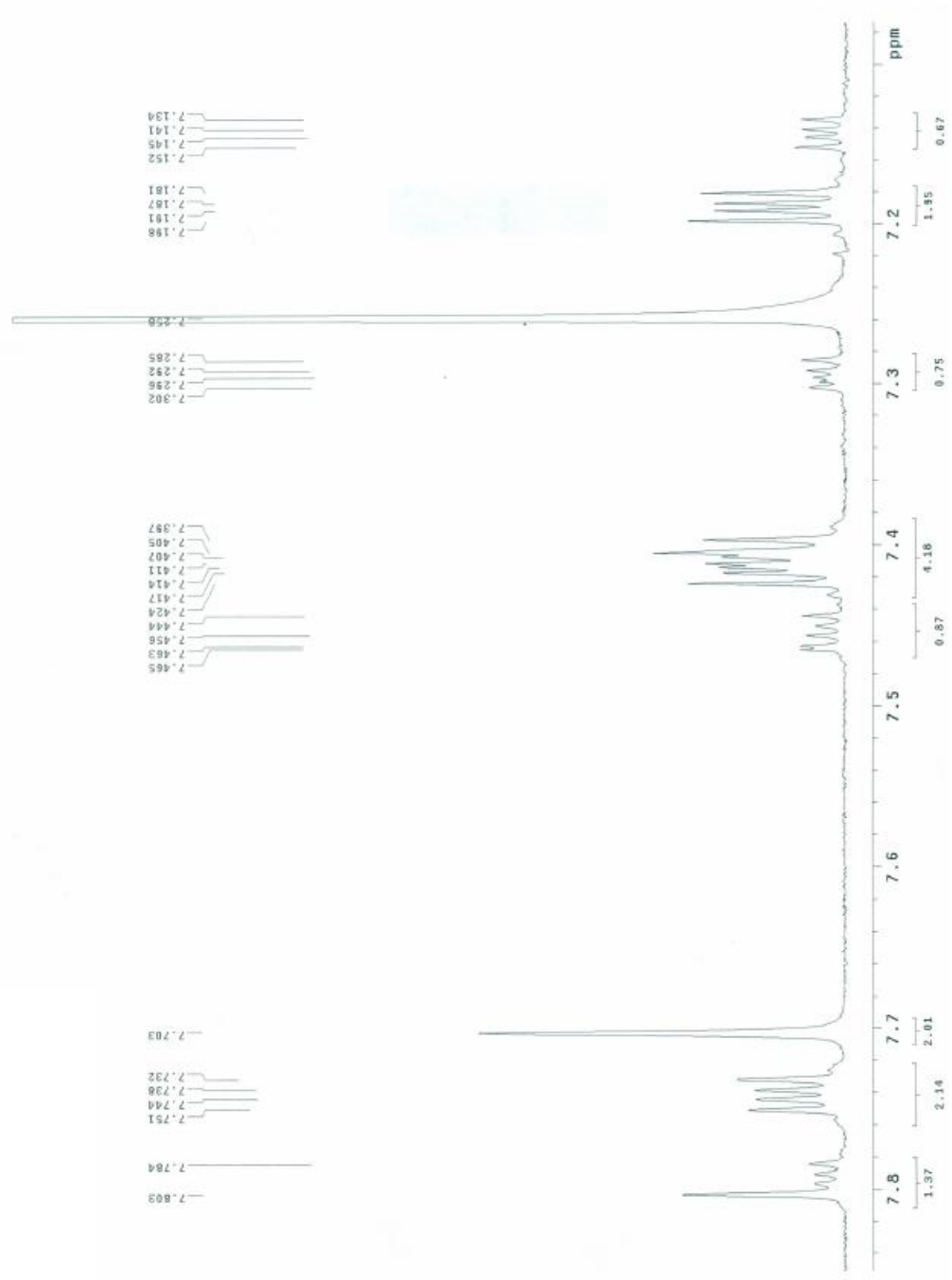
7.134
7.141
7.145
7.152
7.181
7.187
7.191
7.198
7.258
7.285
7.292
7.296
7.302
7.397
7.405
7.407
7.411
7.414
7.417
7.424
7.444
7.456
7.463
7.465
7.703
7.732
7.738
7.744
7.751
7.784
7.803
ppm
7.8
7.7
7.6
7.5
7.4
7.3
7.2
1.37
2.14
2.01
0.87
4.18
0.75
1.35
0.67

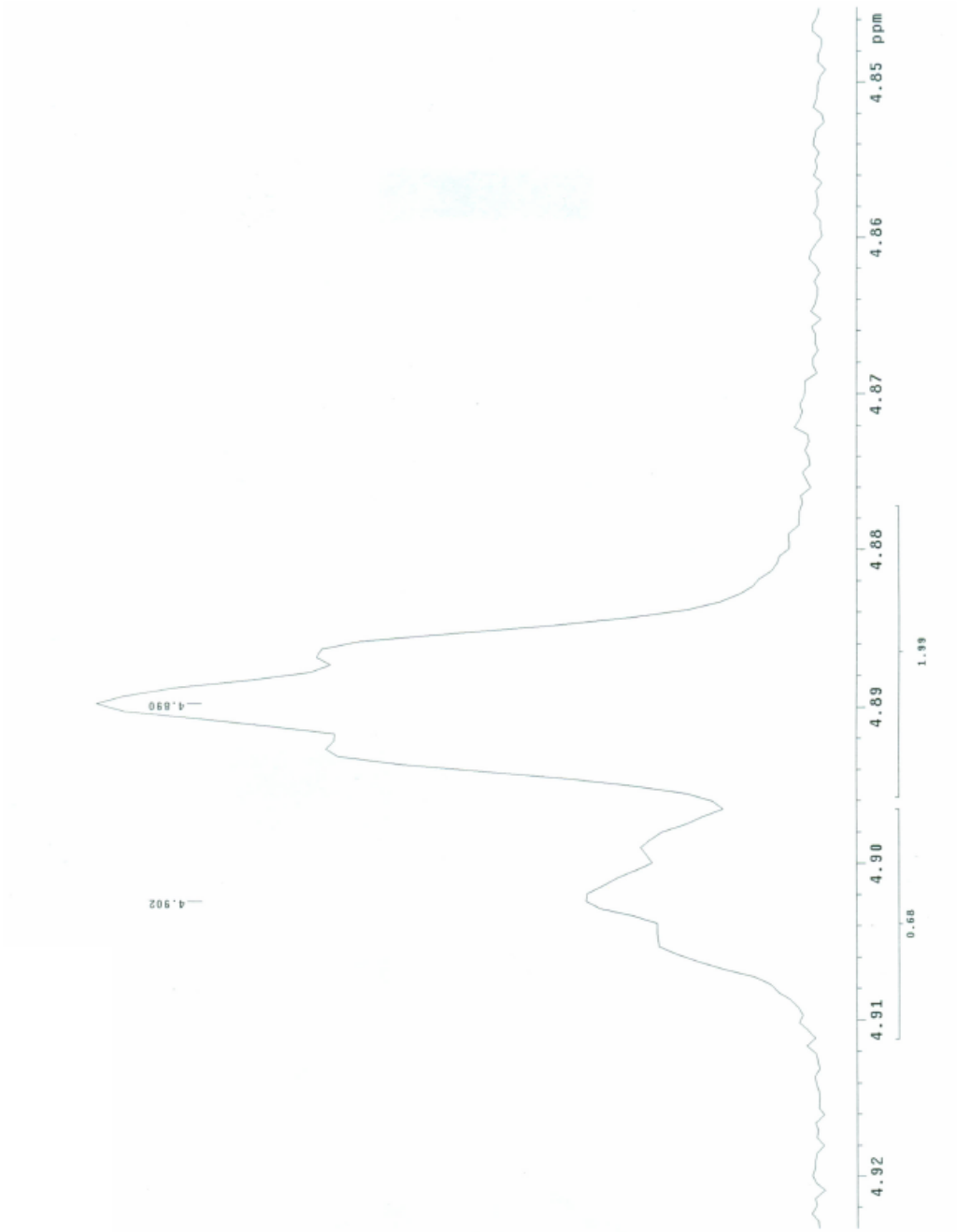
4.85 ppm
4.86
4.87
4.88
4.89
4.90
4.91
4.92
4.890
4.902
1.99
0.68

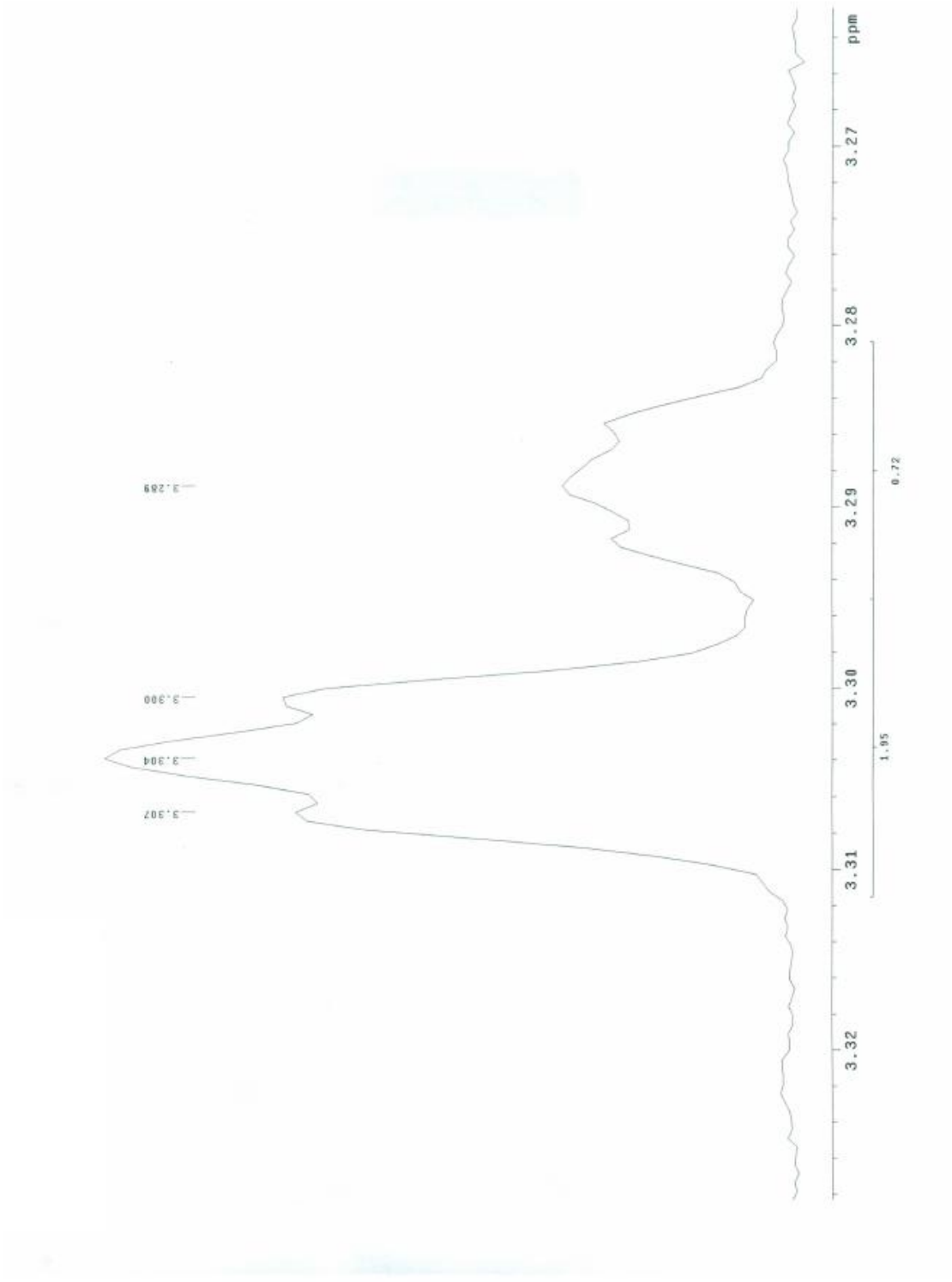
3.269
3.300
3.304
3.307
3.32
3.31
3.30
3.29
3.28
3.27
ppm
1.95
0.72

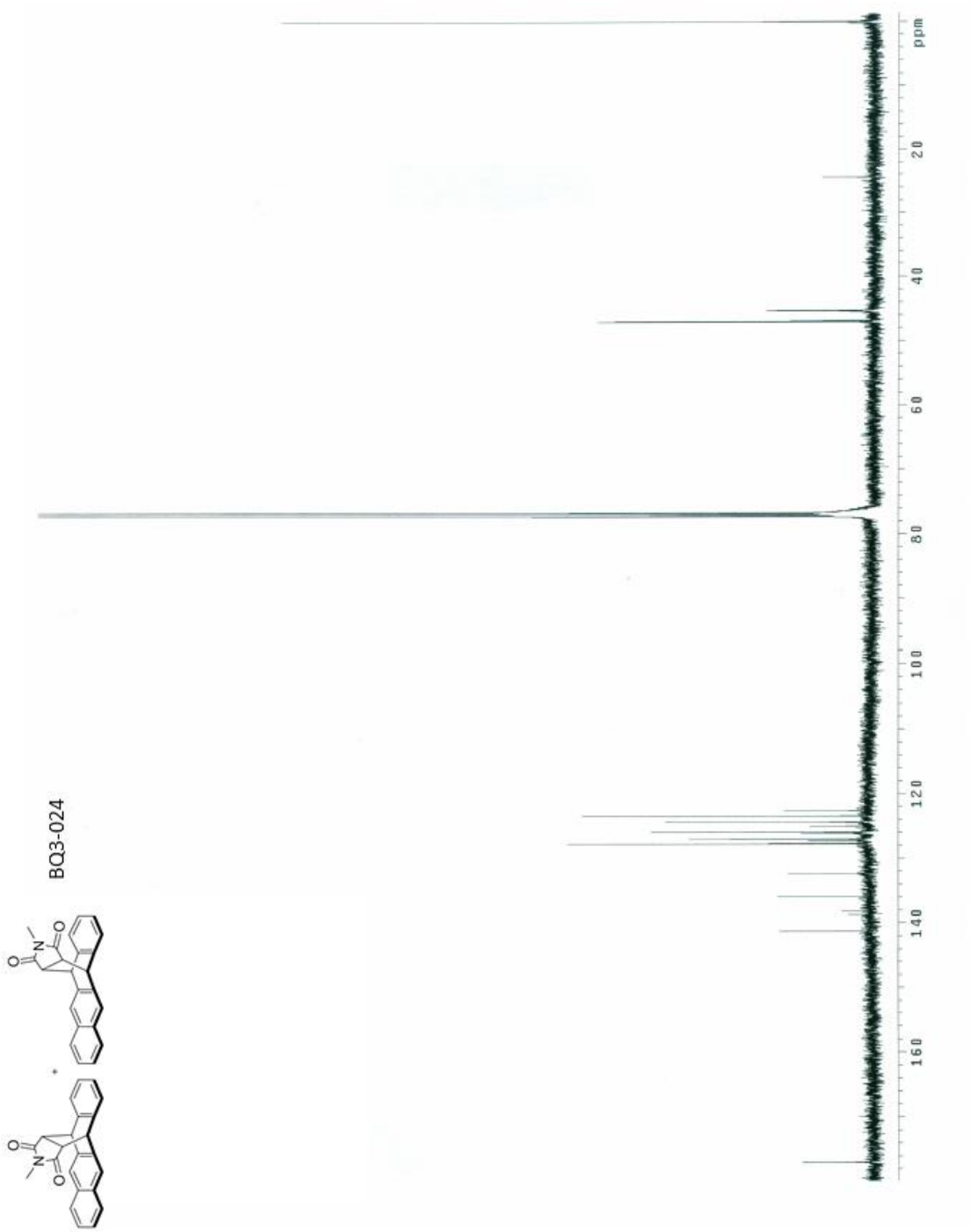
BQ3-024
ppm
20
40
60
80
100
120
140
160

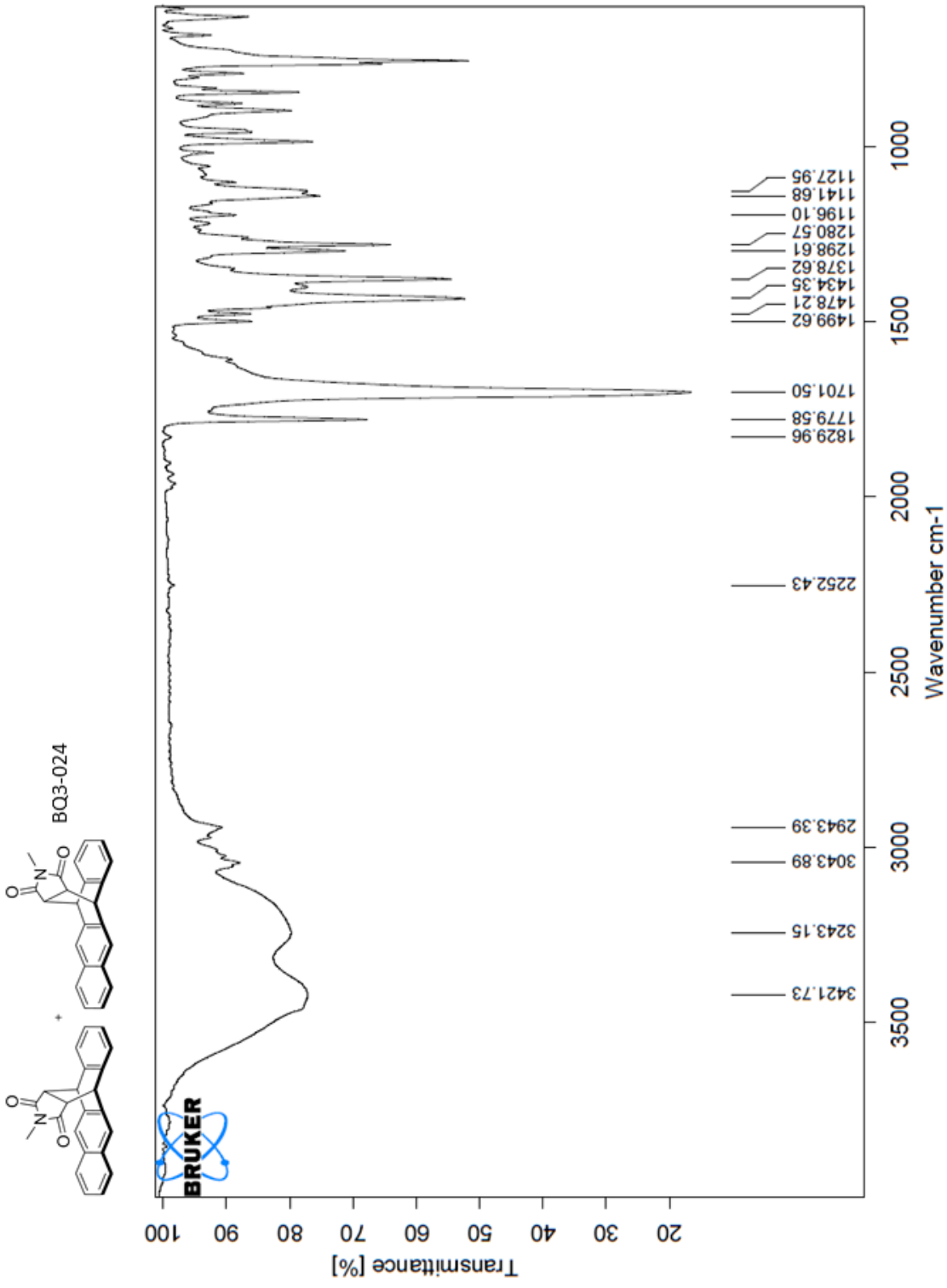
BQ3-024
BRUKER
Transmittance [%]
100
90
80
70
60
50
40
30
20
Wavenumber cm-1
3500
3000
2500
2000
1500
1000
3421.73
3243.15
3043.89
2943.39
2252.43
1829.96
1779.58
1701.50
1499.62
1478.21
1434.35
1378.62
1298.61
1280.57
1196.10
1141.68
1127.95

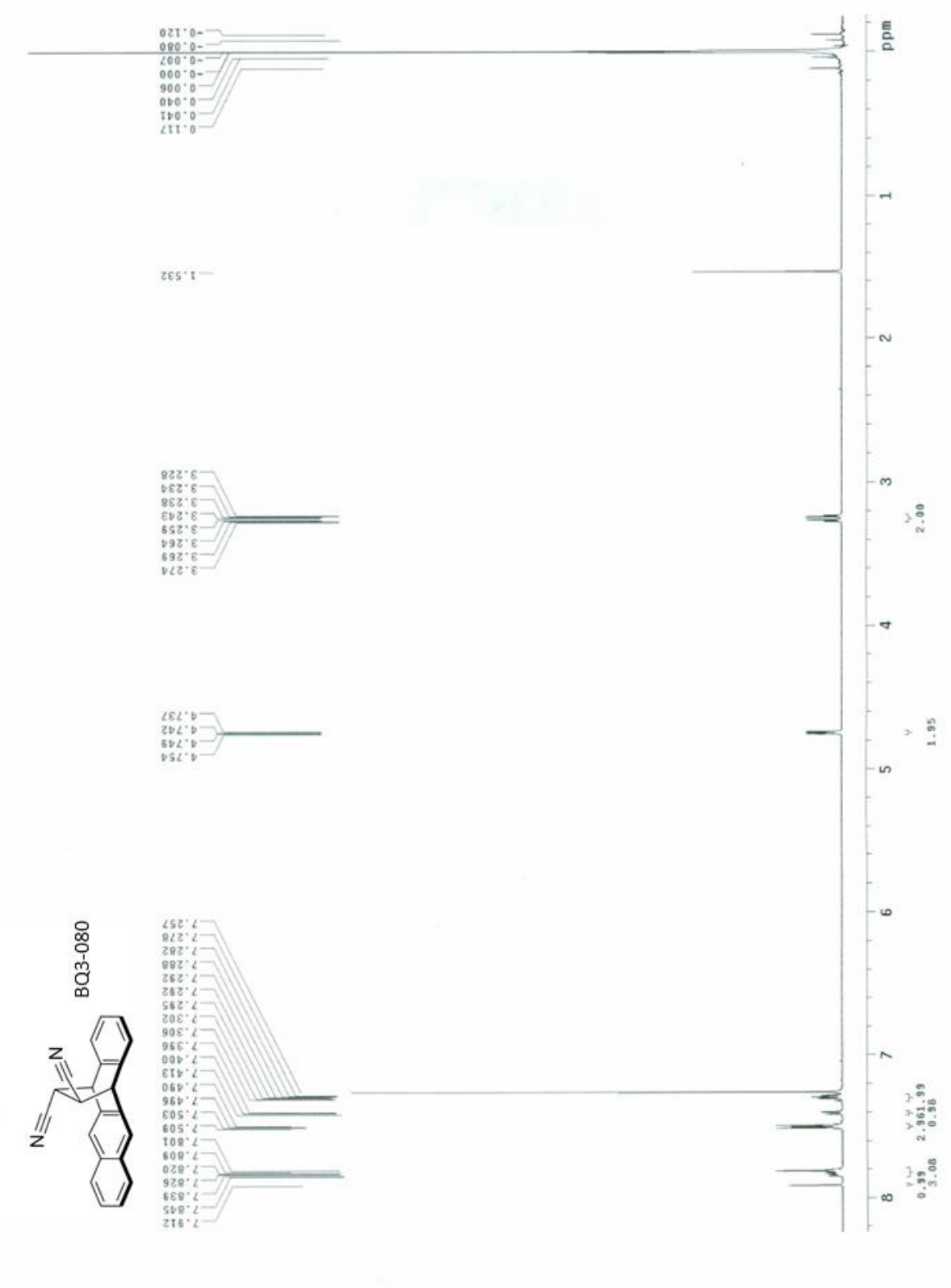
BQ3-080
N
N
ppm
1
2
3
4
5
6
7
8
2.00
1.95
2.961.99
0.98
0.99
3.08

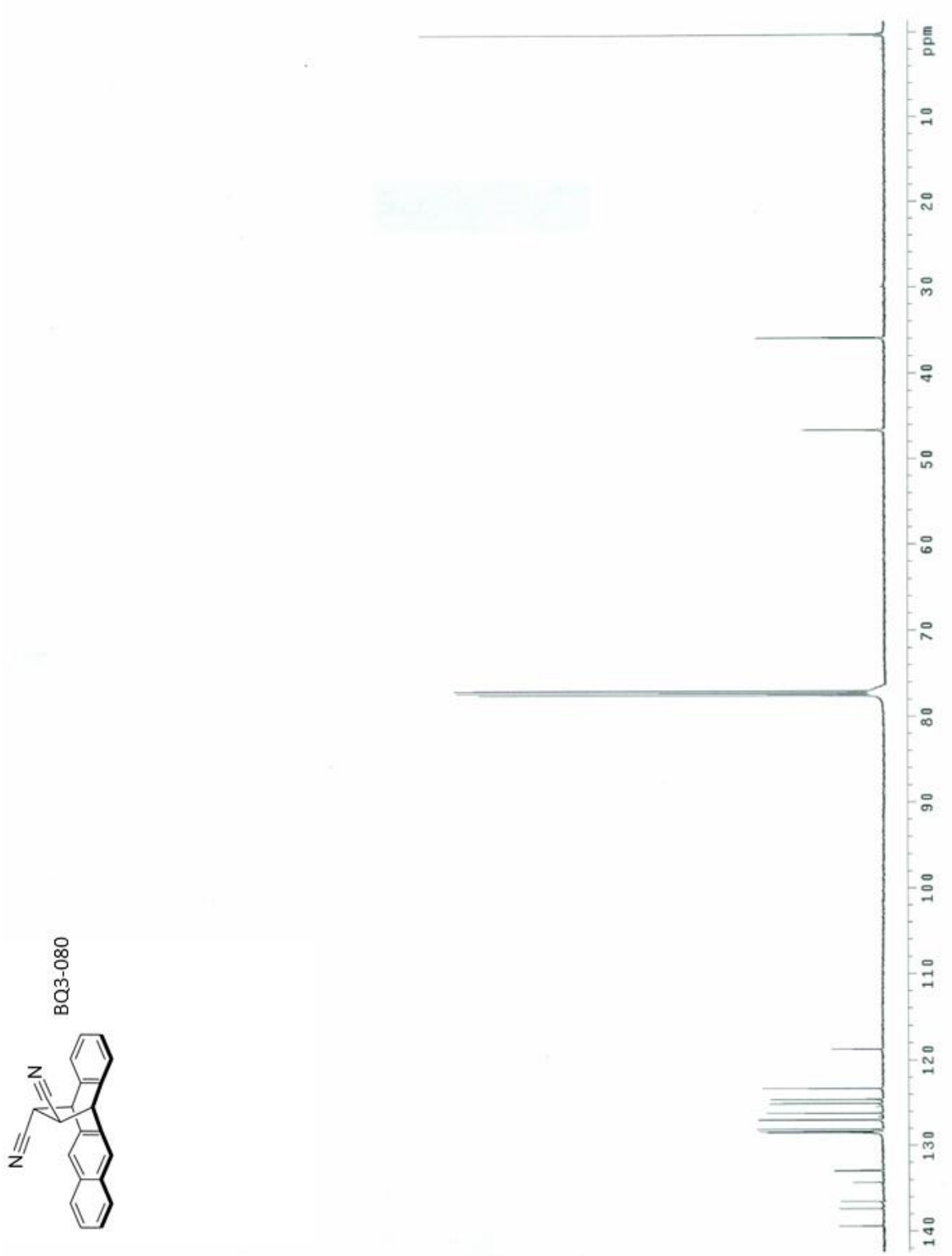
BQ3-080
N
N
ppm
10
20
30
40
50
60
70
80
90
100
110
120
130
140


BQ3-080
N
N
ppm
10
20
30
40
50
60
70
80
90
100
110
120
130
140

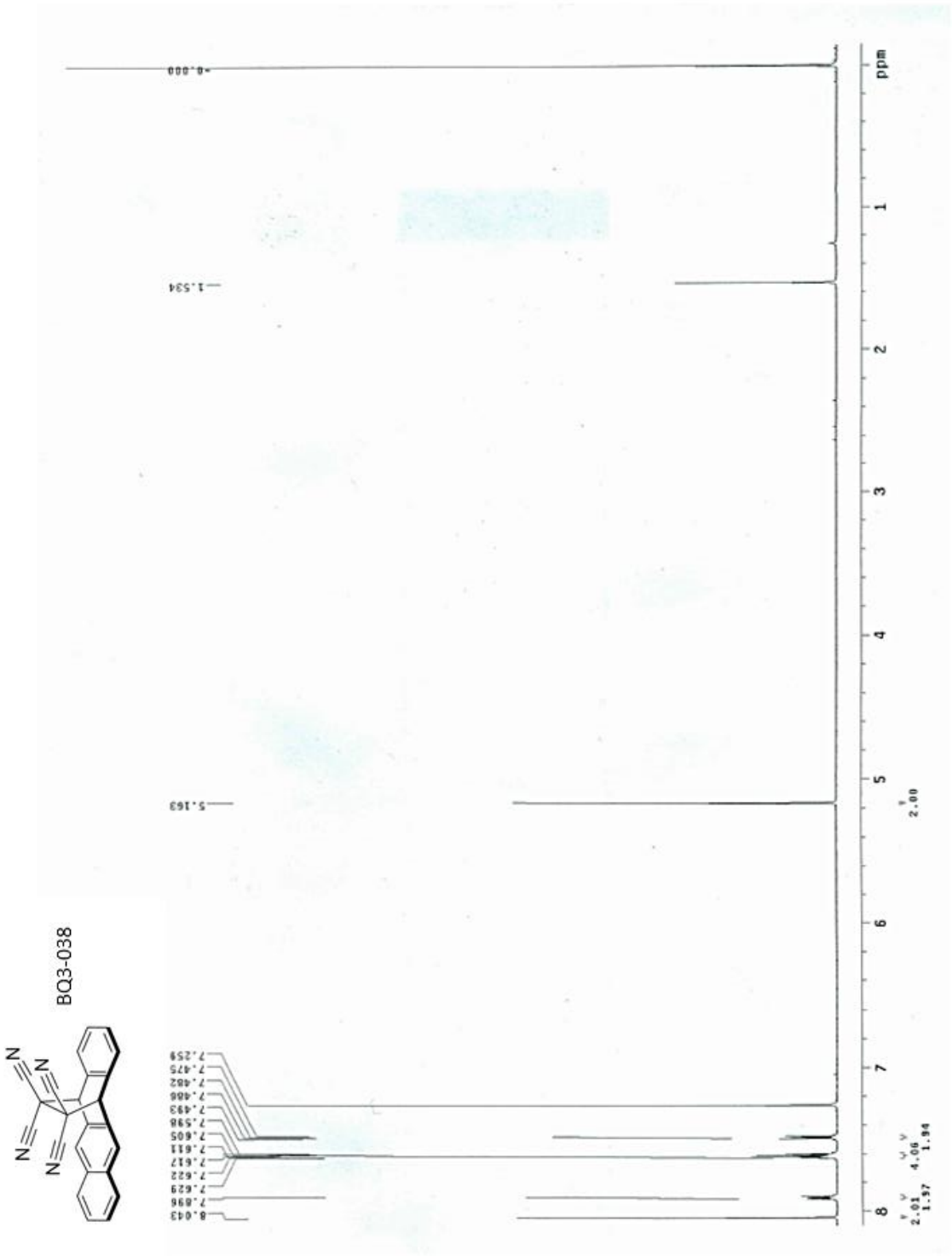
BQ3-038
N
N
N
N
0.000
1.534
5.163
7.259
7.475
7.482
7.486
7.493
7.598
7.605
7.611
7.617
7.622
7.629
7.696
8.043
ppm
1
2
3
4
5
6
7
8
2.00
2.01
1.97
4.06
1.94

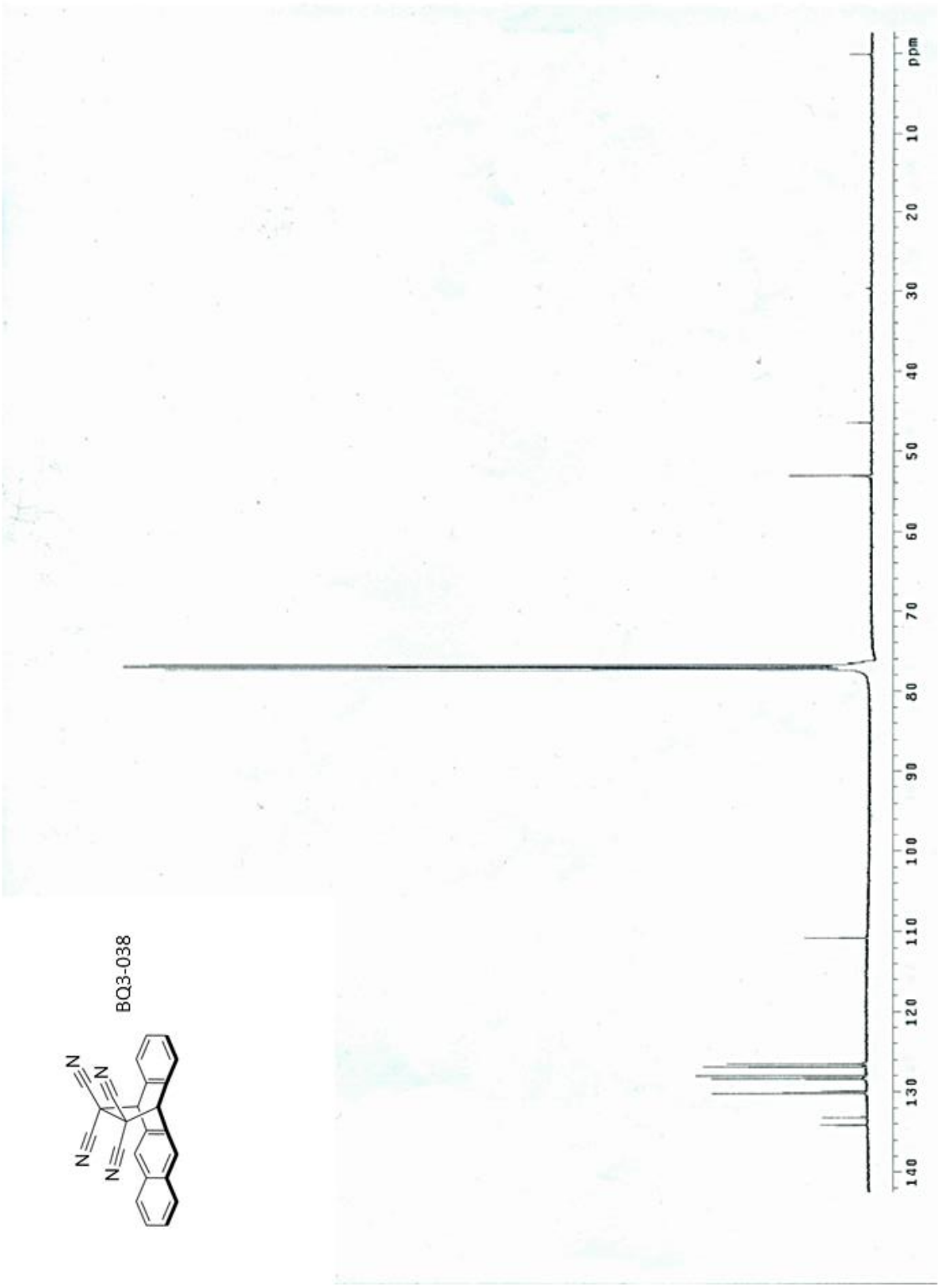
BQ3-038
N
N
N
N
ppm
10
20
30
40
50
60
70
80
90
100
110
120
130
140

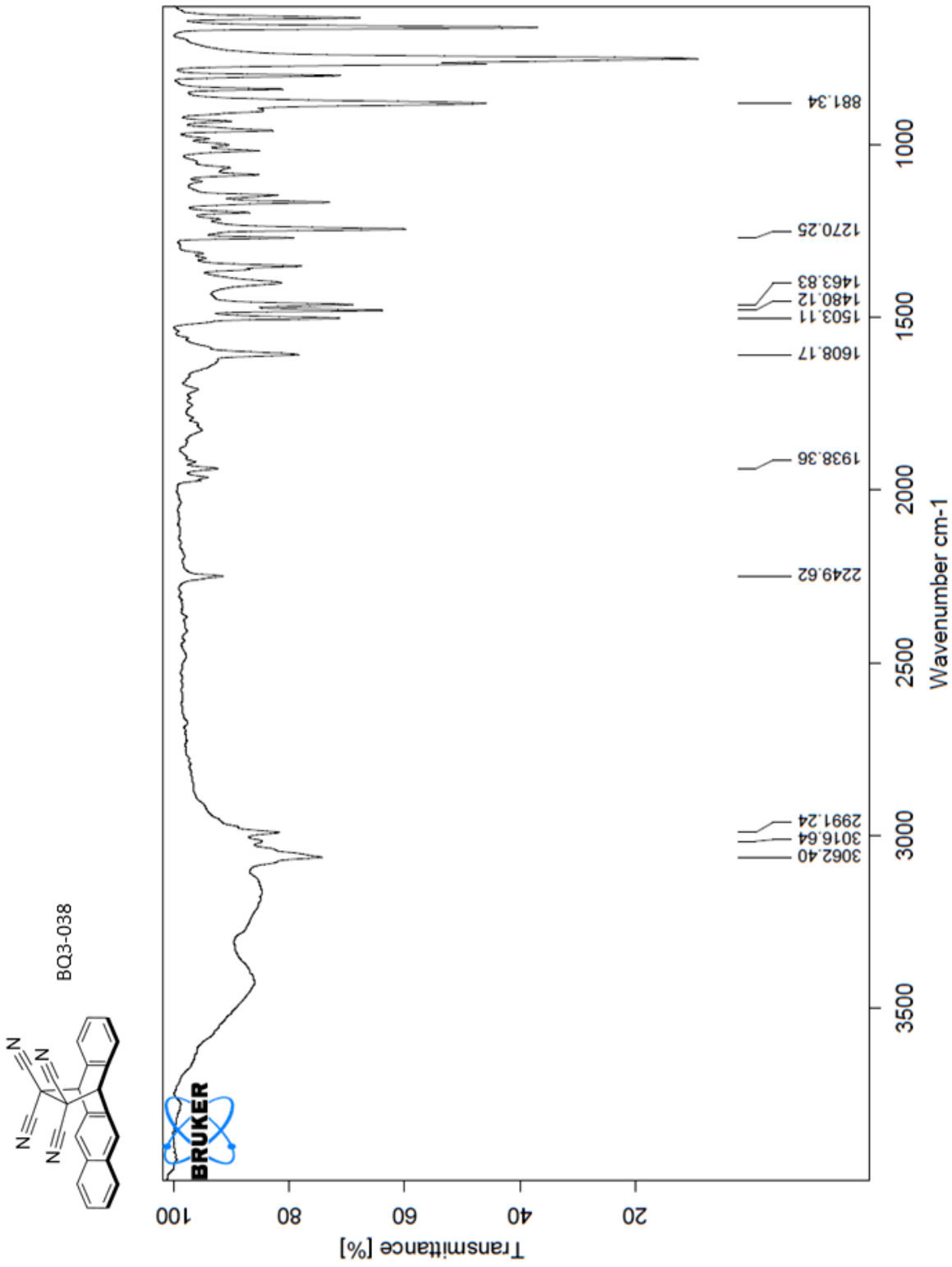
BQ3-038
N
N
N
N
BRUKER
Transmittance [%]
100
80
60
40
20
3500
3000
2500
2000
1500
1000
Wavenumber cm-1
3062.40
3016.64
2991.24
2249.62
1938.36
1608.17
1503.11
1480.12
1463.83
1270.25
881.34

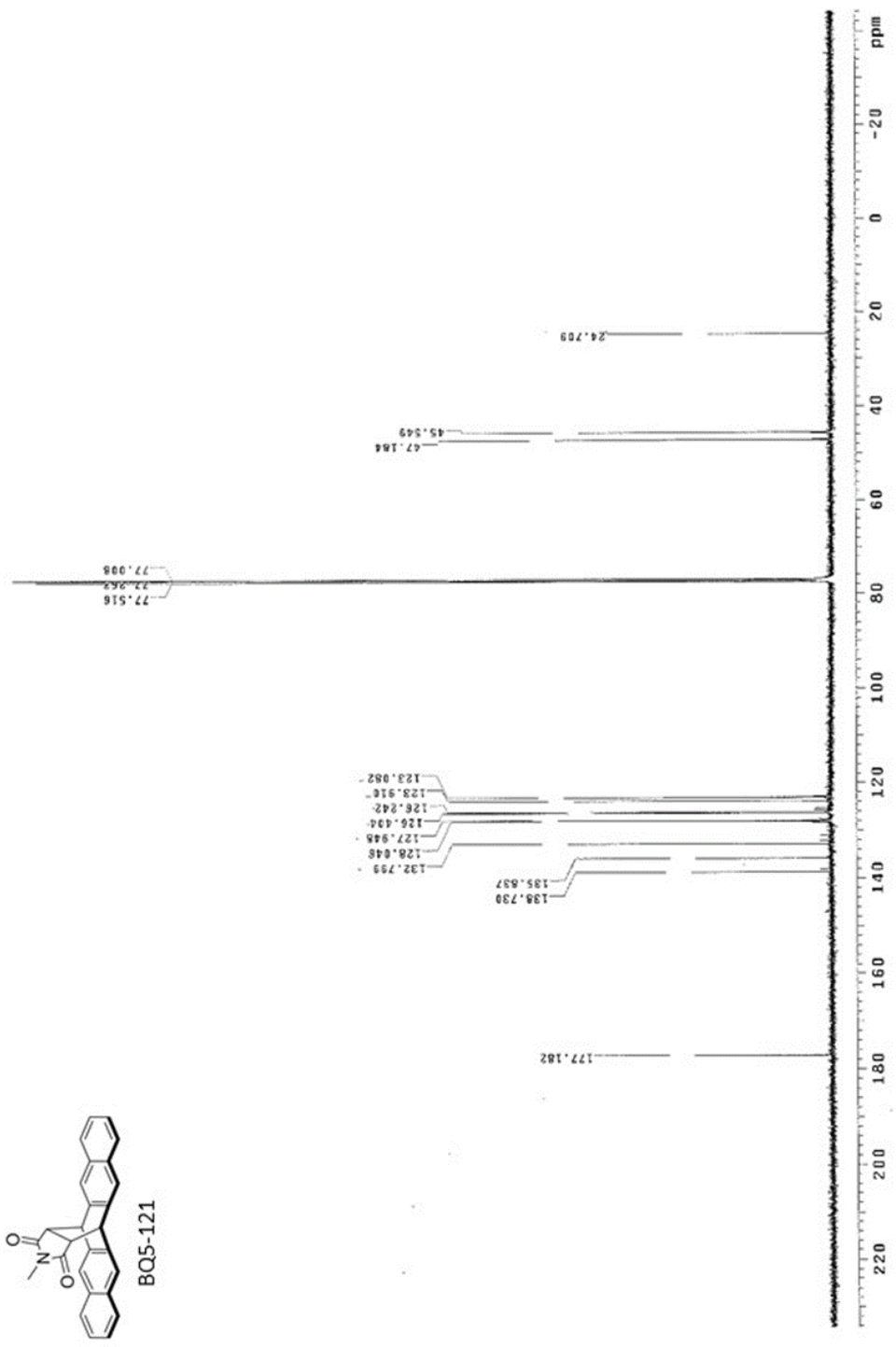
ppm
220
200
180
160
140
120
100
80
60
40
20
0
-20
177.182
138.730
135.837
132.799
128.648
127.945
126.634
126.242
123.916
123.082
77.516
77.088
47.184
45.549
24.709
BQ5-121

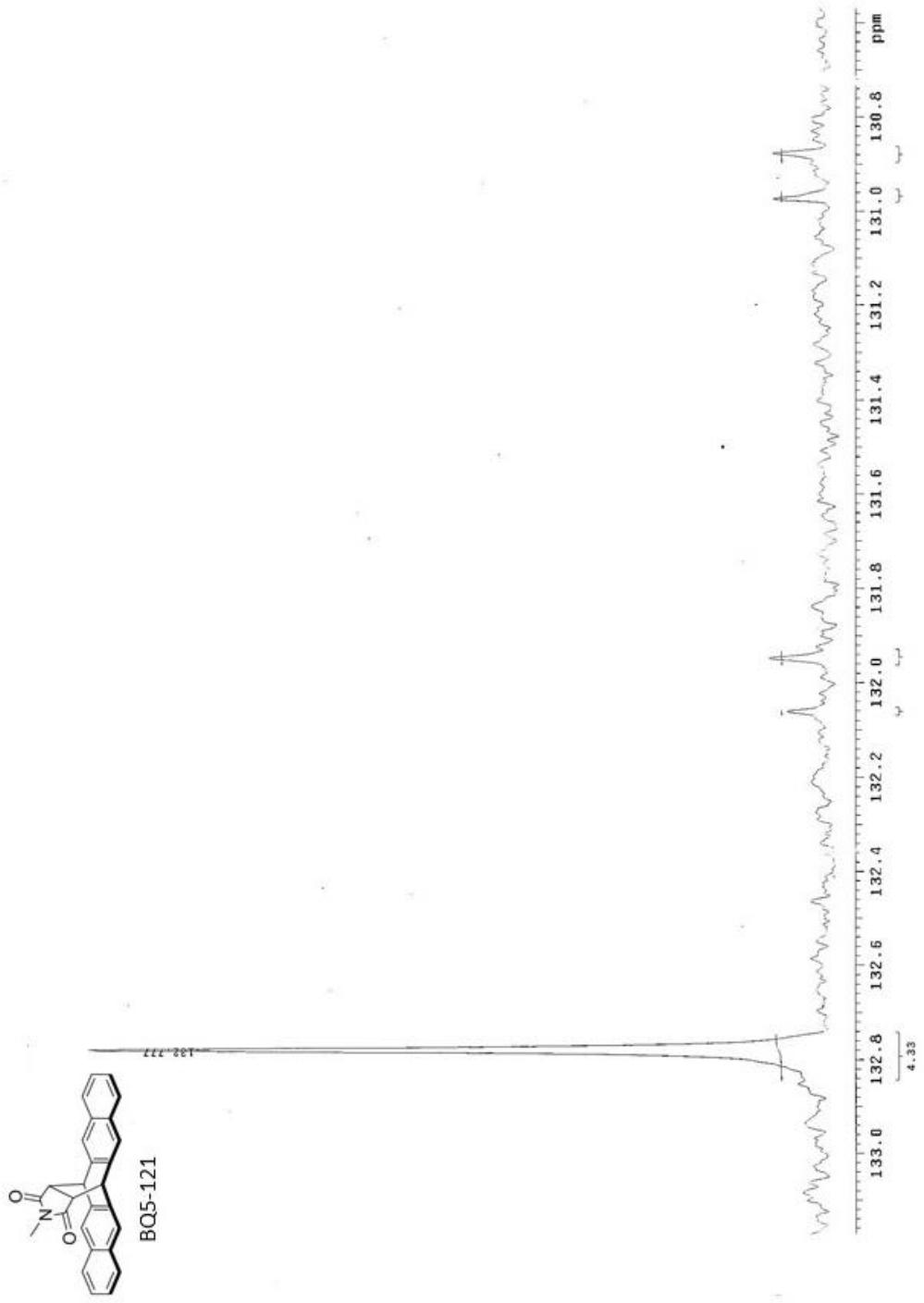
BQ5-121
133.0
132.8
132.6
132.4
132.2
132.0
131.8
131.6
131.4
131.2
131.0
130.8
ppm
4.33

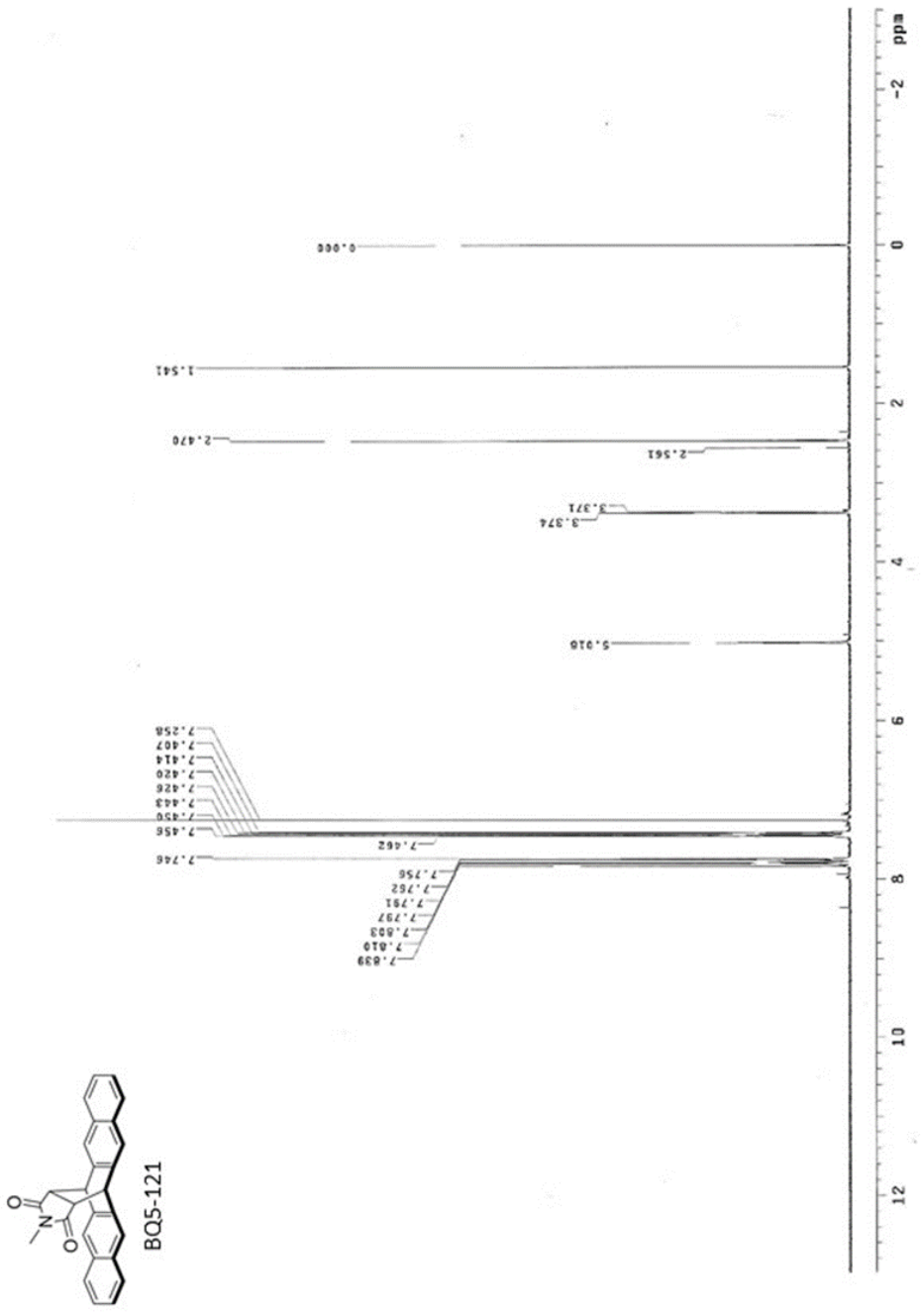
BQ5-121
0.000
1.541
2.470
2.561
3.371
3.374
5.918
7.258
7.407
7.414
7.420
7.426
7.443
7.450
7.456
7.462
7.746
7.756
7.762
7.791
7.797
7.833
7.839
7.840
ppm

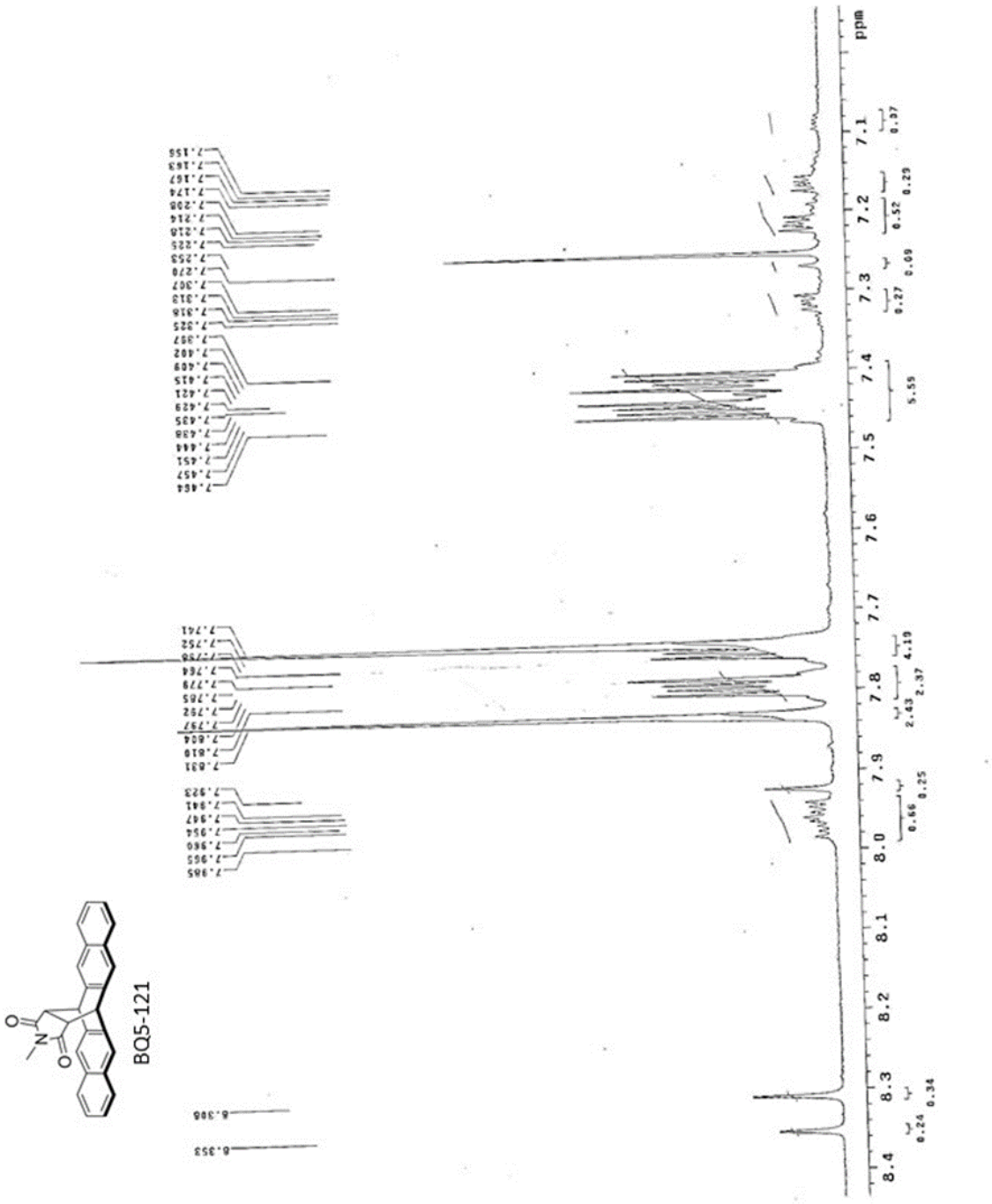
BQ5-121
ppm

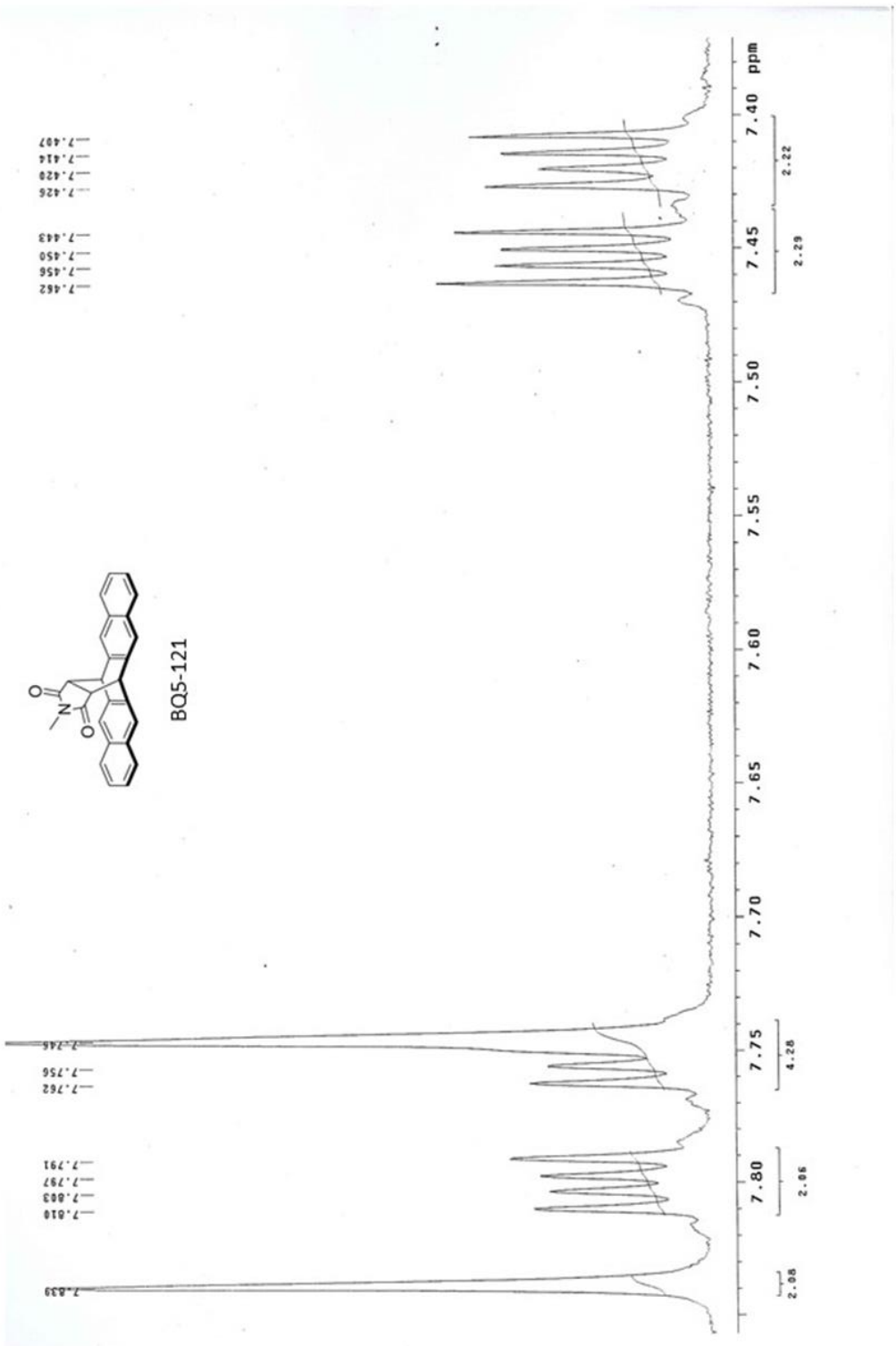
BQ5-121
7.839
7.818
7.803
7.797
7.791
7.762
7.756
7.746
7.462
7.456
7.450
7.443
7.426
7.420
7.414
7.407
7.80
7.75
7.70
7.65
7.60
7.55
7.50
7.45
7.40
ppm
2.08
2.06
4.28
2.29
2.22

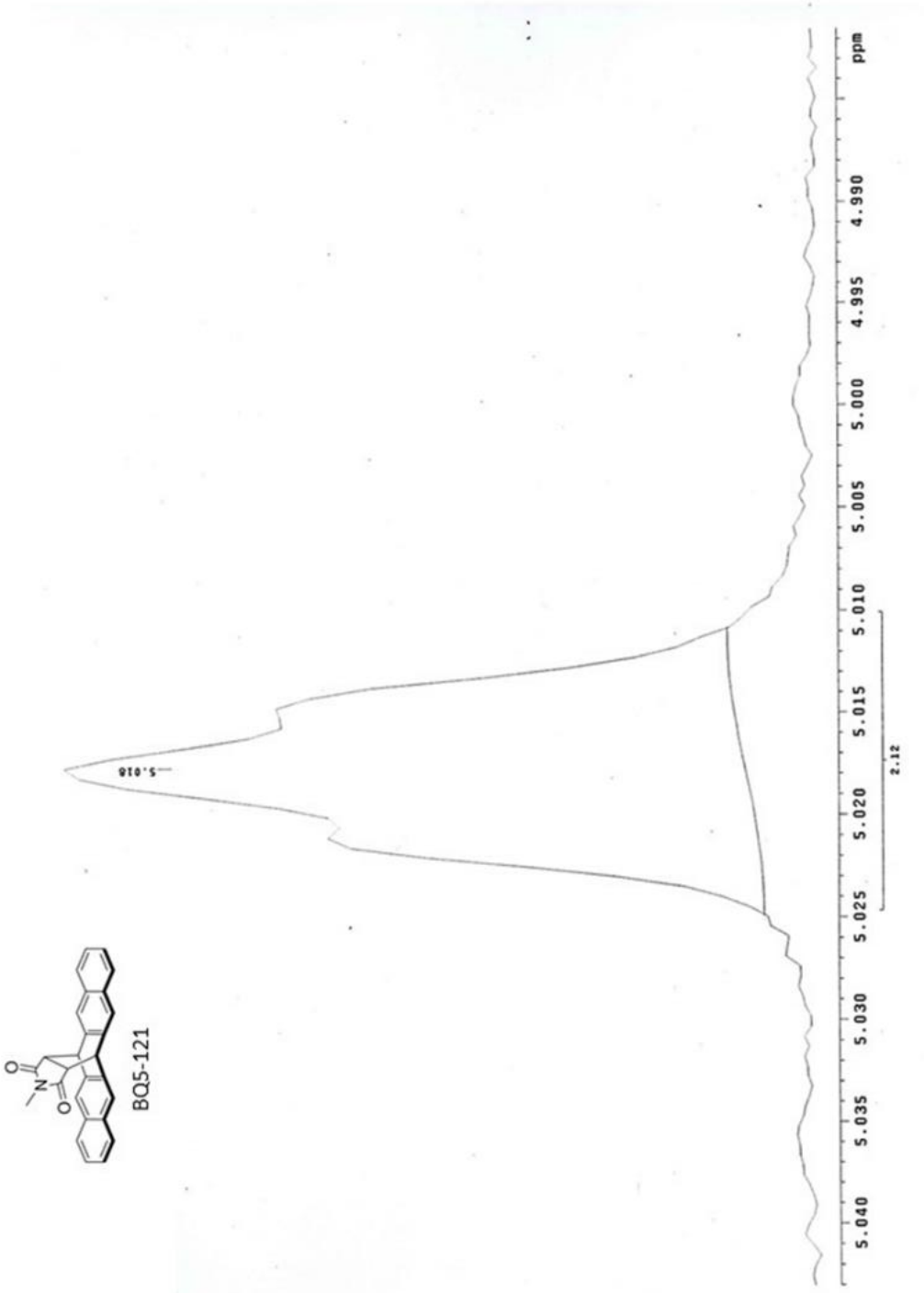
BQ5-121
5.018
2.12
5.040
5.035
5.030
5.025
5.020
5.015
5.010
5.005
5.000
4.995
4.990
ppm

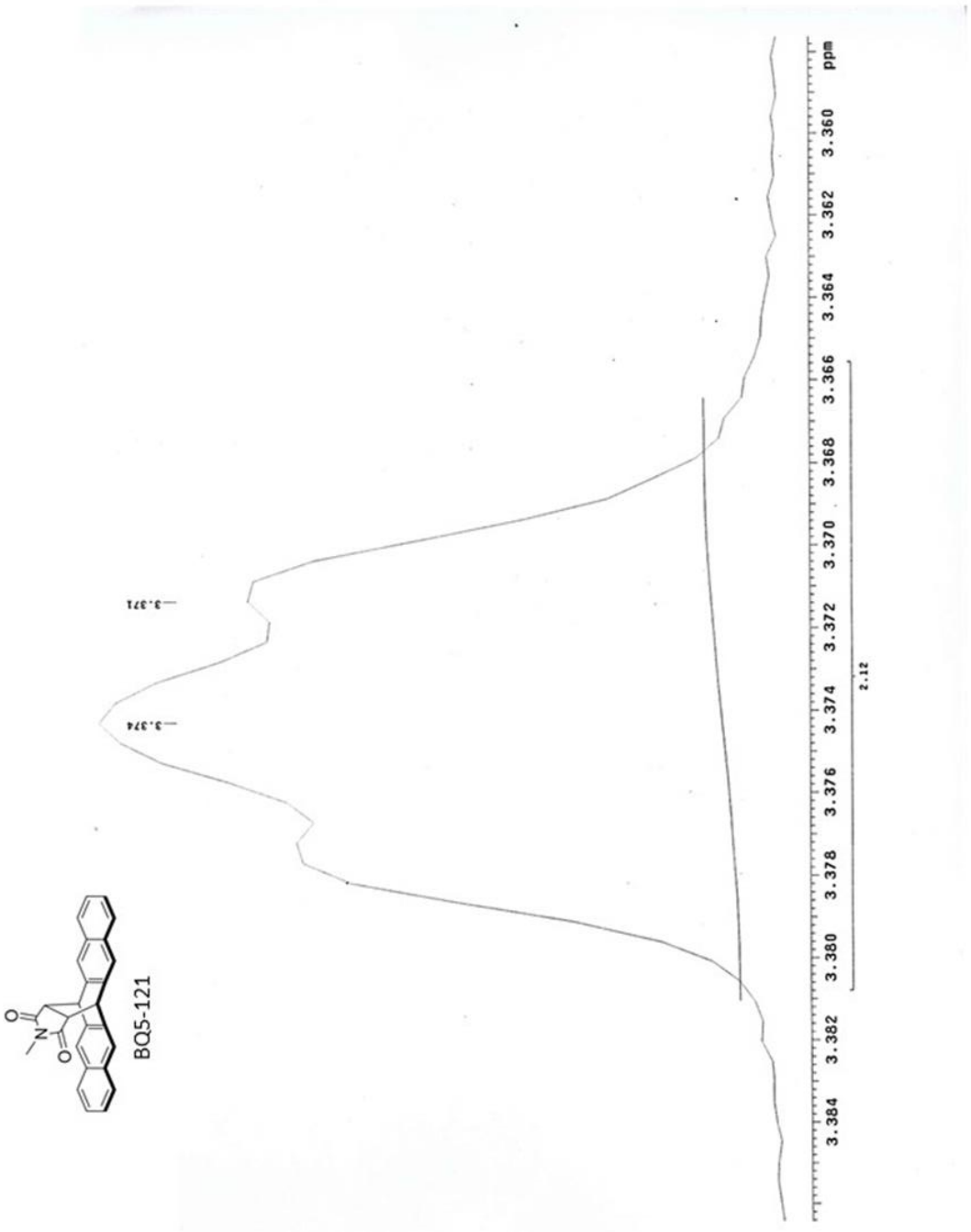
BQ5-121
3.374
3.371
3.384
3.382
3.380
3.378
3.376
3.374
3.372
3.370
3.368
3.366
3.364
3.362
3.360
ppm
2.12

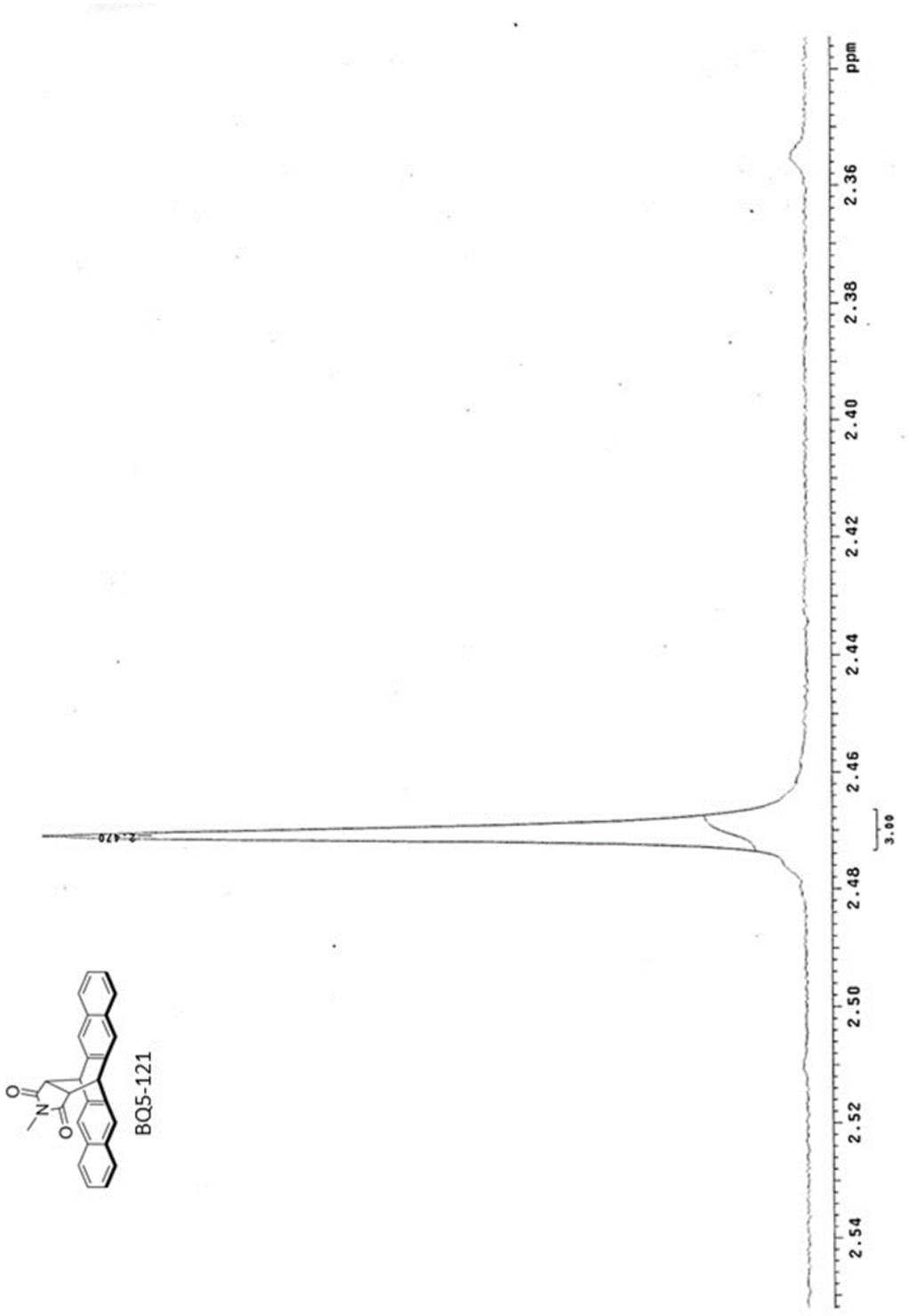
BQ5-121
2.54
2.52
2.50
2.48
2.46
2.44
2.42
2.40
2.38
2.36
ppm
3.00

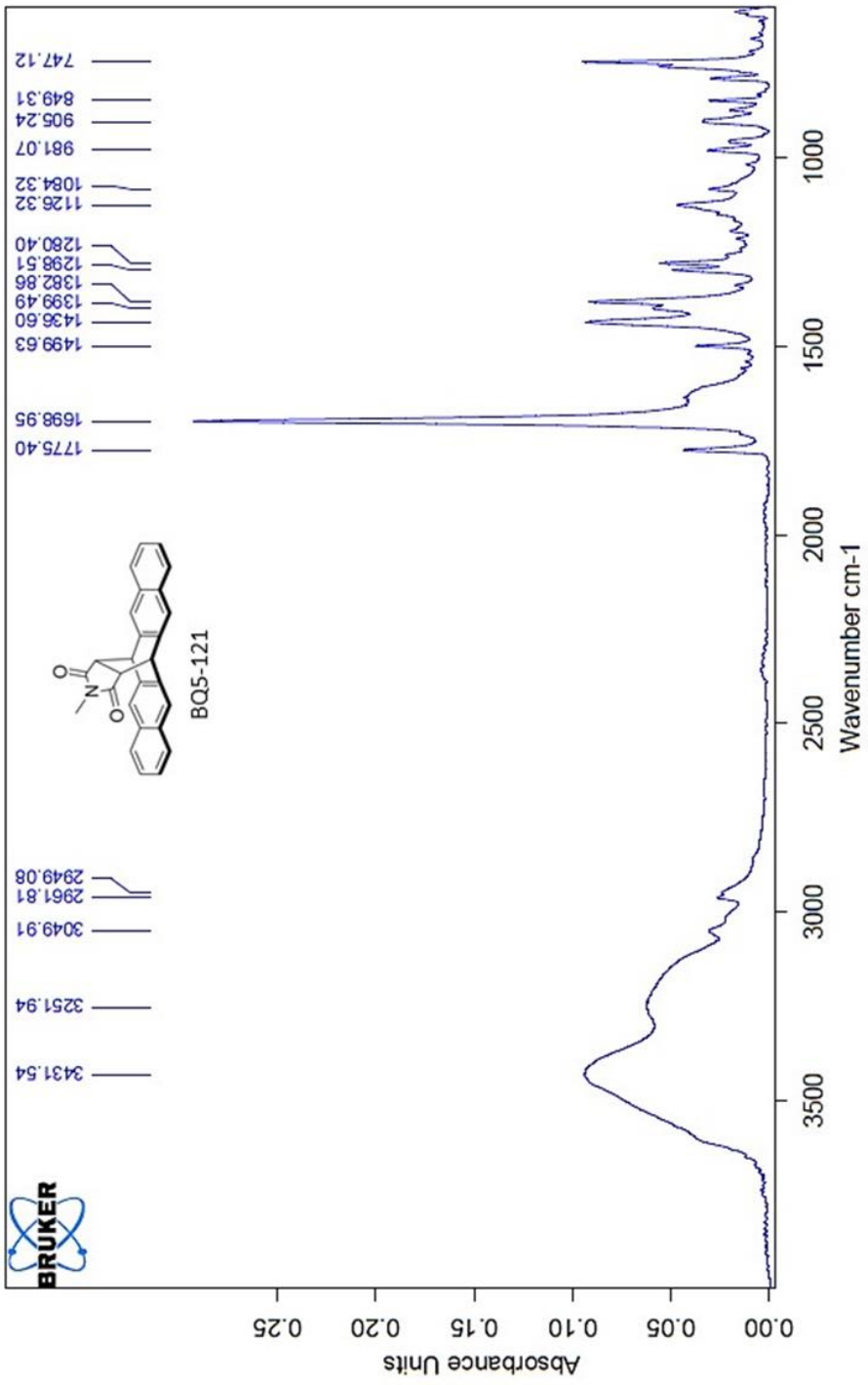
BRUKER
3431.54
3251.94
3049.91
2961.81
2949.08
1775.40
1698.95
1499.63
1436.60
1399.49
1382.86
1298.51
1280.40
1126.32
1084.32
981.07
905.24
849.31
747.12
BQ5-121
Absorbance Units
0.00
0.05
0.10
0.15
0.20
0.25
3500
3000
2500
2000
1500
1000
Wavenumber cm-1

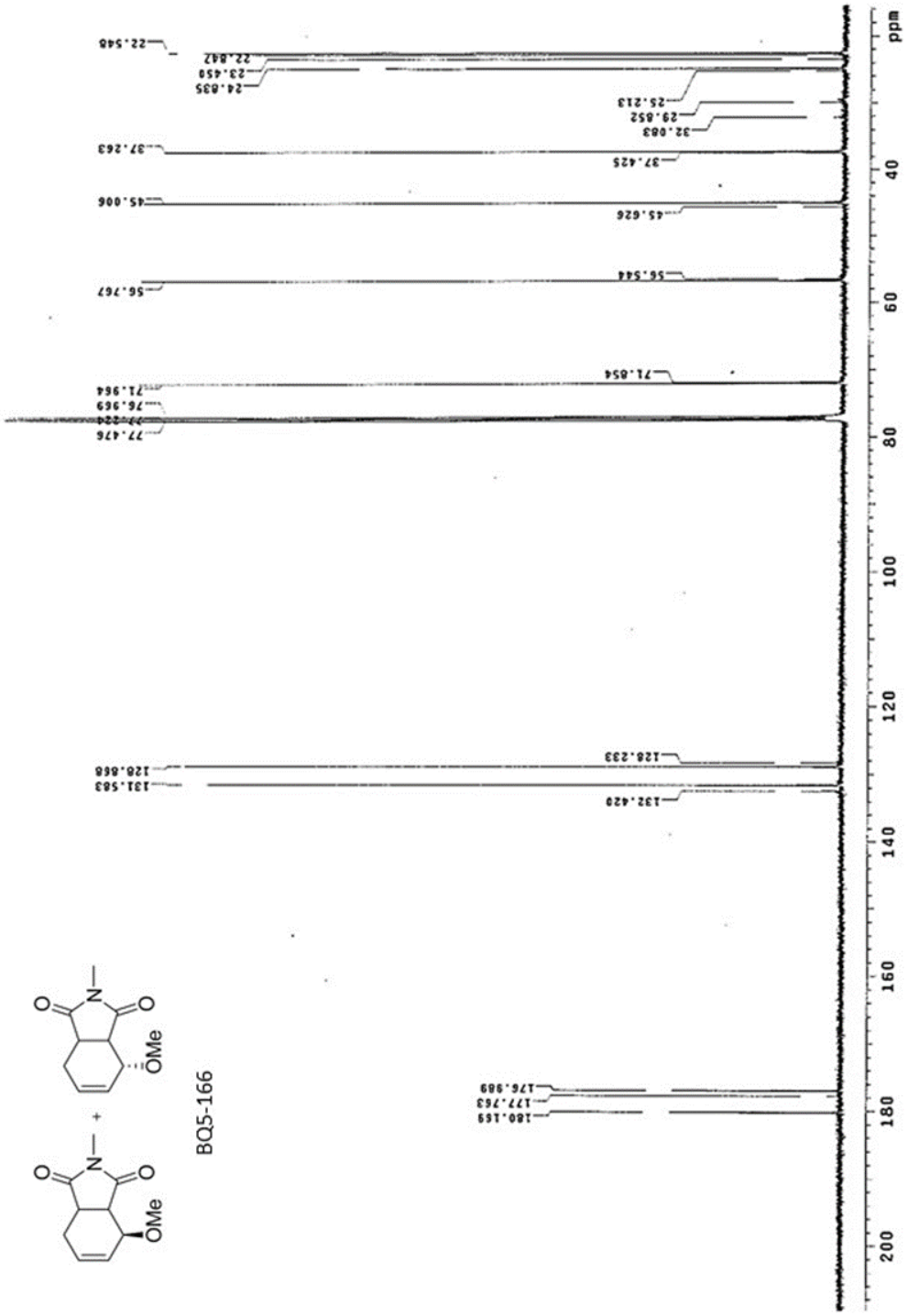
ppm
40
60
80
100
120
140
160
180
200
22.546
22.842
23.458
24.835
25.213
29.852
32.083
37.425
37.263
45.626
45.006
56.544
56.767
71.854
71.964
76.969
77.224
77.476
126.233
126.868
131.583
132.420
176.989
177.763
180.169
OMe
OMe
BQ5-166

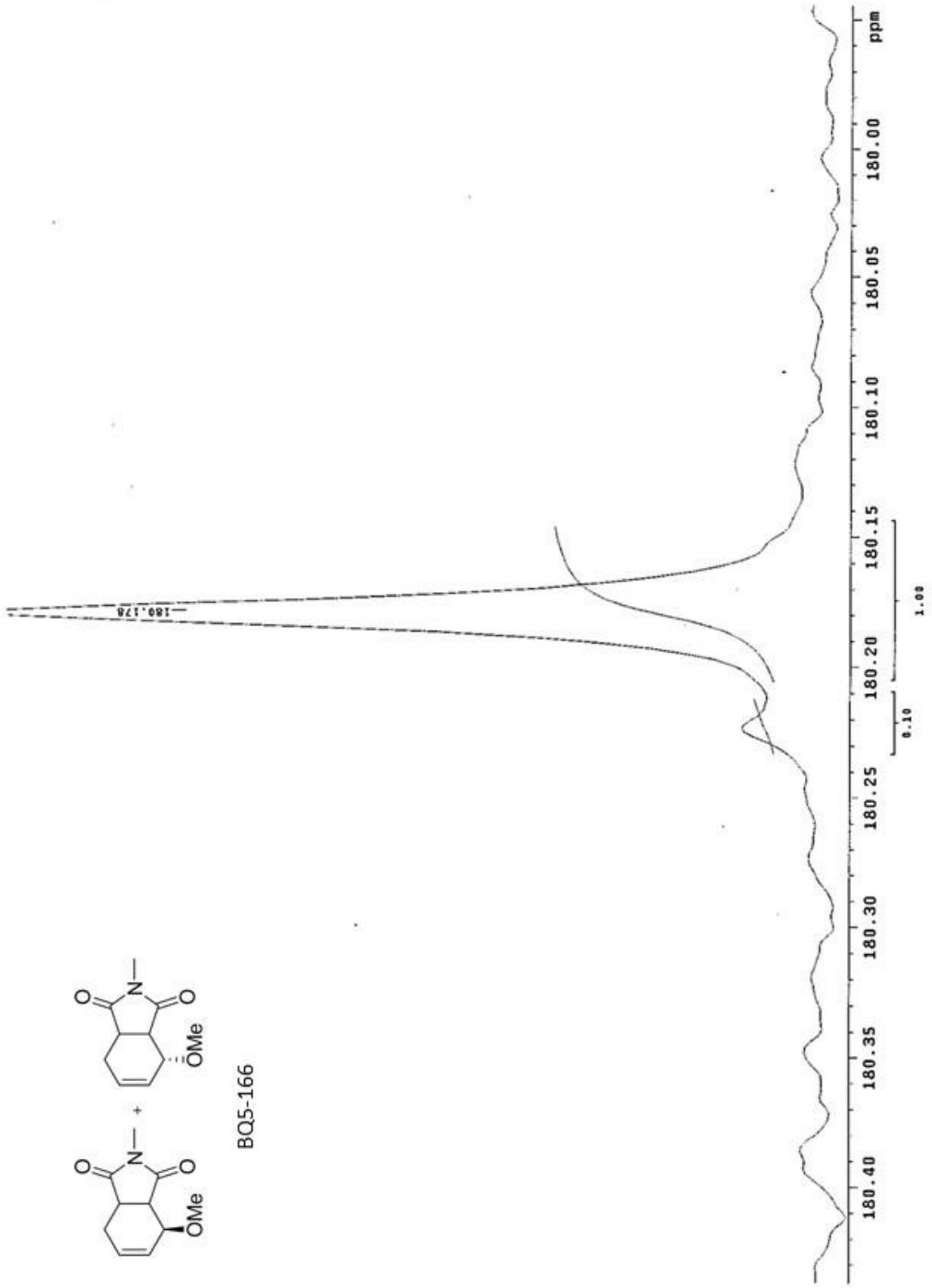
180.40
180.35
180.30
180.25
180.20
180.15
180.10
180.05
180.00
ppm
180.178
0.10
1.00
OMe
OMe
BQ5-166

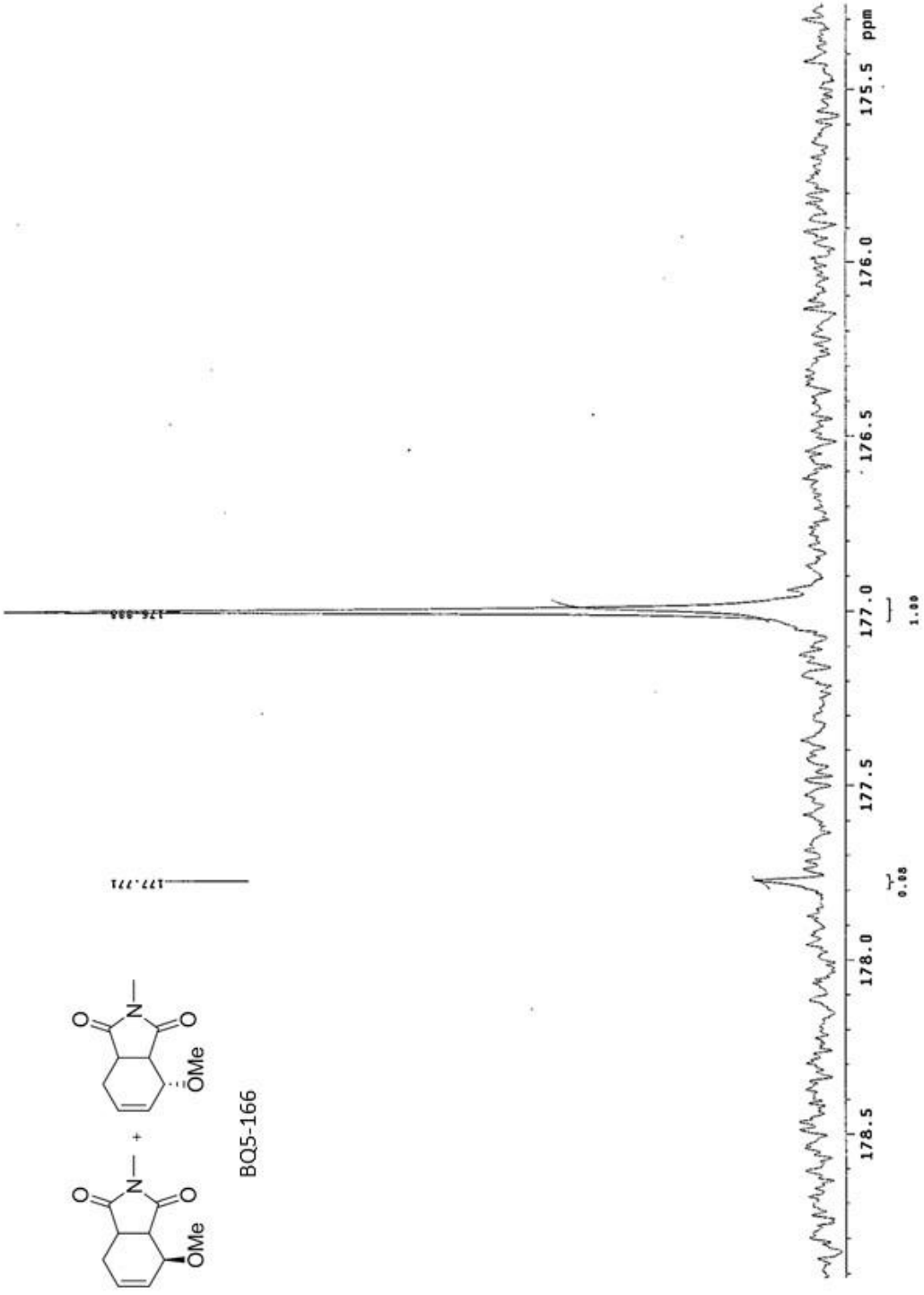
BQ5-166
177.771
176.884
175.5
176.0
176.5
177.0
177.5
178.0
178.5
ppm
1.00
0.88

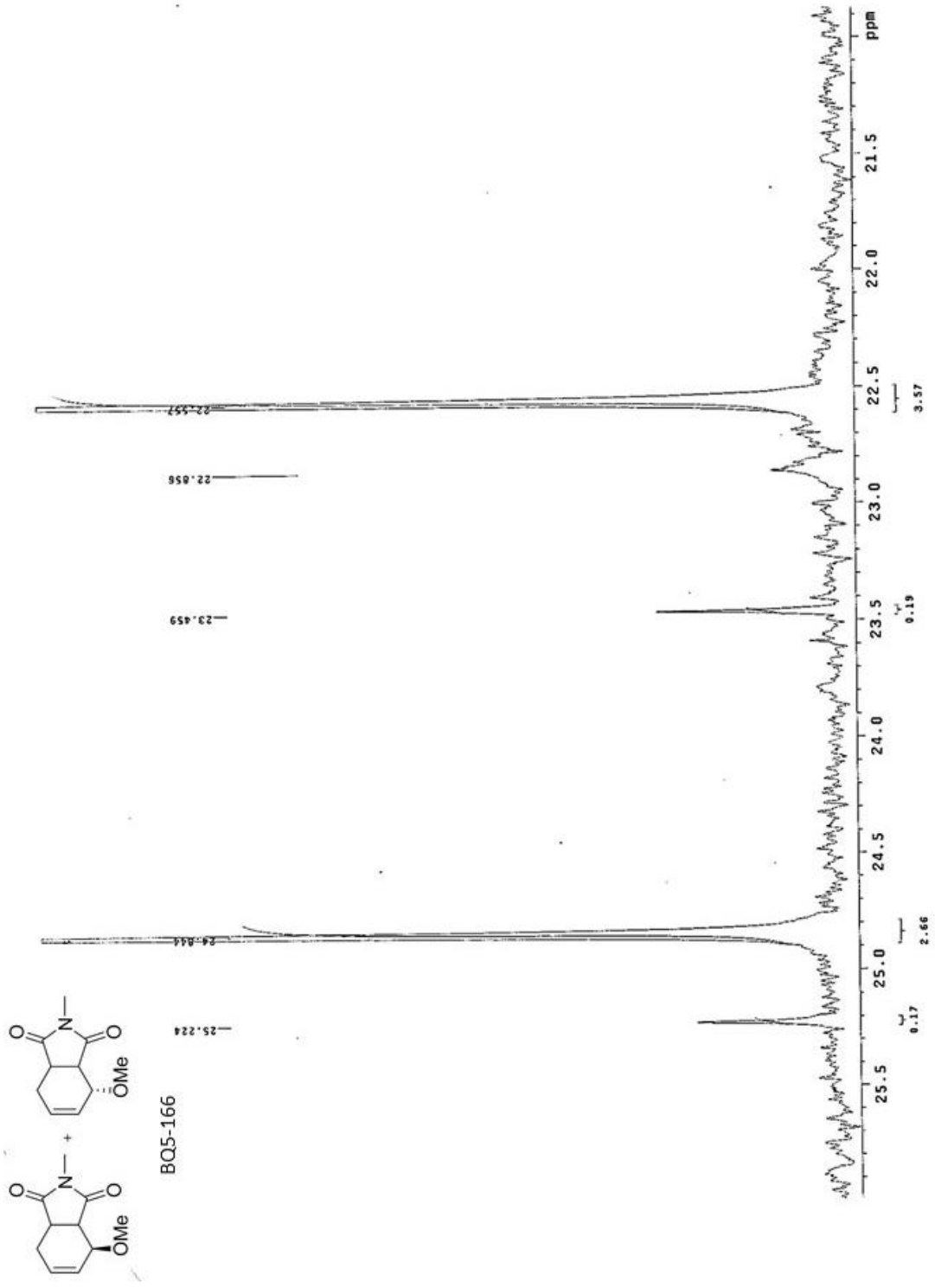
BQ5-166
OMe
OMe
25.224
24.844
23.459
22.856
22.557
ppm
25.5
25.0
24.5
24.0
23.5
23.0
22.5
22.0
21.5
0.17
2.66
0.19
3.57

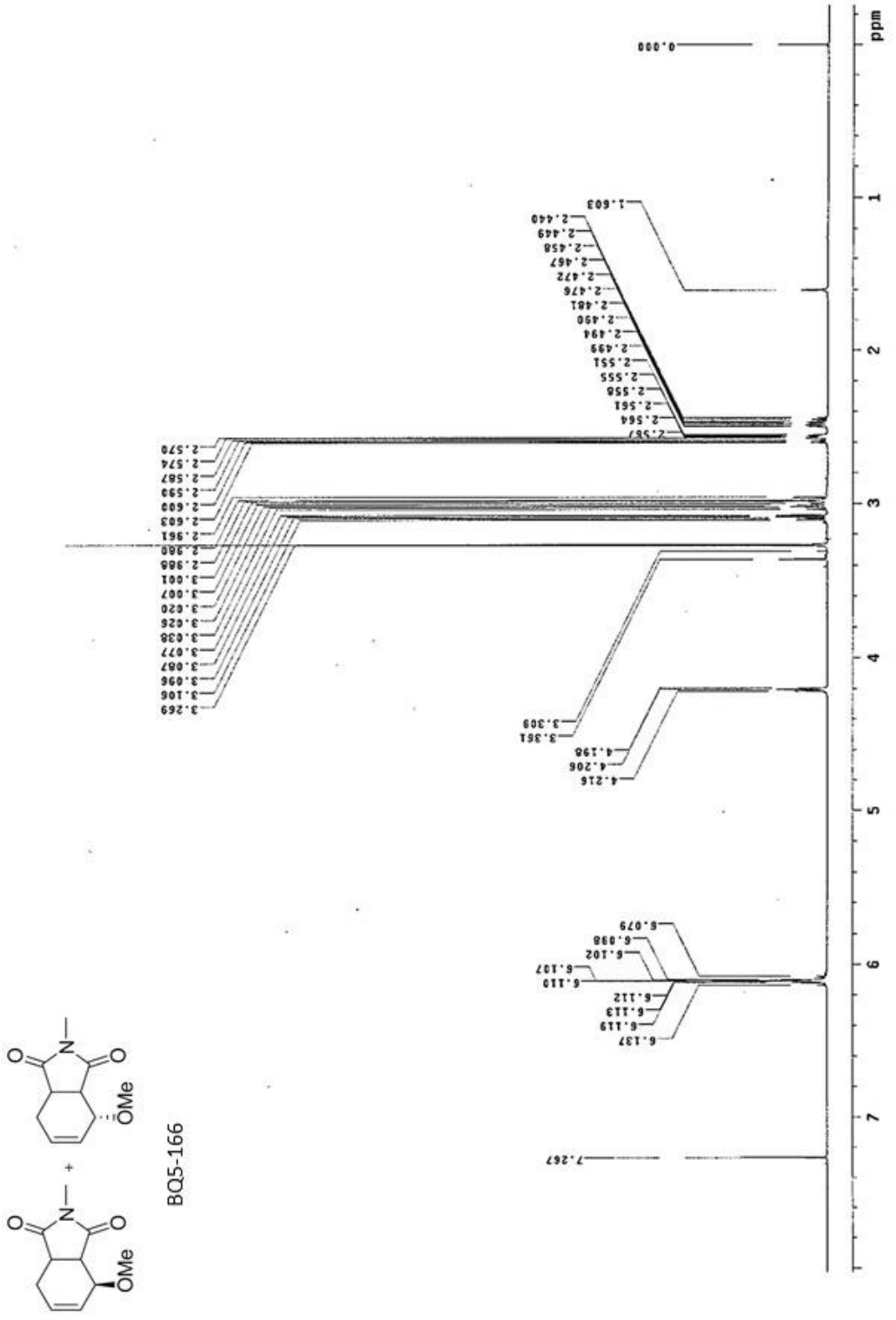
ppm
0.000
1.603
2.440
2.449
2.458
2.467
2.472
2.476
2.481
2.490
2.494
2.499
2.551
2.555
2.558
2.561
2.564
2.567
2.570
2.574
2.587
2.590
2.600
2.603
2.961
2.980
2.986
3.001
3.007
3.020
3.026
3.038
3.077
3.087
3.096
3.106
3.269
3.309
3.361
4.196
4.206
4.216
6.079
6.088
6.102
6.107
6.110
6.112
6.113
6.119
6.137
7.267
OMe
OMe
BQ5-166

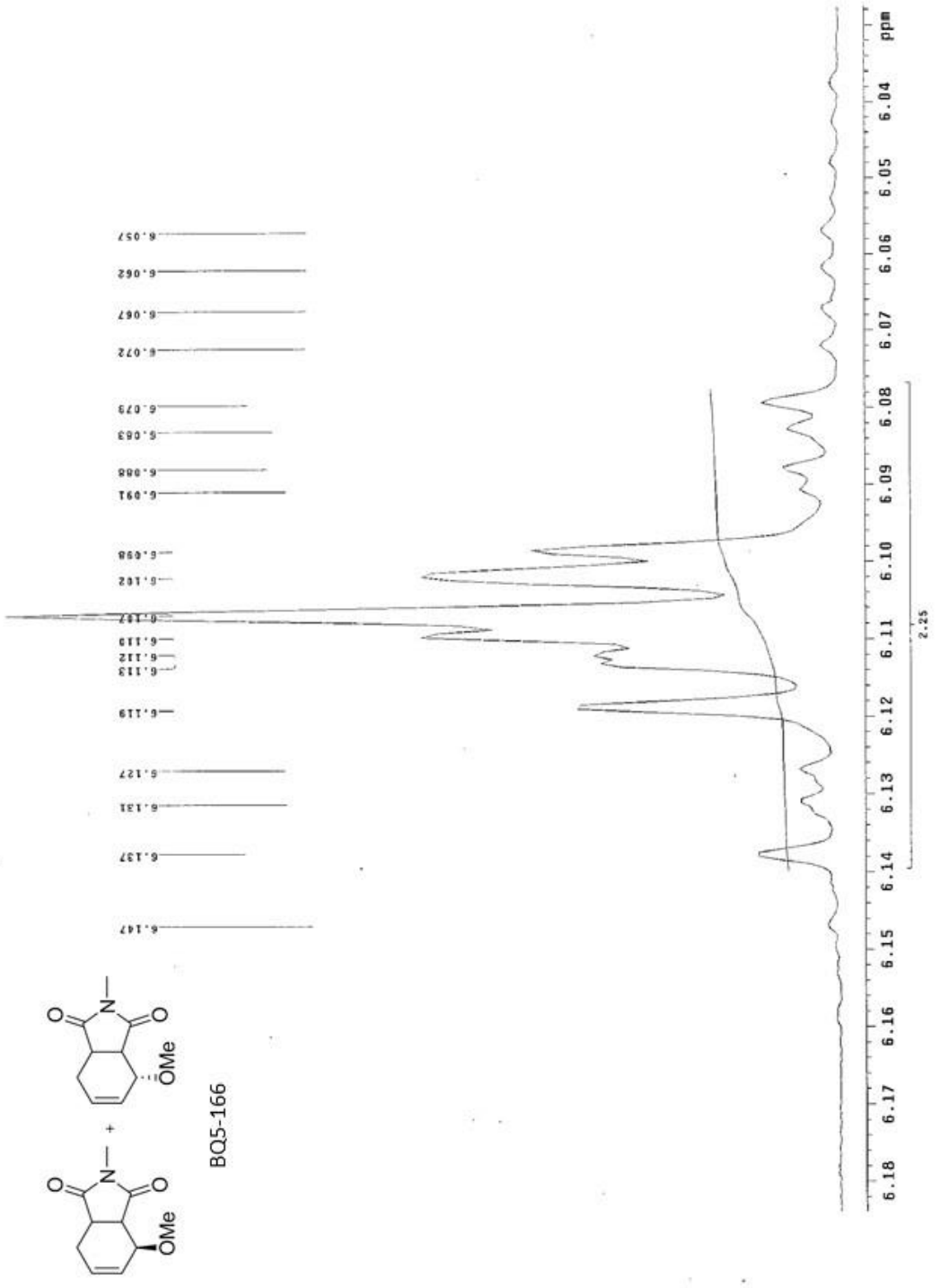
6.057
6.062
6.067
6.072
6.079
6.083
6.088
6.091
6.098
6.102
6.107
6.112
6.113
6.119
6.127
6.131
6.137
6.147
6.04
6.05
6.06
6.07
6.08
6.09
6.10
6.11
6.12
6.13
6.14
6.15
6.16
6.17
6.18
ppm
2.25
OMe
OMe
BQ5-166

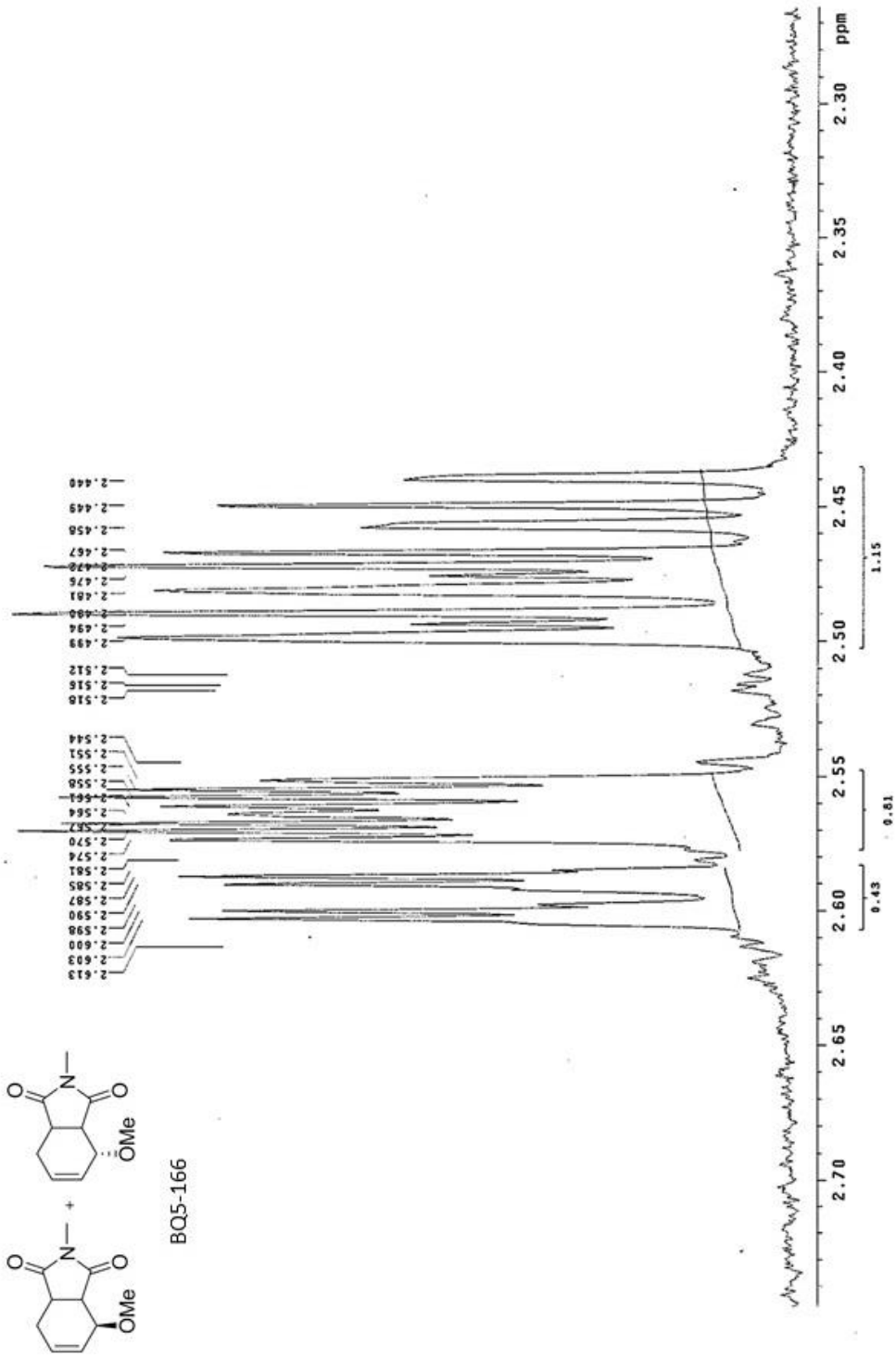
BQ5-166
OMe
OMe
ppm
2.70
2.65
2.60
2.55
2.50
2.45
2.40
2.35
2.30
0.43
0.61
1.15

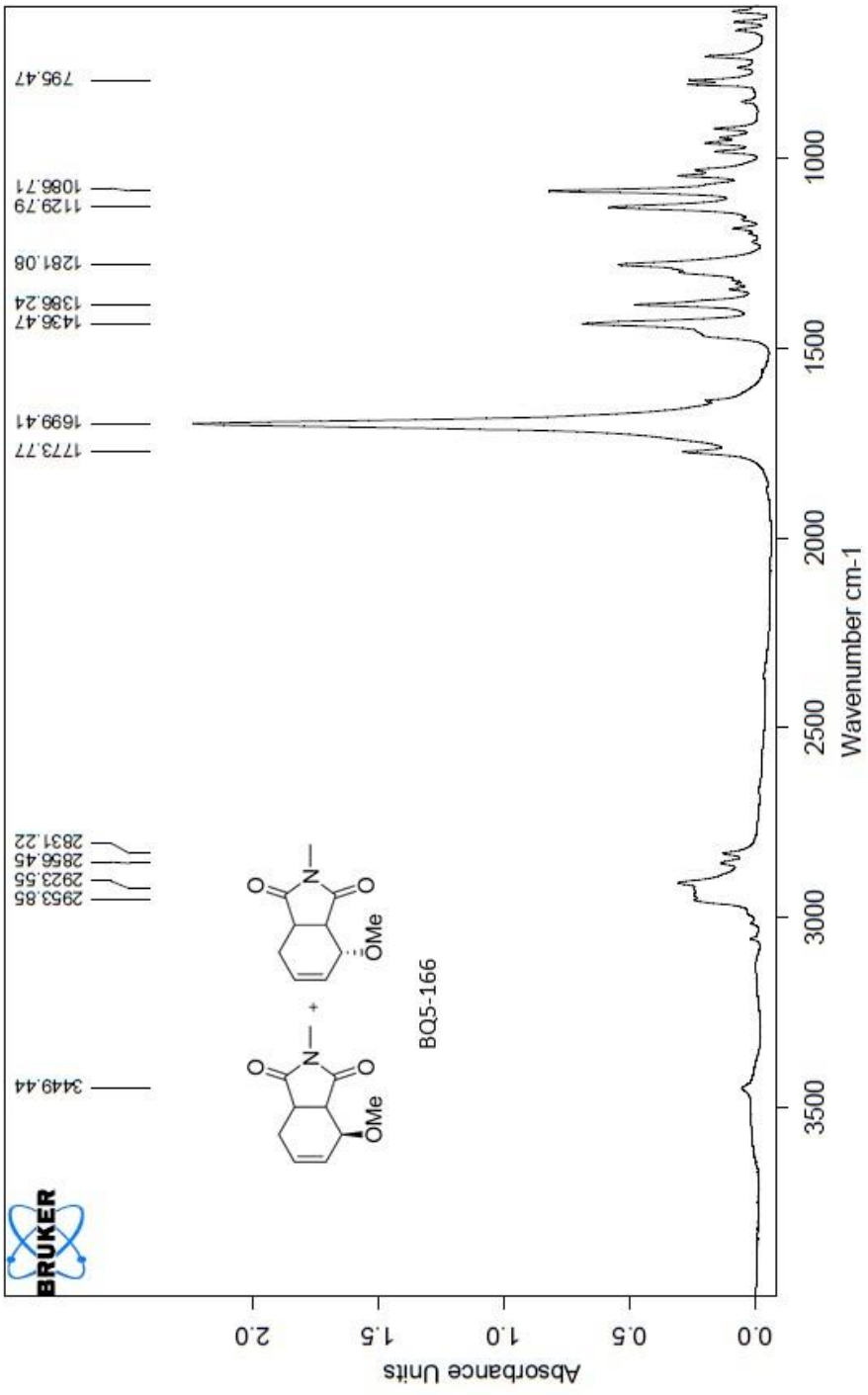
BRUKER
BQ5-166
OMe
OMe
3449.44
2953.85
2923.55
2856.45
2831.22
1773.77
1699.41
1436.47
1386.24
1281.08
1129.79
1086.71
795.47
Absorbance Units
0.0
0.5
1.0
1.5
2.0
3500
3000
2500
2000
1500
1000
Wavenumber cm-1

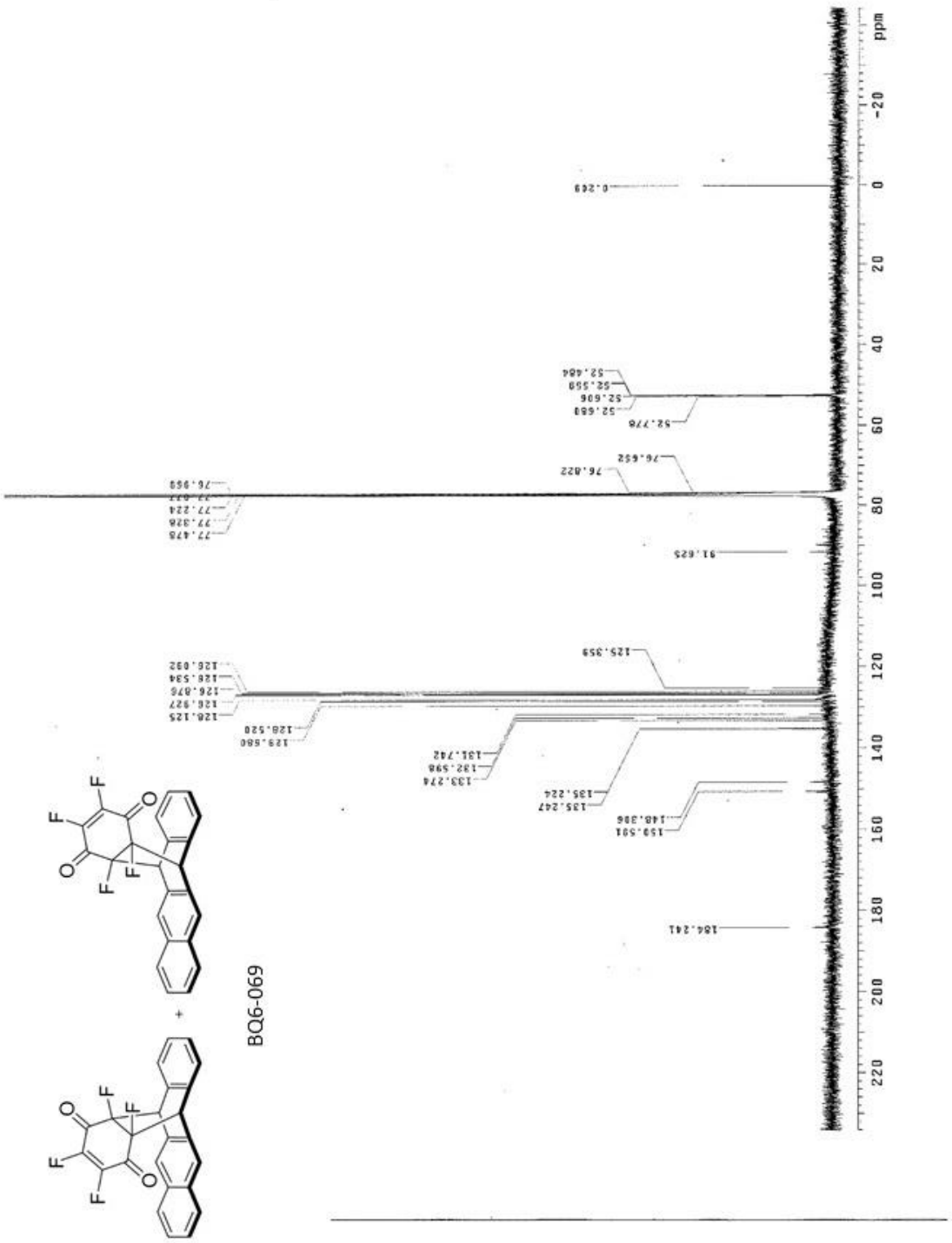
BQ6-069
ppm
0.269
52.464
52.559
52.606
52.688
52.778
76.022
76.652
76.959
77.478
77.326
77.224
91.625
125.359
126.092
126.534
126.876
126.927
126.125
128.520
129.680
131.742
132.598
133.274
135.224
135.247
148.386
159.501
184.241

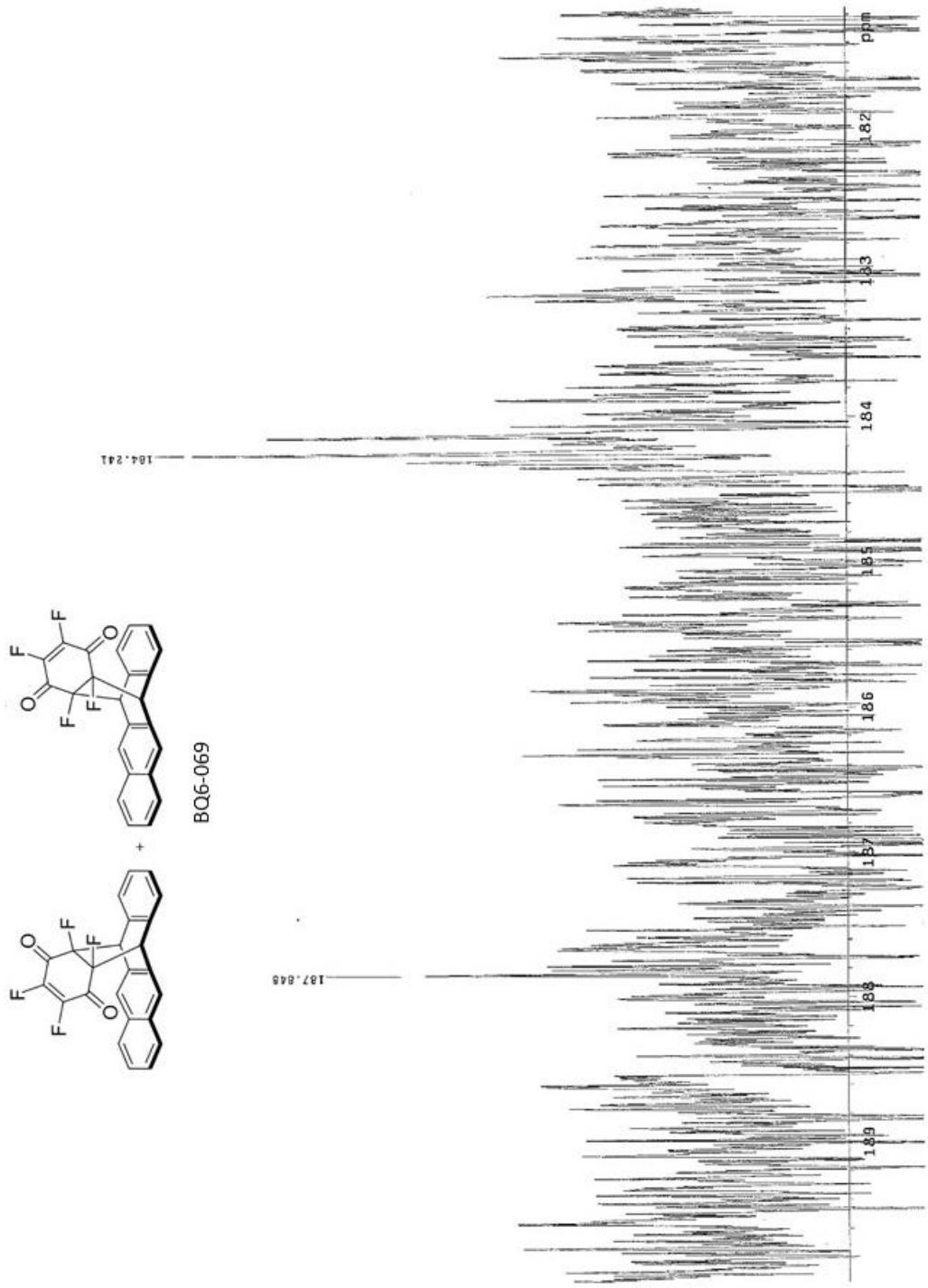
BQ6-069
184.241
187.848
ppm
182
183
184
185
186
187
188
189

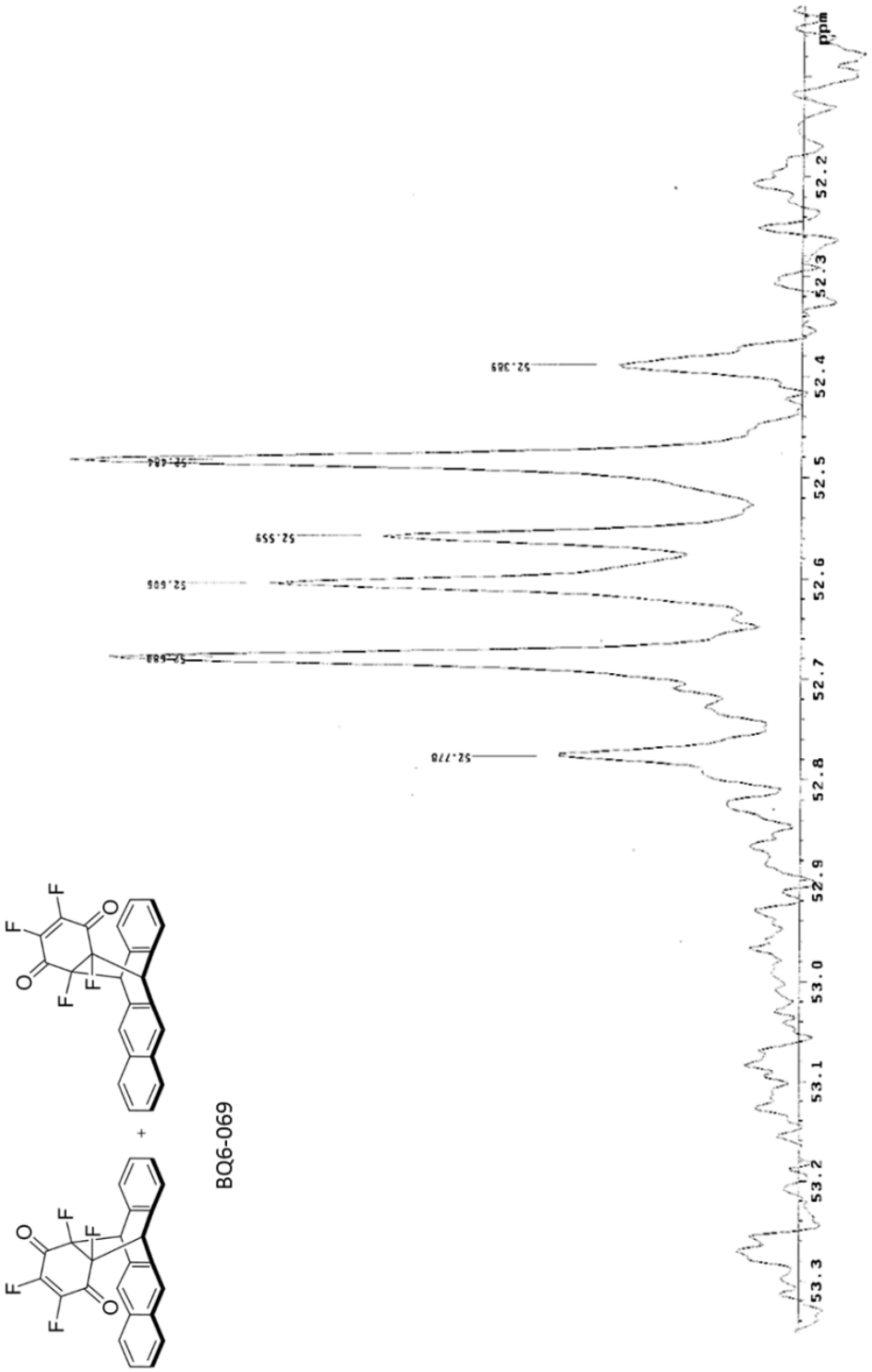
F
O
F
F
O
+
F
O
F
F
O
BQ6-069
52.369
52.559
52.606
52.778
ppm
52.2
52.3
52.4
52.5
52.6
52.7
52.8
52.9
53.0
53.1
53.2
53.3

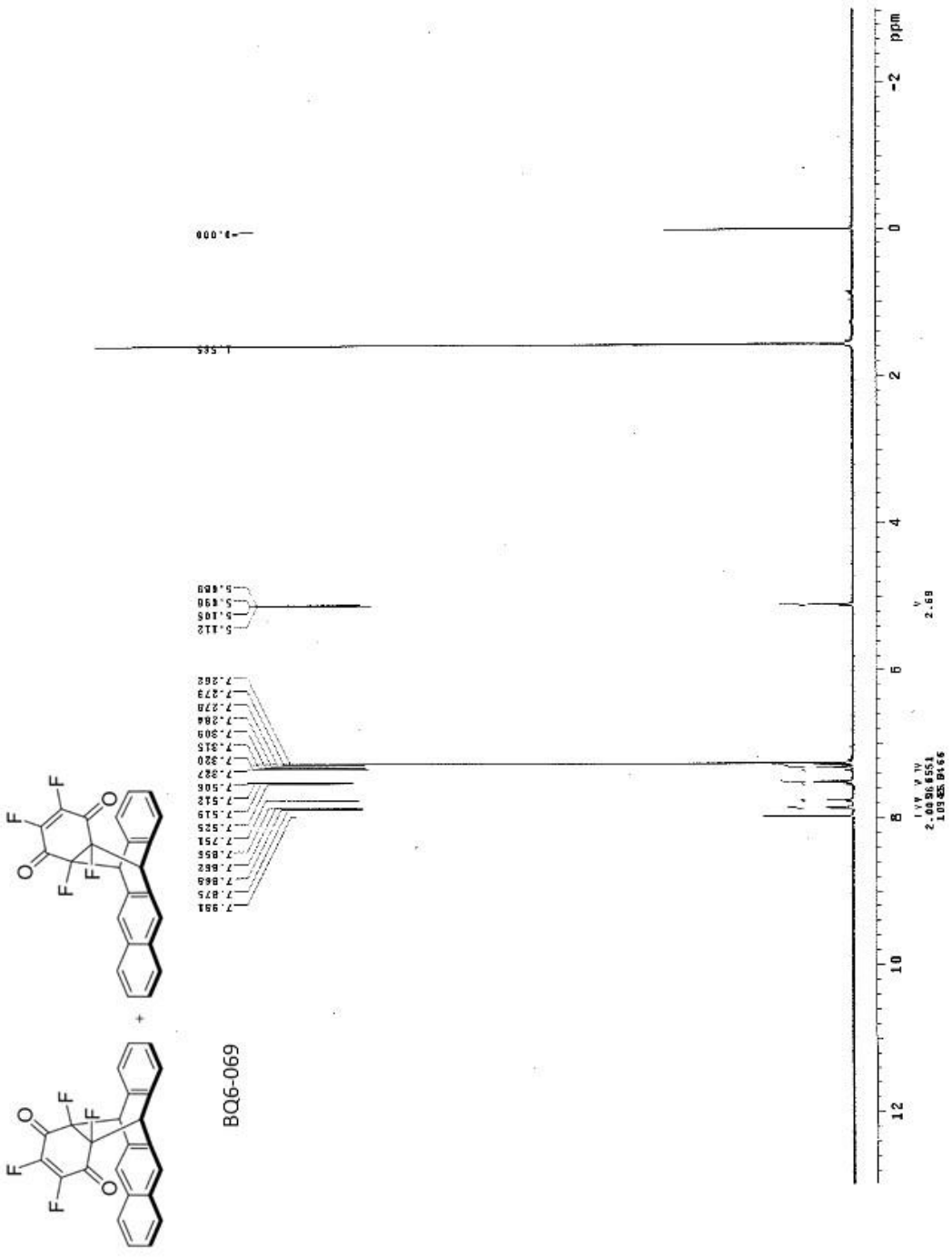
BQ6-069
ppm

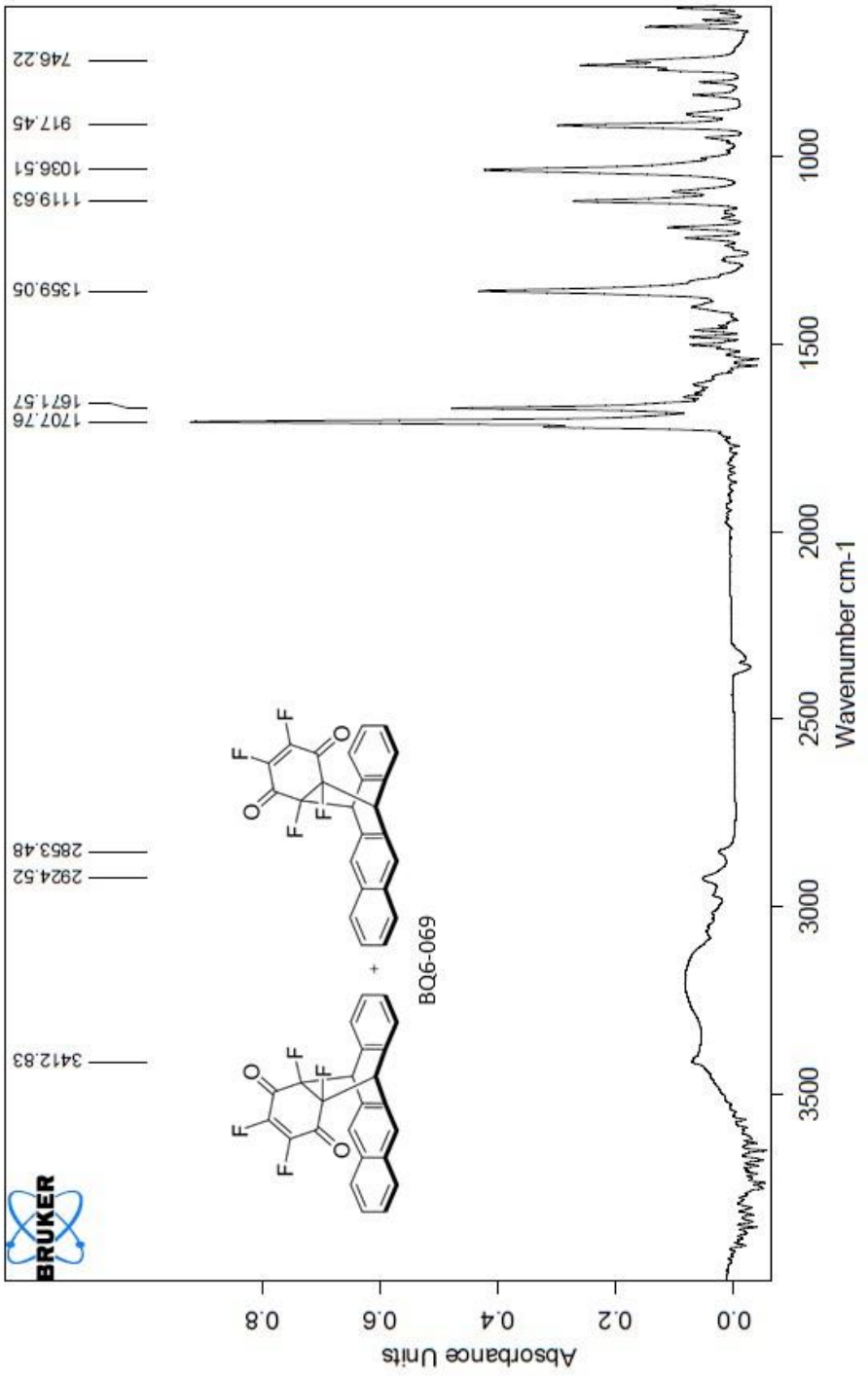
BRUKER
BQ6-069
3412.83
2924.52
2853.48
1671.57
1707.76
1359.05
1119.63
1036.51
917.45
746.22
Absorbance Units
Wavenumber cm-1

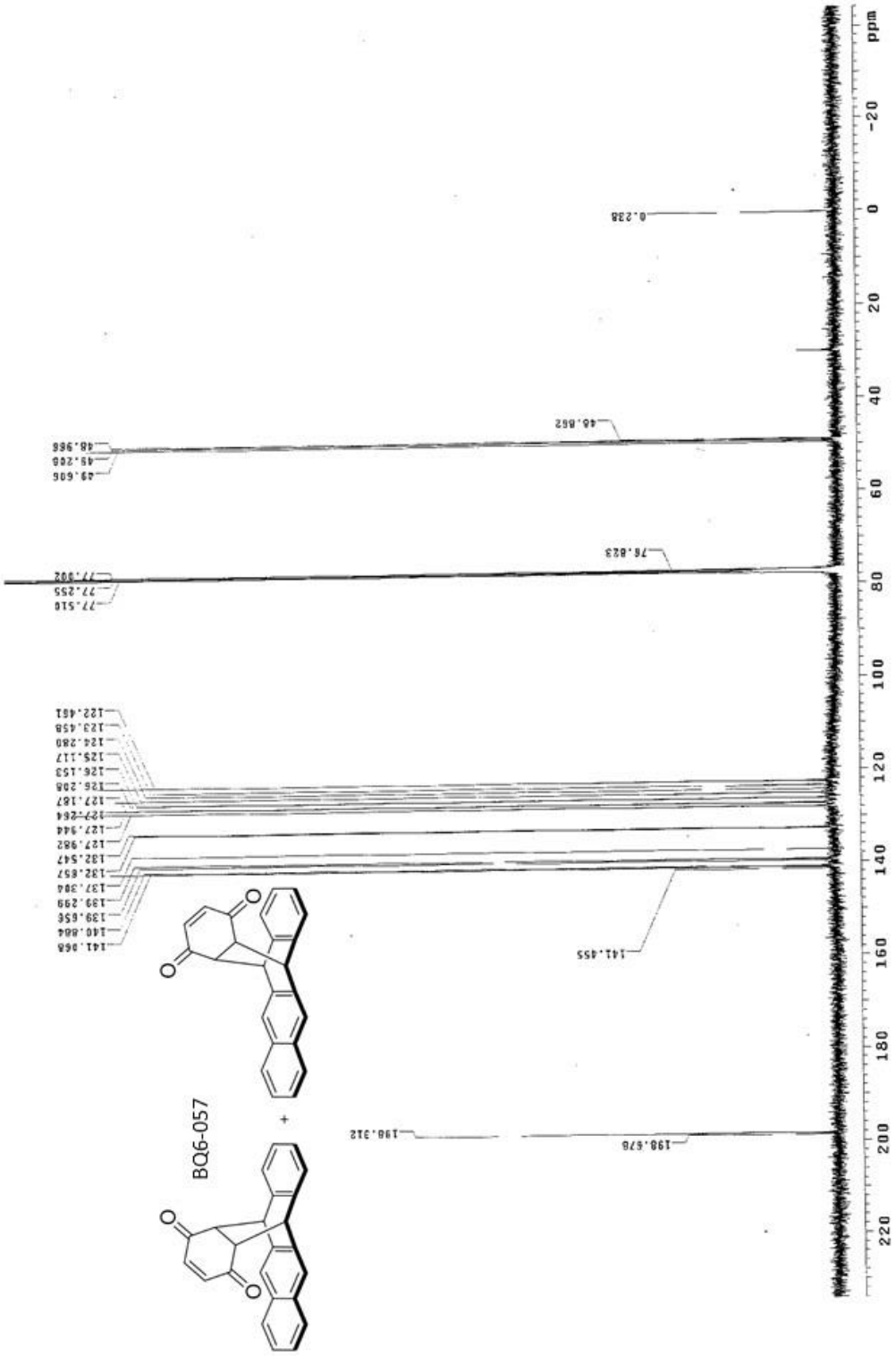
BQ6-057
ppm
198.676
198.342
141.455
141.868
140.884
139.656
139.299
137.304
132.657
132.547
127.982
127.944
127.264
127.187
126.208
126.153
125.117
124.280
123.458
122.461
77.516
77.255
77.002
76.823
49.606
49.208
48.966
46.862
0.238

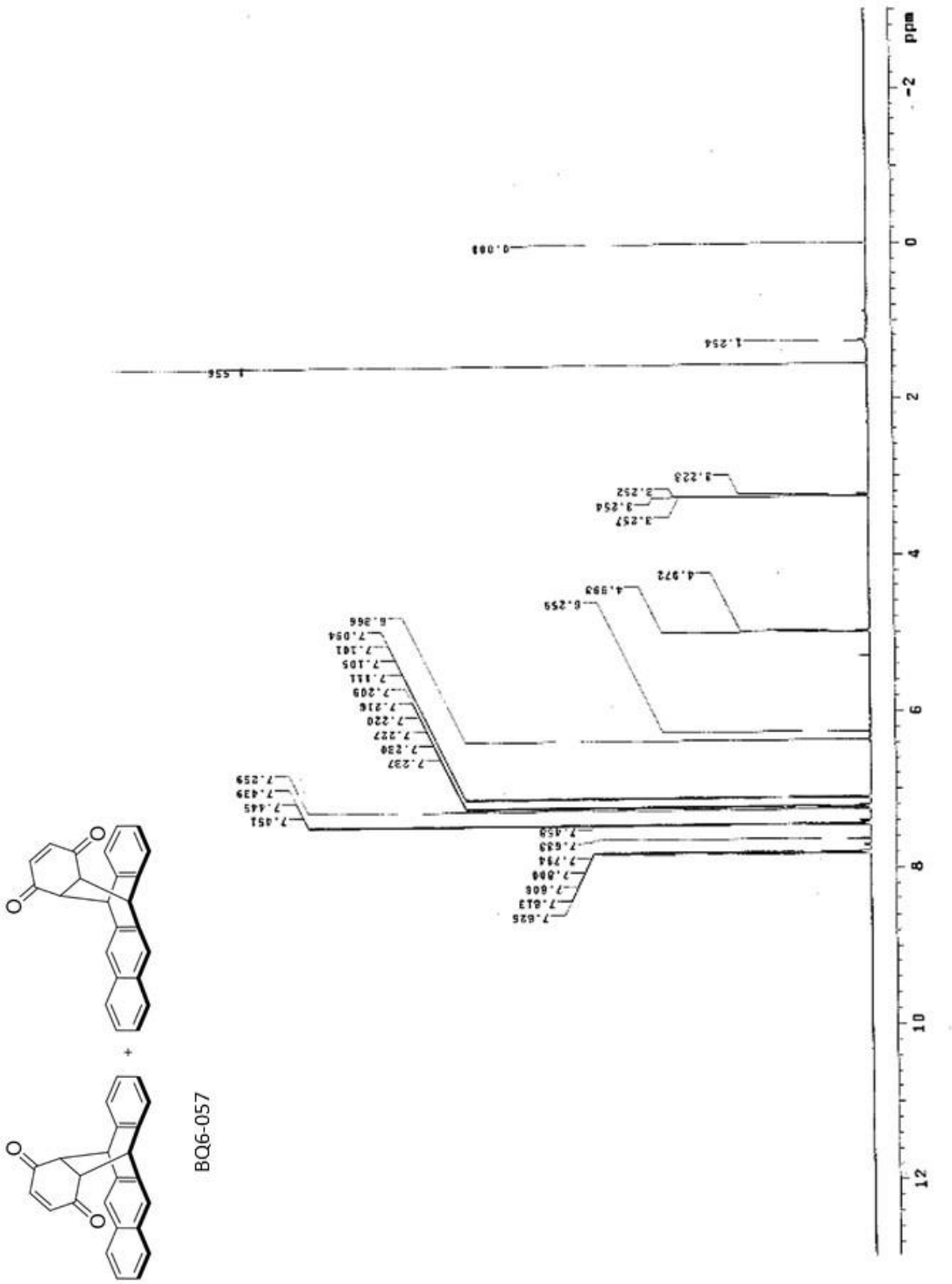
BQ6-057
ppm

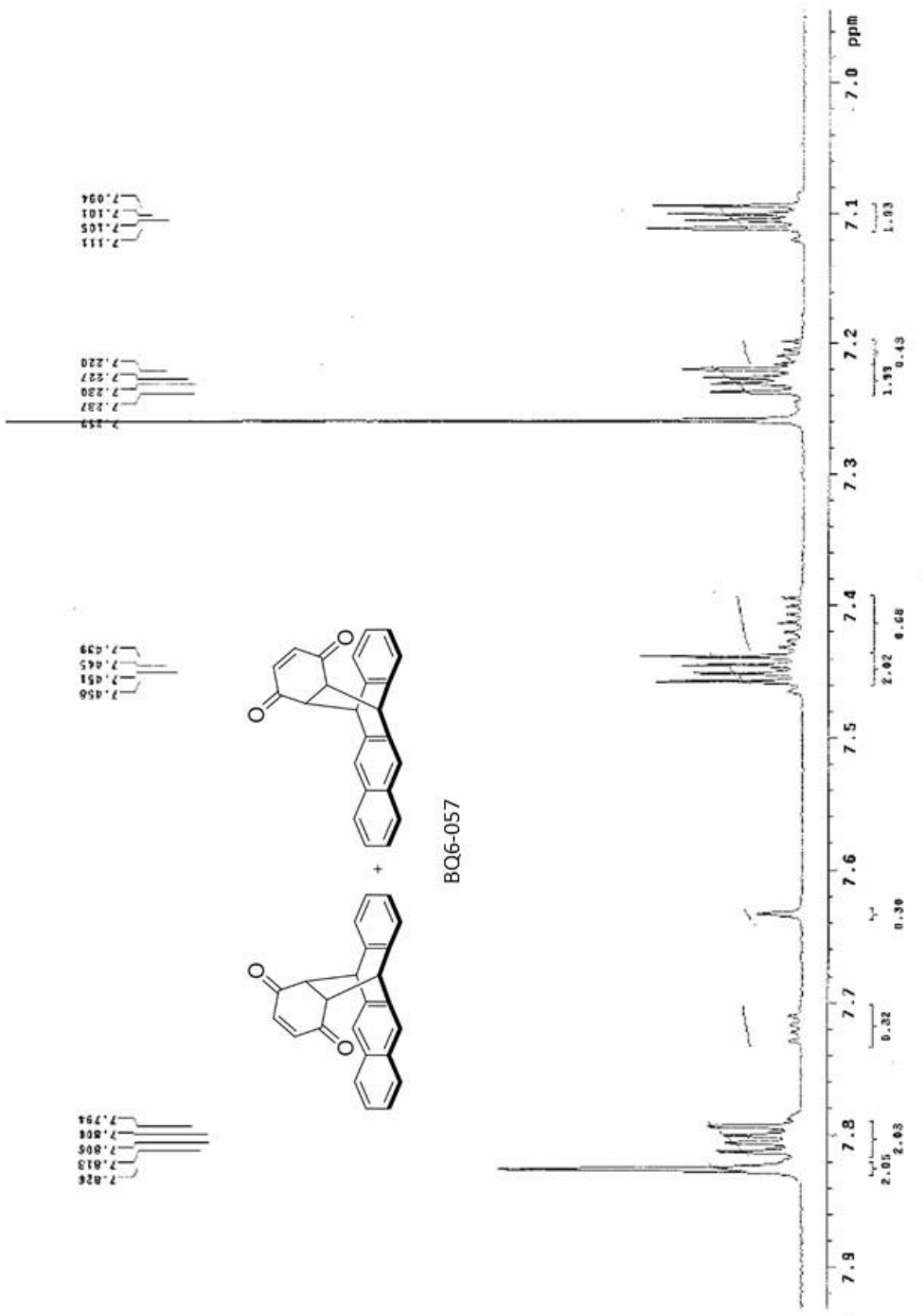
BQ6-057
ppm

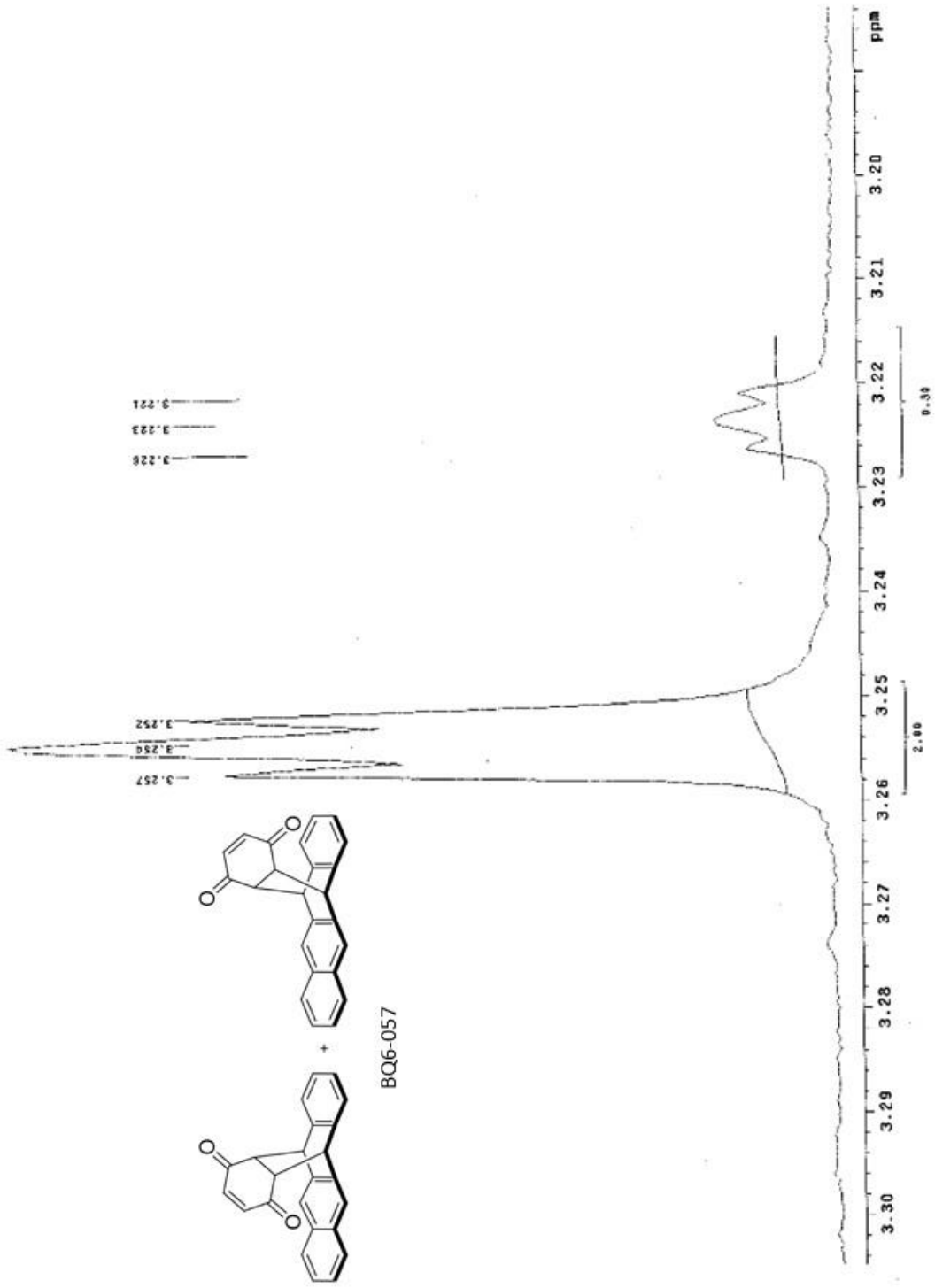
BQ6-057
3.257
3.256
3.252
3.228
3.223
3.221
3.20
3.21
3.22
3.23
3.24
3.25
3.26
3.27
3.28
3.29
3.30
ppm

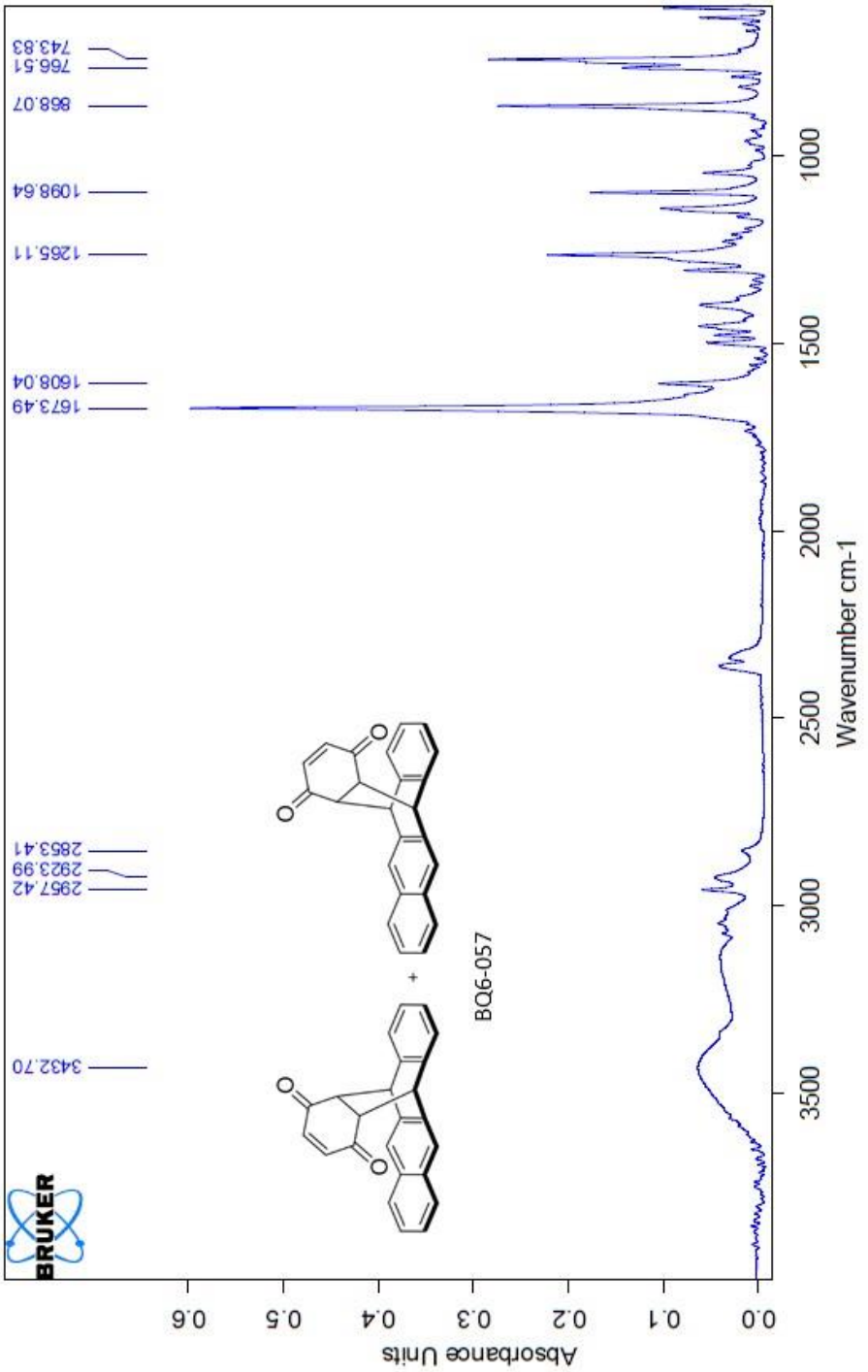
BRUKER
BQ6-057
Absorbance Units
Wavenumber cm-1
0.0
0.1
0.2
0.3
0.4
0.5
0.6
3500
3000
2500
2000
1500
1000
3432.70
2957.42
2923.99
2853.41
1673.49
1608.04
1265.11
1098.64
868.07
766.51
743.83

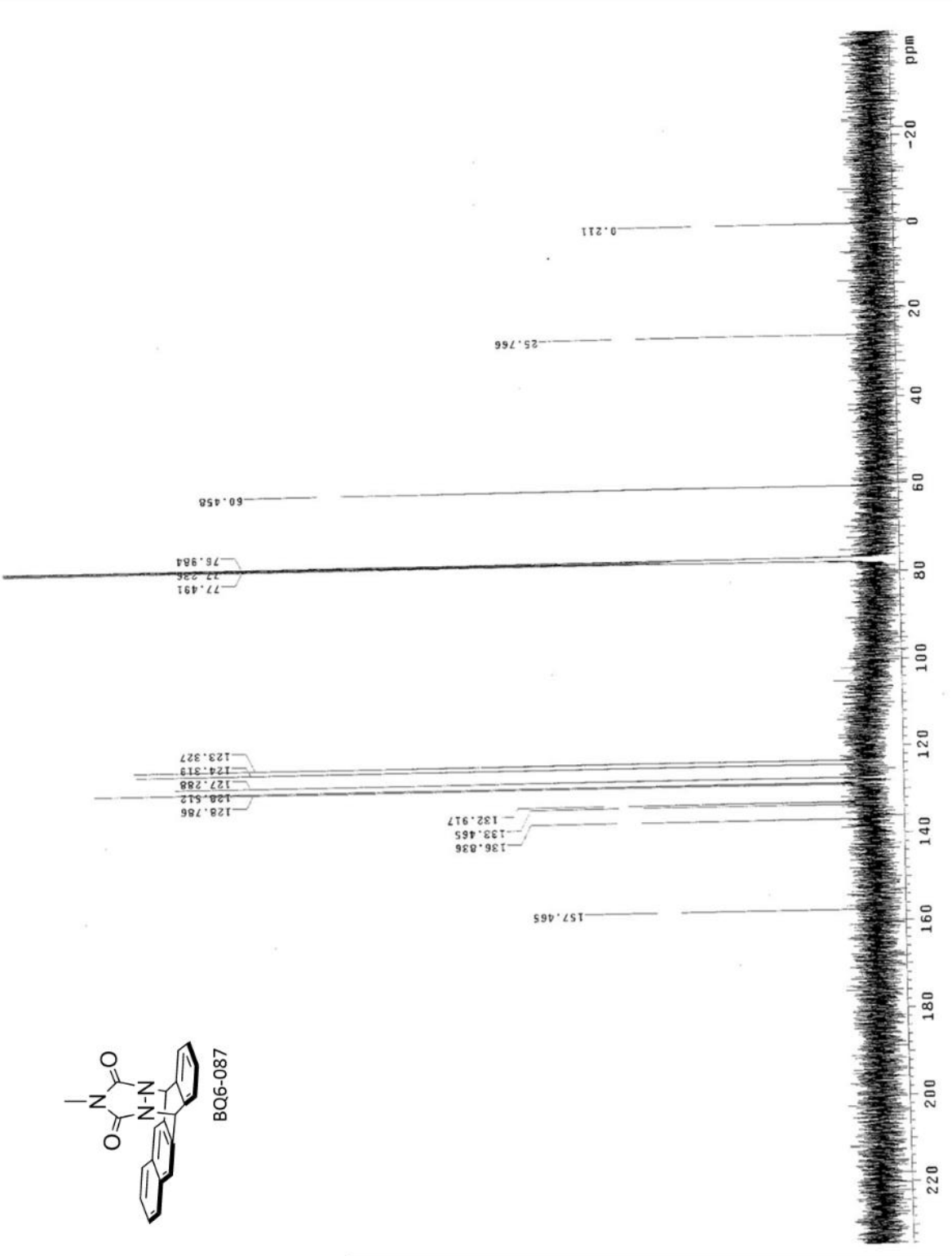
ppm
220
200
180
160
140
120
100
80
60
40
20
0
-20
0.211
25.766
60.458
76.984
77.236
77.491
123.327
124.319
127.288
128.512
128.786
132.917
133.465
136.836
157.465
BQ6-087

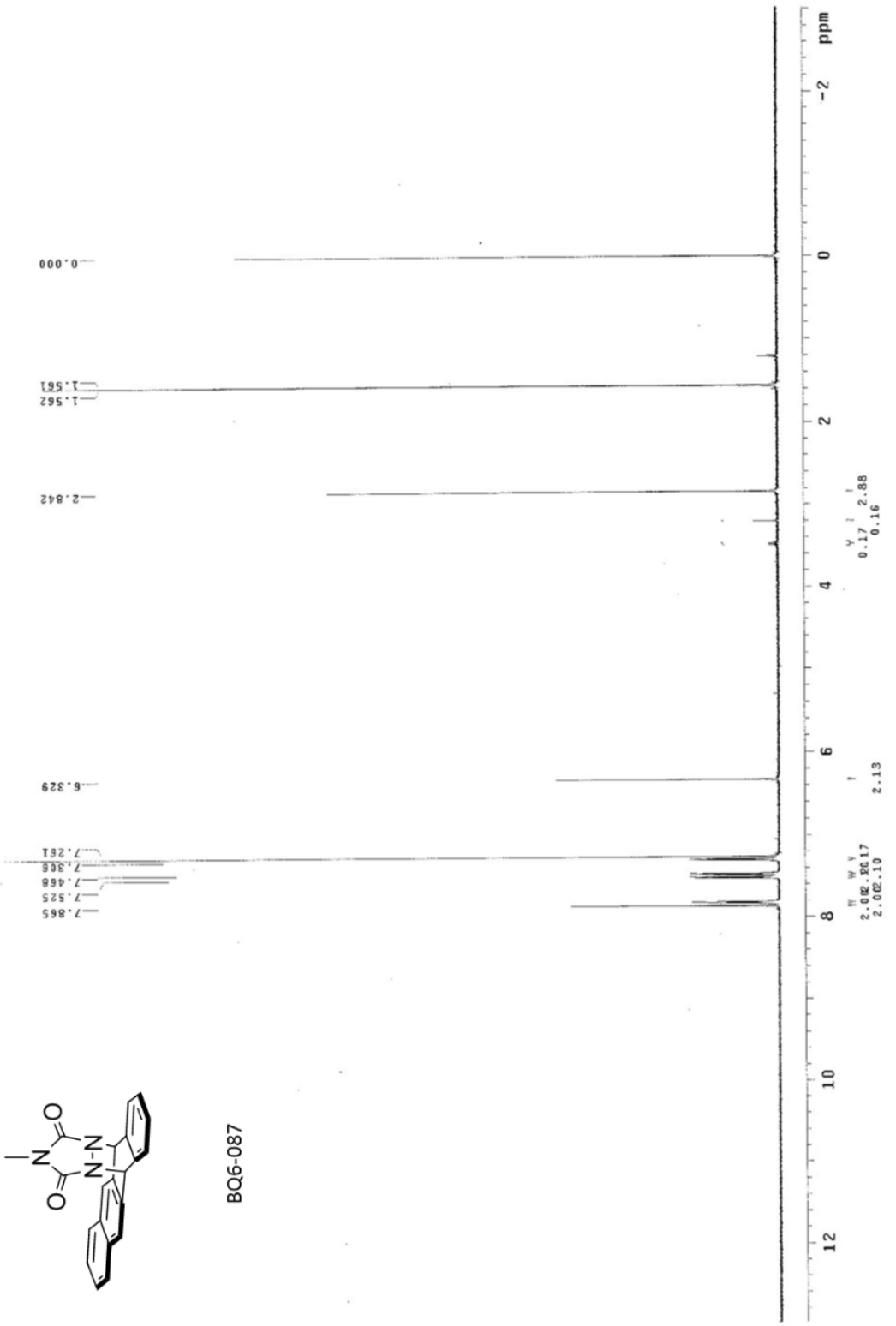
BQ6-087
0.000
1.561
1.562
2.842
6.329
7.261
7.308
7.468
7.525
7.865
ppm
0
2
4
6
8
10
12
2.13
2.88
0.17
0.16
2.017
2.10

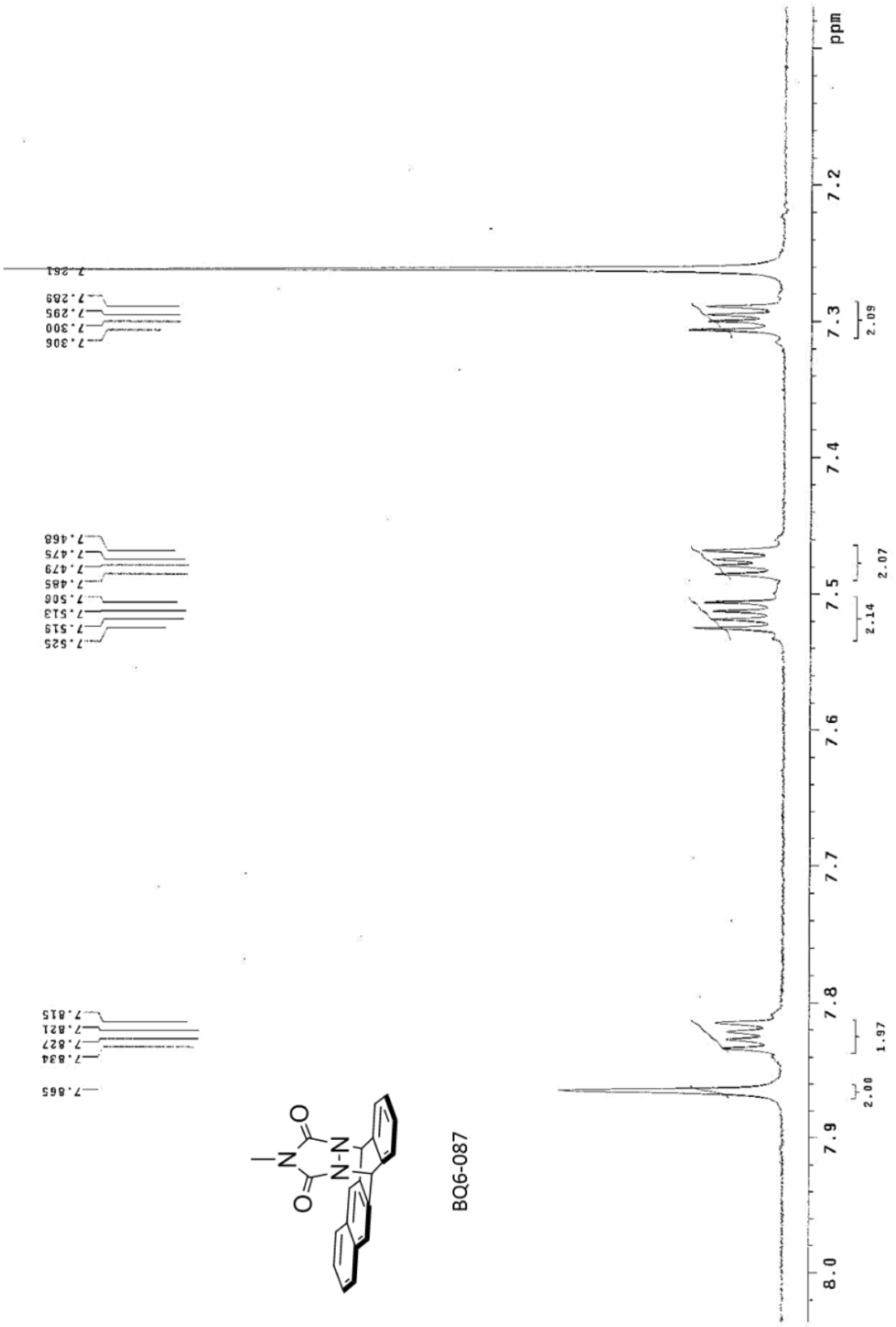
7.261
7.289
7.295
7.300
7.306
7.468
7.475
7.479
7.485
7.506
7.513
7.519
7.525
7.815
7.821
7.827
7.834
7.865
8.0
7.9
7.8
7.7
7.6
7.5
7.4
7.3
7.2
ppm
2.09
2.14
2.07
2.00
1.97
BQ6-087

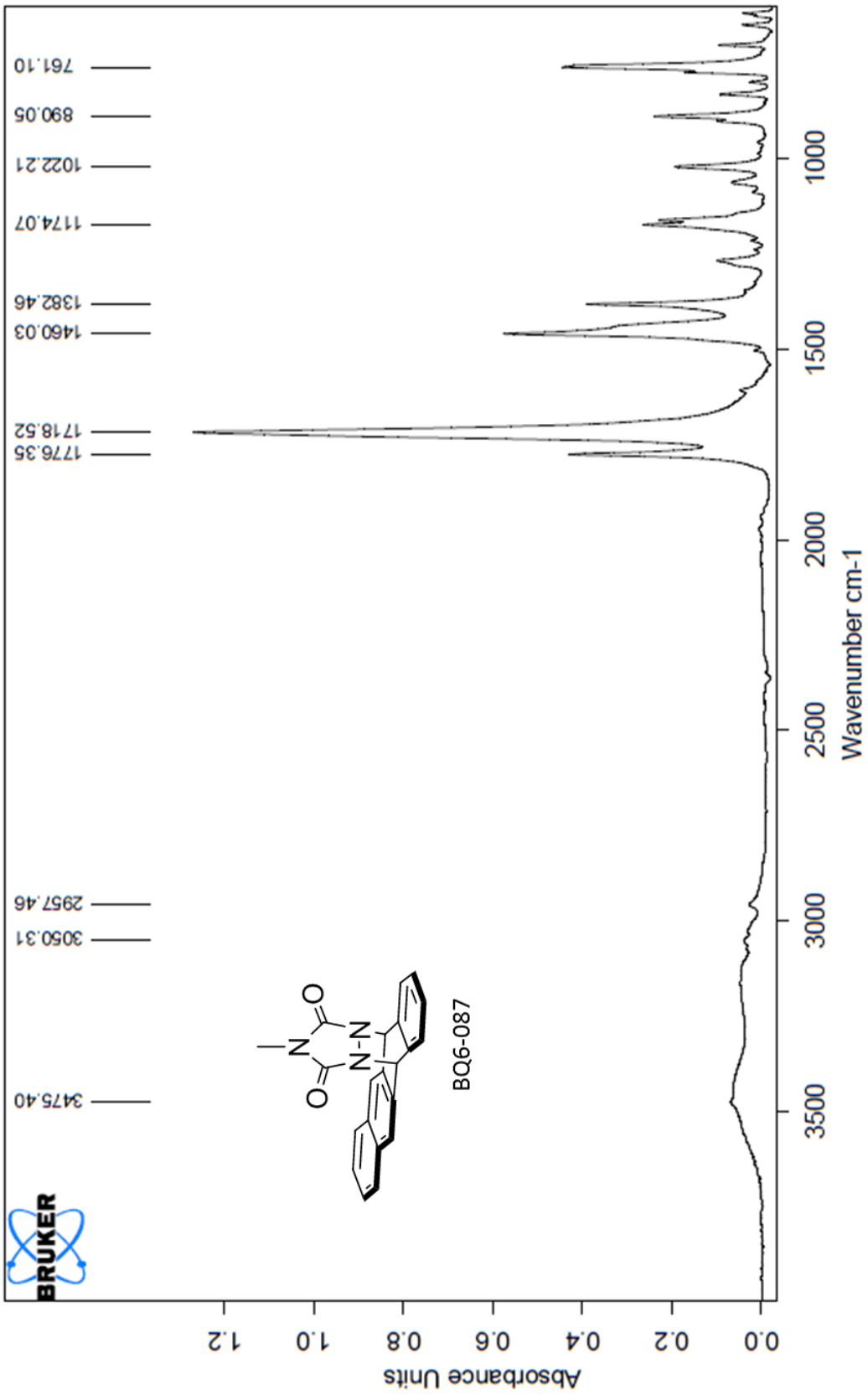
BRUKER
BQ6-087
3475.40
3050.31
2957.46
1776.35
1718.52
1460.03
1382.46
1174.07
1022.21
890.05
761.10
Absorbance Units
Wavenumber cm-1

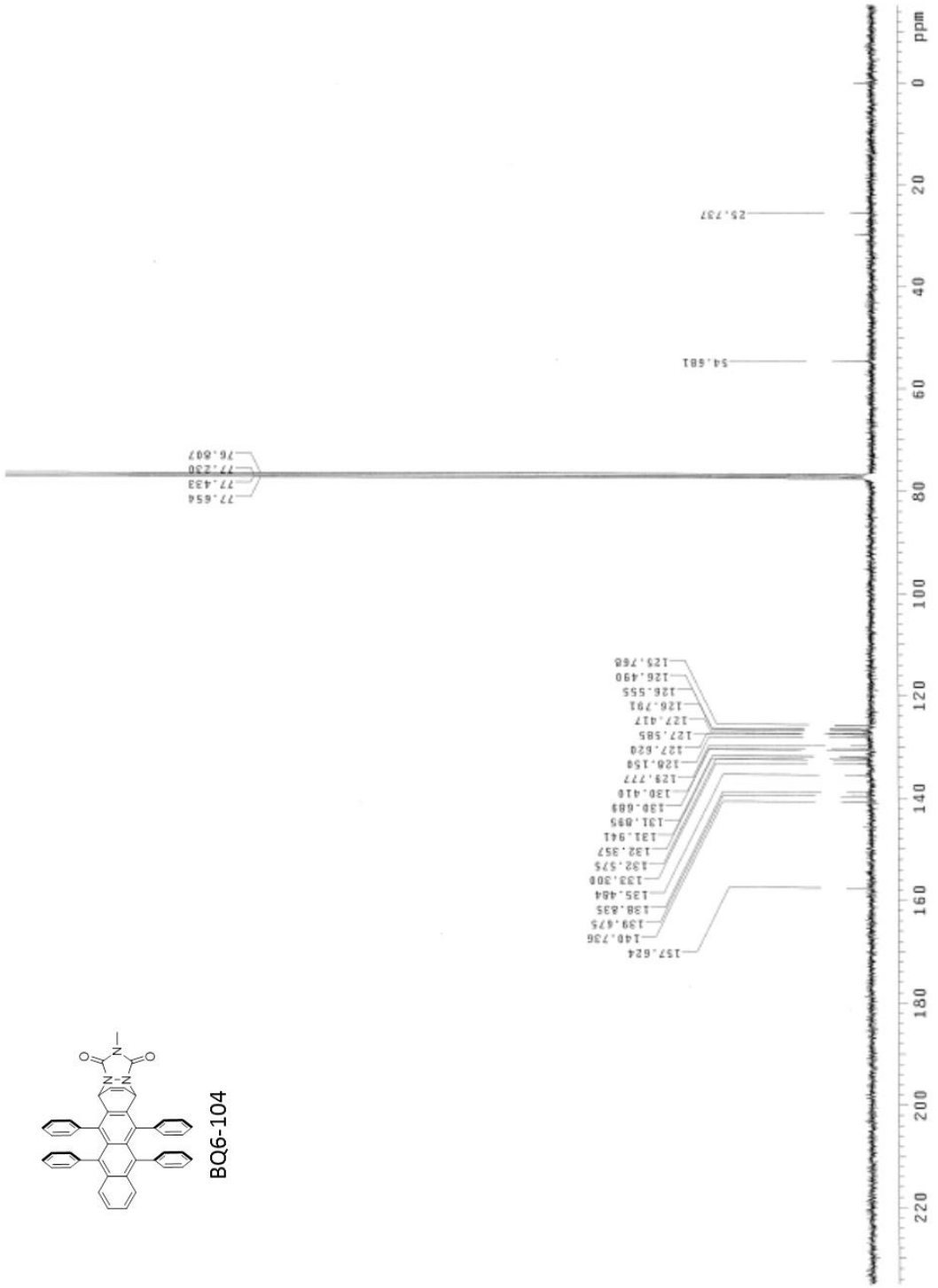
ppm
0
20
40
60
80
100
120
140
160
180
200
220
25.737
54.681
76.807
77.230
77.433
77.654
125.768
126.490
126.555
126.791
127.417
127.585
127.620
128.158
129.777
130.410
130.689
131.095
131.941
132.357
132.575
133.308
135.484
138.835
139.675
140.736
157.624
BQ6-104

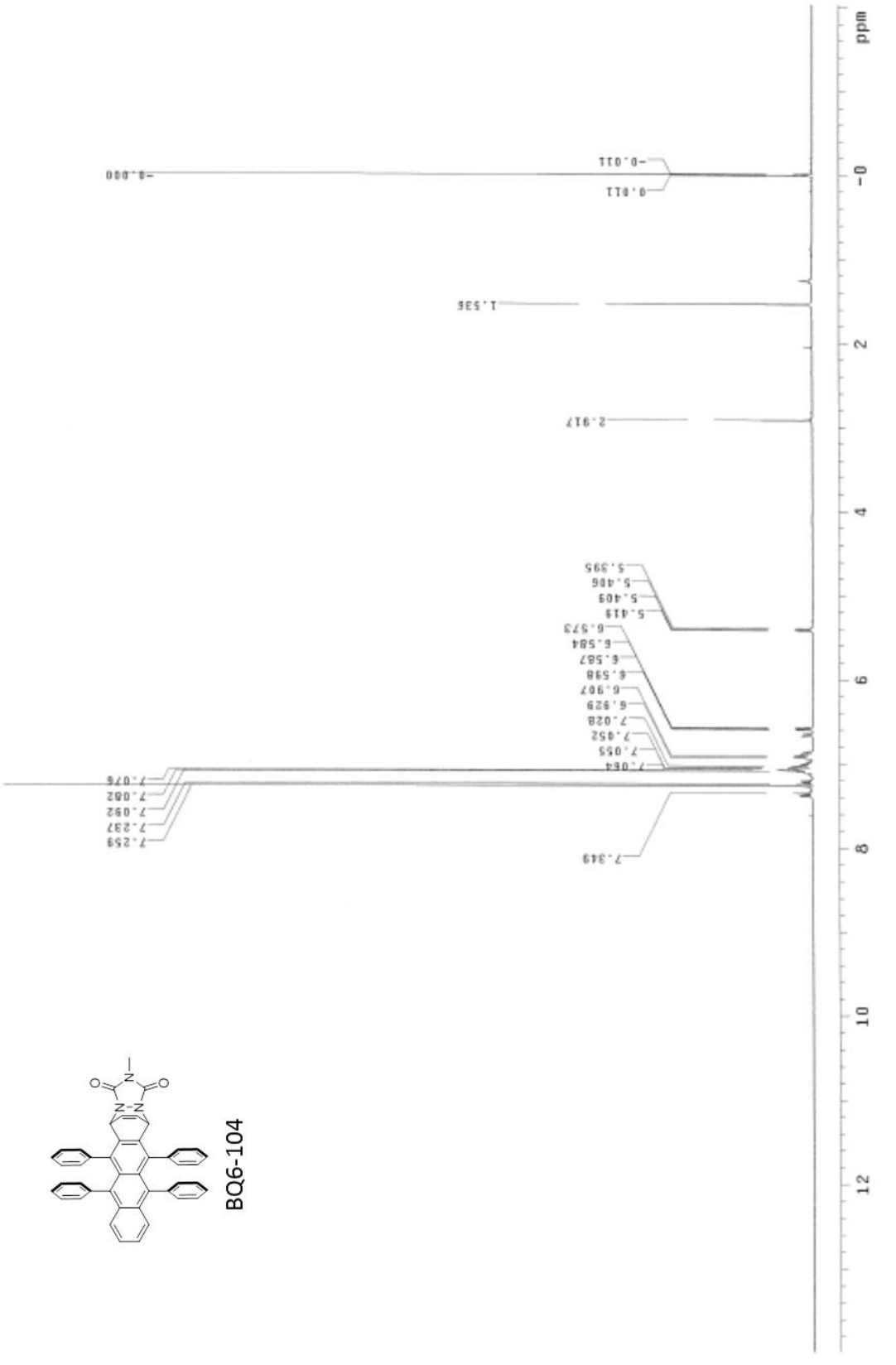
ppm
-0
2
4
6
8
10
12
-0.011
0.011
-0.000
1.536
2.917
5.395
5.406
5.409
5.419
6.573
6.584
6.587
6.598
6.907
6.929
7.028
7.052
7.055
7.064
7.076
7.082
7.092
7.237
7.259
7.349

BQ6-104

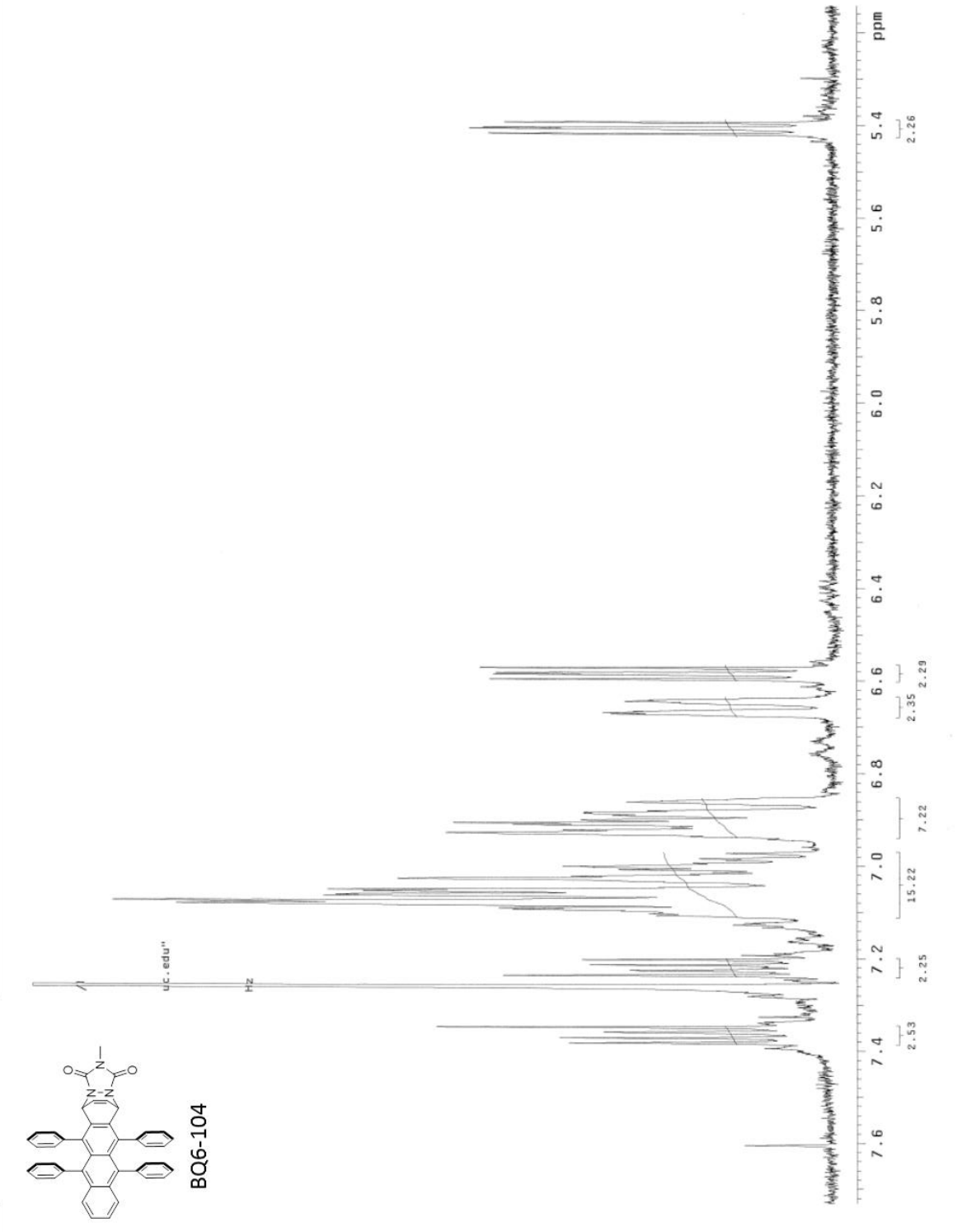
BQ6-104
u.c.epu"
Hz
ppm
7.6
7.4
7.2
7.0
6.8
6.6
6.4
6.2
6.0
5.8
5.6
5.4
2.53
2.25
15.22
7.22
2.35
2.29
2.26

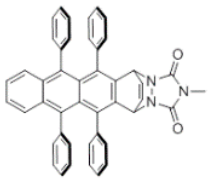

BQ6-104

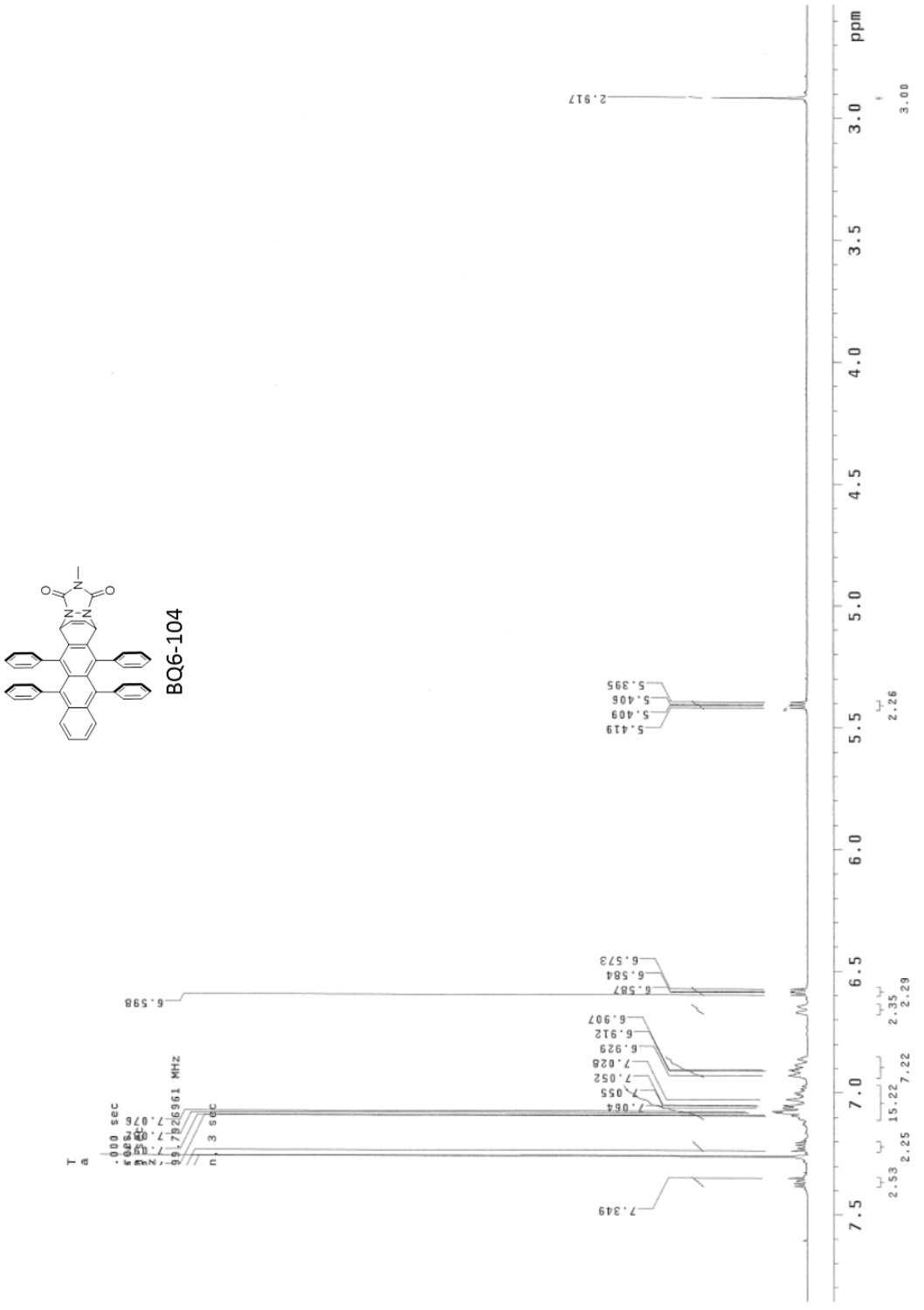
BQ6-104
ppm
2.917
5.419
5.409
5.408
5.395
6.598
6.587
6.584
6.573
6.907
6.912
6.929
7.028
7.052
7.055
7.064
7.349

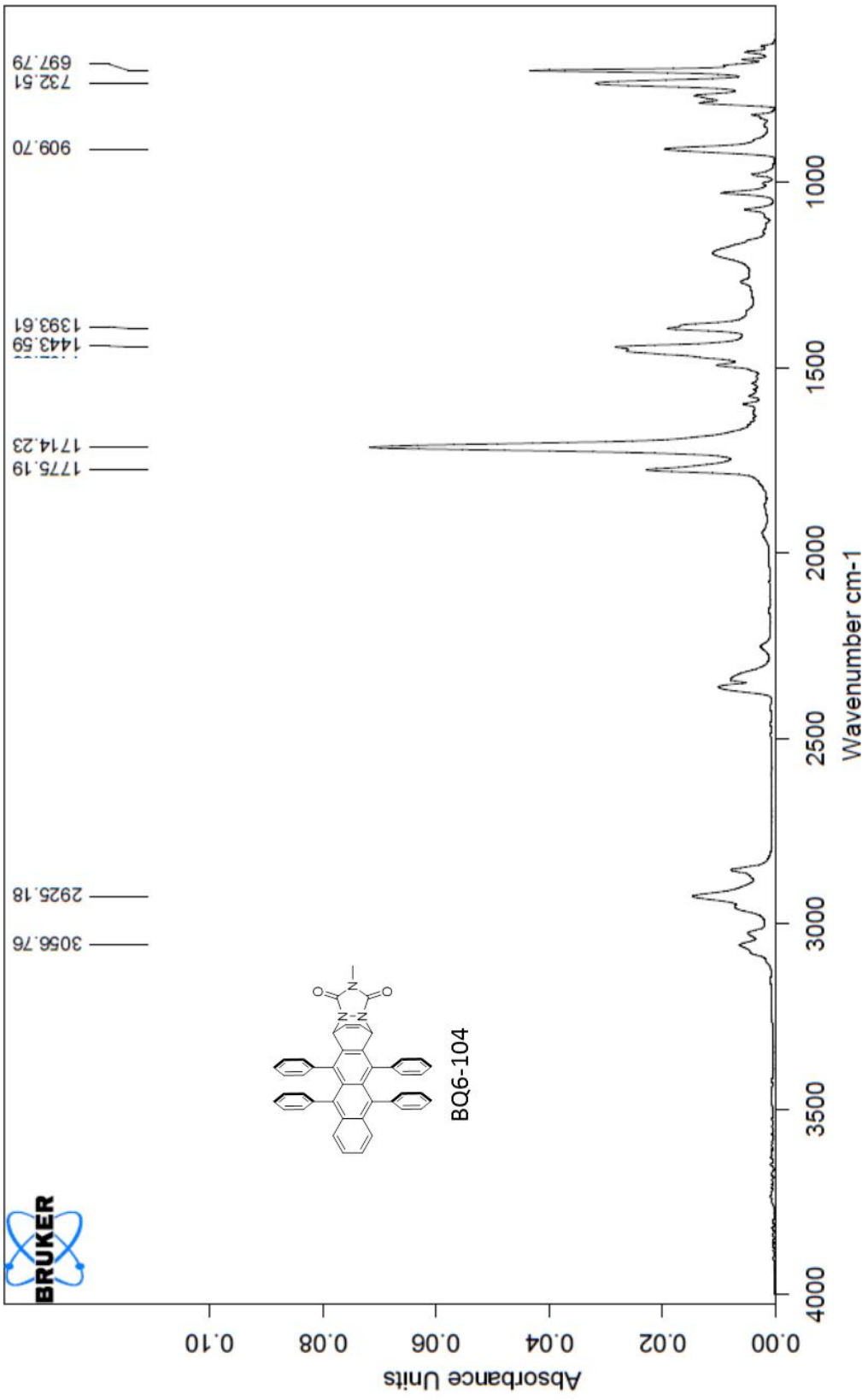
BRUKER
BQ6-104
3056.76
2925.18
1775.19
1714.23
1443.59
1393.61
909.70
732.51
697.79
4000
3500
3000
2500
2000
1500
1000
Wavenumber cm-1
0.00
0.02
0.04
0.06
0.08
0.10
Absorbance Units

APPENDIX B
UV-VIS SPECTROSCOPY OF KINETIC EXPERIMENTS

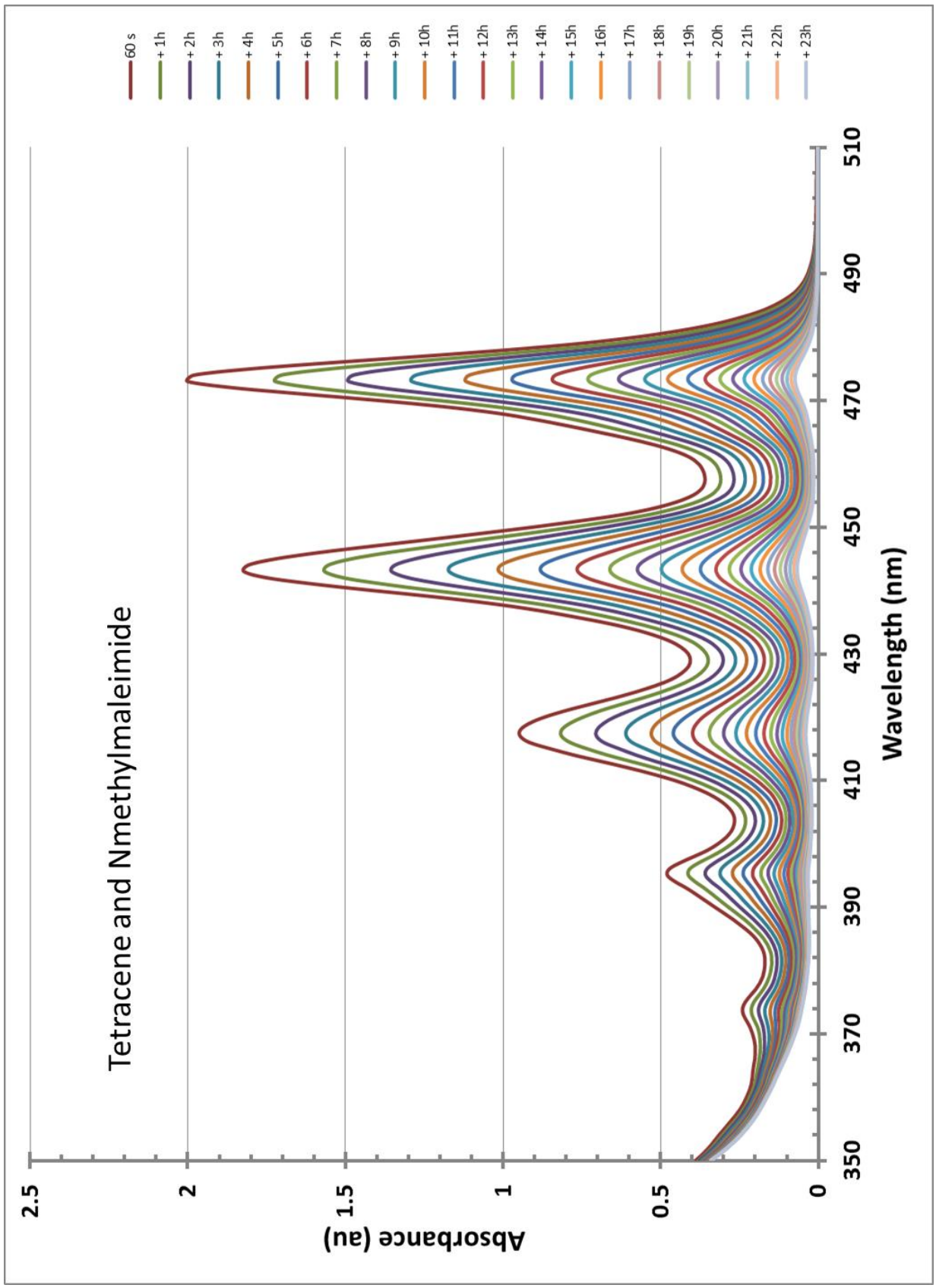
Tetracene and Nmethylmaleimide
60 s
+ 1h
+ 2h
+ 3h
+ 4h
+ 5h
+ 6h
+ 7h
+ 8h
+ 9h
+ 10h
+ 11h
+ 12h
+ 13h
+ 14h
+ 15h
+ 16h
+ 17h
+ 18h
+ 19h
+ 20h
+ 21h
+ 22h
+ 23h
Absorbance (au)
2.5
2
1.5
1
0.5
0
Wavelength (nm)
350
370
390
410
430
450
470
490
510

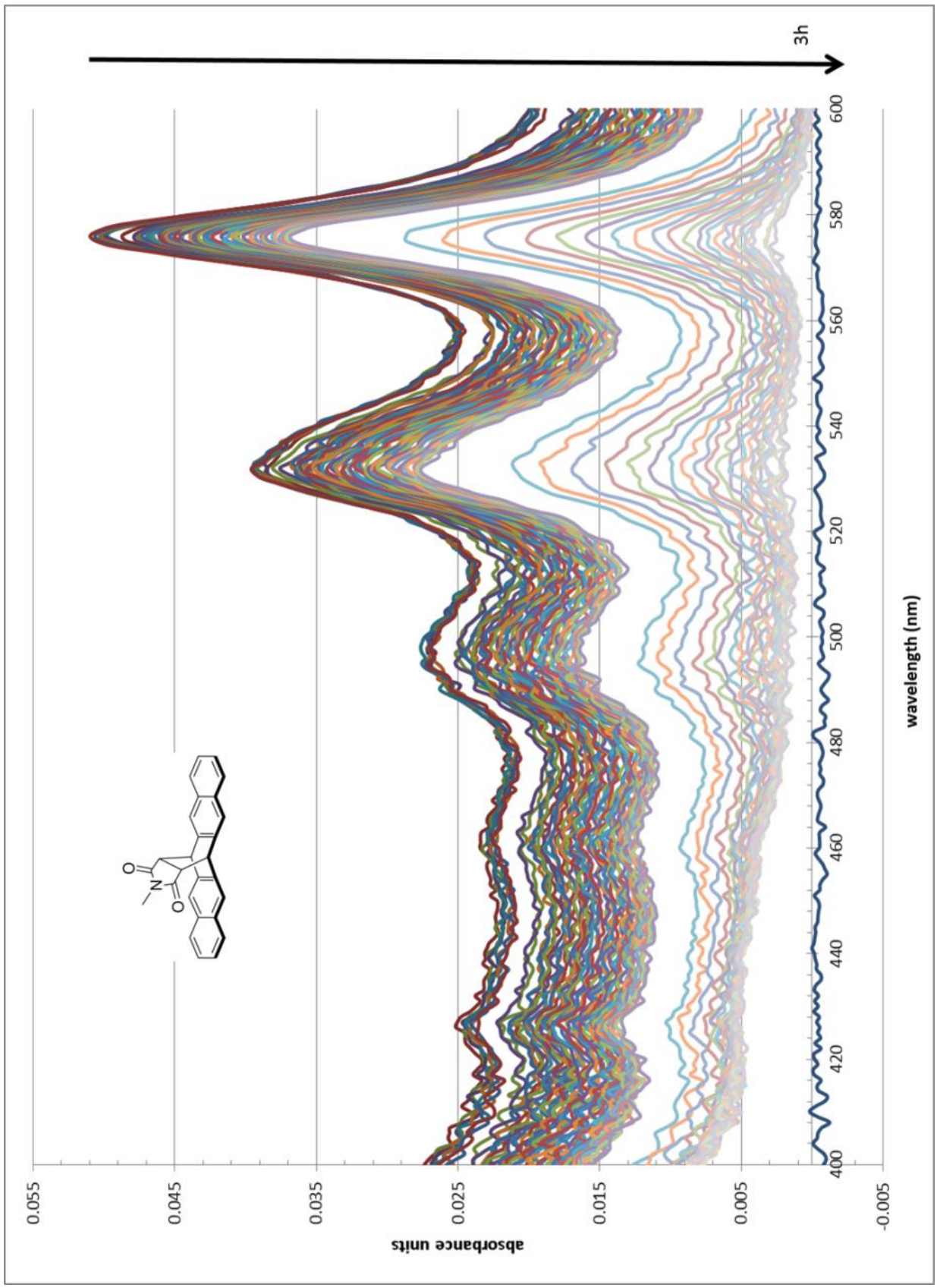
3h
absorbance units
0.055
0.045
0.035
0.025
0.015
0.005
-0.005
400
420
440
460
480
500
520
540
560
580
600
wavelength (nm)
O
N
O

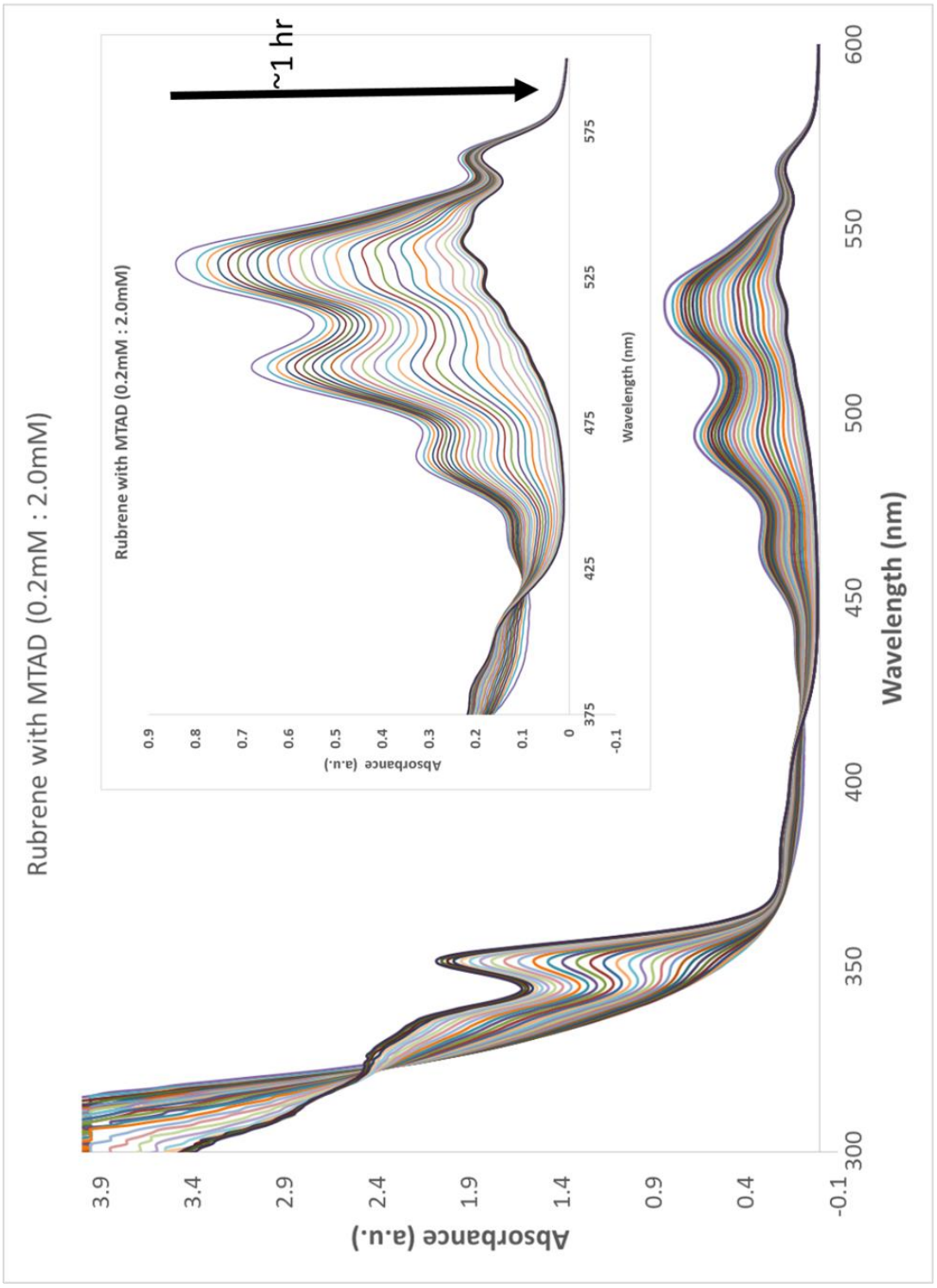
Rubrene with MTAD (0.2mM : 2.0mM)
Absorbance (a.u.)
Wavelength (nm)
~1 hr
Rubrene with MTAD (0.2mM : 2.0mM)
Absorbance (a.u.)
Wavelength (nm)

REFERENCE LIST

(1) Lee, Y.-H. Non-Doped Active Layer, Benzo[k]fluoranthene-Based Linear Acenes, for Deep Blue- to Green-Emissive Organic Light-Emitting Diodes. *Org. Electron.* **2013**, *14*, 1064–1072.

(2) Zhang, F.; Melzer, C.; Gassmann, A.; Seggern, H. von; Schwalm, T.; Gawrisch, C.; Rehahn, M. High-Performance N-Channel Thin-Film Transistors with Acene-Based Semiconductors. *Organic Electronics* **2013**, *14*, 888–896.

(3) Kim, D. H. Directed Self-Assembly of Organic Semiconductors via Confined Evaporative Capillary Flows for Use in Organic Field-Effect Transistors. *Org. Electron.* **2014**, *15*, 2322–2327.

(4) Shaheen, S. E.; Brabec, C. J.; Sariciftci, N. S.; Padinger, F.; Fromherz, T.; Hummelen, J. C. 2.5% Efficient Organic Plastic Solar Cells. *Appl. Phys. Lett.* **2001**, *78*, 841.

(5) Forrest, S. R. The Path to Ubiquitous and Low-Cost Organic Electronic Appliances on Plastic. *Nature* **2004**, *428*, 911–918.

(6) Bao, Z.; Lovinger, A. J.; Dodabalapur, A. Organic Field-effect Transistors with High Mobility Based on Copper Phthalocyanine. *Applied Physics Letters* **1996**, *69*, 3066–3068.

(7) Mcculloch, I.; Heeney, M.; Bailey, C.; Genevicius, K.; Macdonald, I.; Shkunov, M.; Sparrowe, D.; Tierney, S.; Wagner, R.; Zhang, W. M.; *et al.* Liquid-Crystalline Semiconducting Polymers with High Charge-Carrier Mobility. *Nat. Mater.* **2006**, *5*, 328–333.

(8) Roncali, J. Conjugated Poly(thiophenes): Synthesis, Functionalization, and Applications. *Chem. Rev.* **1992**, *92*, 711–738.

(9) Kang, C.; Wade, J.; Yun, S.; Lim, J.; Cho, H.; Roh, J.; Lee, H.; Nam, S.; Bradley, D. D. C.; Kim, J.-S.; *et al.* Organic Electronics: 1 GHz Pentacene Diode Rectifiers Enabled by Controlled Film Deposition on SAM-Treated Au Anodes. *Adv. Electron. Mater.* **2016**, *2*, 1500282.

(10) Sekitani, T.; Zschieschang, U.; Klauk, H.; Someya, T. Flexible Organic Transistors and Circuits with Extreme Bending Stability. *Nat. Mater.* **2010**, *9*, 1015–1022.

(11) J. H. on F.; Pm, 2016 at 12:12. Samsung Galaxy S7 sweeps DisplayMate rankings with the best OLED panel ever tested http://www.extremetech.com/mobile/223461-galaxy-s7-sweeps-displaymate-rankings-as-the-best-oled-panel-ever (accessed Aug 3, 2016).

(12) LG Chem developed plastic-based “truly” flexible OLED lighting panels, to mass produce them in 2015 | OLED-Info http://www.oled-info.com/lg-chem-developed-new-plastic-based-truly-flexible-oled-lighting-panels-mass-produce-them-2015 (accessed Aug 3, 2016).

(13) Facchetti, A. π-Conjugated Polymers for Organic Electronics and Photovoltaic Cell Applications. *Chem. Mater.* **2011**, *23*, 733–758

(14) Park, B.; Kim, Y. J.; Graham, S.; Reichmanis, E. Change in Electronic States in the Accumulation Layer at Interfaces in a Poly(3-Hexylthiophene) Field-Effect Transistor and the Impact of Encapsulation. *ACS Appl. Mater. Interfaces* **2011**, *3*, 3545–3551.

(15) Buriak, J. M. Organometallic Chemistry on Silicon Surfaces: Formation of Functional Monolayers Bound through Si-C Bonds. *Chem. Commun.* **1999**, 1051–1060.

(16) Zamborini, F. P.; Crooks, R. M. Corrosion Passivation of Gold by N-Alkanethiol Self-Assembled Monolayers: Effect of Chain Length and End Group. *Langmuir* **1998**, *14*, 3279–3286.

(17) Hau, S. K.; Yip, H.-L.; Acton, O.; Baek, N. S.; Ma, H.; Jen, A. K.-Y. Interfacial Modification to Improve Inverted Polymer Solar Cells. *J. Mater. Chem.* **2008**, *18*, 5113–5119.

(18) Ulman, A. Formation and Structure of Self-Assembled Monolayers. *Chem. Rev.* **1996**, *96*, 1533–1554.

(19) Love, J. C.; Estroff, L. A.; Kriebel, J. K.; Nuzzo, R. G.; Whitesides, G. M. Self-Assembled Monolayers of Thiolates on Metals as a Form of Nanotechnology. *Chem. Rev.* **2005**, *105*, 1103–1169.

(20) Prime, K.; Whitesides, G. Self-Assembled Organic Monolayers - Model Systems for Studying Adsorption of Proteins at Surfaces. *Science* **1991**, *252*, 1164–1167.

(21) Feng, X.; Fryxell, G. E.; Wang, L. Q.; Kim, A. Y.; Liu, J.; Kemner, K. M. Functionalized Monolayers on Ordered Mesoporous Supports. *Science* **1997**, *276*, 923–926.

(22) Linford, M. R.; Fenter, P.; Eisenberger, P. M.; Chidsey, C. E. D. Alkyl Monolayers on Silicon Prepared from 1-Alkenes and Hydrogen-Terminated Silicon. *J. Am. Chem. Soc.* **1995**, *117*, 3145–3155.

(23) Tsetseris, L. Modification of the Electronic Properties of Rubrene Crystals by Water and Oxygen-Related Species. *Org. Electron.* **2009**, *10*, 333–340.

(24) Calhoun, M. F.; Sanchez, J.; Olaya, D.; Gershenson, M. E.; Podzorov, V. Electronic Functionalization of the Surface of Organic Semiconductors with Self-Assembled Monolayers. *Nat. Mater.* **2007**, *7*, 84–89.

(25) Maboudian, R.; Ashurst, W. R.; Carraro, C. Tribological Challenges in Micromechanical Systems. *Tribology Letters* **2013**, *12*, 95–100.

(26) Judy, J. W. Microelectromechanical Systems (MEMS): Fabrication, Design and Applications. *Smart Mater. Struct.* **2001**, *10*, 1115.

(27) Mayer, T. M.; Elam, J. W.; George, S. M.; Kotula, P. G.; Goeke, R. S. Atomic-Layer Deposition of Wear-Resistant Coatings for Microelectromechanical Devices. *Applied Physics Letters* **2003**, *82*, 2883–2885.

(28) Clear, S. C.; Nealey, P. F. Chemical Force Microscopy Study of Adhesion and Friction between Surfaces Functionalized with Self-Assembled Monolayers and Immersed in Solvents. *Journal of Colloid and Interface Science* **1999**, *213*, 238–250.

(29) Wasserman, S. R.; Biebuyck, H.; Whitesides, G. M. Monolayers of 11-Trichlorosilylundecyl Thioacetate: A System That Promotes Adhesion between Silicon Dioxide and Evaporated Gold. *Journal of Materials Research* **1989**, *4*, 886–892.

(30) Petrenko, V. F.; Peng, S. Reduction of Ice Adhesion to Metal by Using Self-Assembling Monolayers (SAMs). *Canadian Journal of Physics* **2003**, *81*, 387–393.

(31) Mrksich, M. A Surface Chemistry Approach to Studying Cell Adhesion. *Chemical Society Reviews* **2000**, *29*, 267–273.

(32) Ostuni, E.; Yan, L.; Whitesides, G. M. The Interaction of Proteins and Cells with Self-Assembled Monolayers of Alkanethiolates on Gold and Silver. *Colloids and Surfaces B: Biointerfaces* **1999**, *15*, 3–30.

(33) Mrksich, M.; Whitesides, G. M. Using Self-Assembled Monolayers to Understand the Interactions of Man-Made Surfaces with Proteins and Cells. *Annual Review of Biophysics and Biomolecular Structure* **1996**, *25*, 55–78.

(34) Stornetta, R. L.; Moreira, T. S.; Takakura, A. C.; Kang, B. J.; Chang, D. A.; West, G. H.; Brunet, J. F.; Mulkey, D. K.; Bayliss, D. A.; Guyenet, P. G. Expression of Phox2b by Brainstem Neurons Involved in Chemosensory Integration in the Adult Rat. *J. Neurosci.* **2006**, *26*, 10305–10314.

(35) Laibinis, P. E.; Whitesides, G. M. Self-Assembled Monolayers of N-Alkanethiolates on Copper Are Barrier Films That Protect the Metal against Oxidation by Air. *J. Am. Chem. Soc.* **1992**, *114*, 9022–9028.

(36) Uozumi, Y.; Nakazono, M. Amphiphilic Resin-Supported Rhodium-Phosphine Catalysts for C-C Bond Forming Reactions in Water. *Adv. Synth. Catal.* **2002**, *344*, 274–277.

(37) Ishii, H.; Sugiyama, K.; Ito, E.; Seki, K. Energy Level Alignment and Interfacial Electronic Structures at Organic/Metal and Organic/Organic Interfaces. *Adv. Mater.* **1999**, *11*, 605–625.

(38) Templeton, A. C.; Wuefling, W. P.; Murray, R. W. Monolayer-Protected Cluster Molecules. *Acc. Chem. Res.* **2000**, *33*, 27–36.

(39) Frankamp, B. L.; Boal, A. K.; Tuominen, M. T.; Rotello, V. M. Direct Control of the Magnetic Interaction between Iron Oxide Nanoparticles through Dendrimer-Mediated Self-Assembly. *Journal of the American Chemical Society* **2005**, *127*, 9731–9735.

(40) Prodan, E.; Radloff, C.; Halas, N. J.; Nordlander, P. A Hybridization Model for the Plasmon Response of Complex Nanostructures. *Science* **2003**, *302*, 419–422.

(41) Yoshizawa, M.; Tamura, M.; Fujita, M. Diels-Alder in Aqueous Molecular Hosts: Unusual Regioselectivity and Efficient Catalysis. *Science* **2006**, *312*, 251–254.

(42) Hamers, R. J.; Coulter, S. K.; Ellison, M. D.; Hovis, J. S.; Padowitz, D. F.; Schwartz, M. P.; Greenlief, C. M.; John N. Russell, J. Cycloaddition Chemistry of Organic Molecules with Semiconductor Surfaces. *Acc. Chem. Res.* **2000**, *33*, 617–624.

(43) Moses, J. E.; Moorhouse, A. D. The Growing Applications of Click Chemistry. *Chem. Soc. Rev.* **2007**, *36*, 1249–1262.

(44) Tarasow, T. M.; Tarasow, S. L.; Eaton, B. E. RNA-Catalysed Carbon-Carbon Bond Formation. *Nature* **1997**, *389*, 54–57.

(45) Qualizza, B. A.; Prasad, S.; Chiarelli, M. P.; Ciszek, J. W. Functionalization of Organic Semiconductor Crystals via the Diels-Alder Reaction. *Chem. Comm.* **2013**, *49*, 4495–4497.

(46) Menard, E.; Marchenko, A.; Podzorov, V.; Gershenson, M. E.; Fichou, D.; Rogers, J. A. Nanoscale Surface Morphology and Rectifying Behavior of a Bulk Single-Crystal Organic Semiconductor. *Adv. Mater.* **2006**, *18*, 1552–1556.

(47) Yamashita, Y. Organic Semiconductors for Organic Field-Effect Transistors. *Sci. Technol. Adv. Mater.* **2009**, *10*, 24313.

(48) Olsen, H.; Snyder, J. P. Concerted Thermal Cycloreversion of Unsaturated Azo N-Oxides. *J. Am. Chem. Soc.* **1977**, *99*, 1524–1536.

(49) Wise, K. E.; Wheeler, R. A. Donor-Acceptor-Assisted Diels-Alder Reaction of Anthracene and Tetracyanoethylene. *J. Phys. Chem. A.* **1999**, *103*, 8279–8287.

(50) Brown, P.; Cookson, R. C. Kinetics of Addition of Tetracyanoethylene to Anthracene and Bicyclo[2,2,1]heptadiene. *Tetrahedron* **1965**, *21*, 1977–1991.

(51) Andrews, L. J.; Keefer, R. M. A Kinetic Study of the Diels-Alder Reaction of Various Anthracene and Maleic Anhydride Derivatives. *J. Am. Chem. Soc.* **1955**, *77*, 6284–6289.

(52) Kiselev, V. D.; Konovalov, A. I. Internal and External Factors Influencing the Diels-Alder Reaction. *J. Phys. Org. Chem.* **2009**, *22*, 466–483.

(53) Karama, U.; El-Azhary, A. A.; Almansour, A. I.; Al-Kahtani, A. A.; Al-Turki, T. M.; Jaafar, M. H. Computational and Spectral Investigation of 5,12-Dihydro-5,12-Ethanonaphthacene-13-Carbaldehyde. *Molecules* **2011**, *16*, 6741–6746.

(54) Biermann, D.; Schmidt, W. Diels-Alder Reactivity of Polycyclic Aromatic Hydrocarbons. 1. Acenes and Bezologs. *J. Am. Chem. Soc.* **1980**, *102*, 3163–3173.

(55) Qualizza, B. A.; Ciszek, J. W. Experimental Survey of the Kinetics of Acene Diels–Alder Reactions. *J. Phys. Org. Chem.* **2015**, *28*, 629–634.

(56) Ciszek, J. W.; Qualizza, B. A.; Prasad, S. Surface-Modified Organic Semiconductors. US20150060831 A1, March 5, 2015.

(57) Lee, B.; Choi, T.; Cheong, S.-W.; Podzorov, V. Nanoscale Conducting Channels at the Surface of Organic Semiconductors Formed by Decoration of Molecular Steps with Self-Assembled Molecules. *Adv. Funct. Mater.* **2009**, *19*, 3726–3730.

(58) Laudise, R. A.; Kloc, C.; Simpkins, P. G.; Siegrist, T. Physical Vapor Growth of Organic Semiconductors. *J. Crys. Growth* **1998**, *187*, 449–454.

(59) Boyd, R. H. Thermochemistry of Cyanocarbons. *The Journal of Chemical Physics* **1963**, *38*, 2529–2535.

(60) Koschel, H.; Held, G.; Trischberger, P.; Widdra, W.; Steinrück, H.-P. Benzene Adsorption on a Pseudomorphic Cu Monolayer on Ni(111) – a Combined TPD and ARUPS Study. *Surface Science* **1999**, *437*, 125–136.

(61) Breitbach, J.; Franke, D.; Hamm, G.; Becker, C.; Wandelt, K. Adsorption of Benzene on Ordered Sn/Pt(1 1 1) Surface Alloys. *Surface Science* **2002**, *507–510*, 18–22.

(62) Katash, I.; Luo, X.; Sukenik, C. N. In Situ Sulfonation of Alkyl Benzene Self-Assembled Monolayers: Product Distribution and Kinetic Analysis. *Langmuir* **2008**, *24*, 10910–10919.

(63) Holmes, D.; Kumaraswamy, S.; Matzger, A. J.; Vollhardt, K. P. C. On the Nature of Nonplanarity in the [N]Phenylenes. *Chem. Eur. J.* **1999**, *5*, 3399–3412.

(64) Kwon, Y.; Mrksich, M. Dependence on the Rate of an Interfacial Diels-Alder Reaction on the Steric Environment of the Immobilized Dienophile: An Example of Enthalpy-Entropy Compensation. *J. Am. Chem. Soc.* **2002**, *124*, 806–812.

(65) Jarzeba, W.; Murata, S.; Tachiya, M. Ultrafast Dynamics of the Excited Tetracyanoethylene-Toluene Electron Donor-Acceptor Complex. *Chemical Physics Letters* **1999**, *301*, 347–355.

(66) Clar, E. *Polycyclic Hydrocarbons*; Academic Press: New York, 1964.

(67) Coppo, P.; Yeates, S. G. Shining Light on a Pentacene Derivative: The Rate of Photoinduced Cycloadditions. *Adv. Mater.* **2005**, *17*, 3001–3005.

(68) Hoffman, R. V. *Organic Chemistry An Intermediate Text*; second.; John Wiley & Sons, Inc.: Hoboken, 2004.

(69) Schleyer, P. von R.; Manoharan, M.; Jiao, H.; Stahl, F. The Acenes: Is There a Relationship between Aromatic Stabilization and Reactivity? *Org. Lett.* **2001**, *3*, 3643–3646.

(70) Portella, G.; Poater, J.; Solà, M. Assessment of Clar's Aromatic π-Sextet Rule by Means of PDI, NICS and HOMA Indicators of Local Aromaticity. *J. Phys. Org. Chem.* **2005**, *18*, 785–791.

(71) Sauer, J.; Weist, H.; Mielert, A. Eine Studie Der DIELS-ALDER-Reaktion, I. Die Reaktivitat von Dienophilen Gegenuber Cyclopentadien Und 9,10-Dimethyl-Anthracen. *Chem. Ber.* **1964**, *97*, 3183–3207.

(72) Tobia, D.; Harrison, R.; Phillips, B.; White, T. L.; DiMare, M.; Rickborn, B. Unusual Stability of N-Methylmaleimide Cycloadducts: Characterization of Isobenzofuran Retro Diels-Alder Reactions. *J. Org. Chem.* **1993**, *58*, 6701–6706.

(73) Sustmann, R. Orbital Energy Control of Cycloaddition Reactivity. *Pure Appl. Chem.* **1974**, *40*, 569–593.

(74) Sauer, J.; Sustmann, R. Mechanistic Aspects of Diels-Alder Reactions: A Critical Survey. *Angew. Chem., Int. Ed. Engl.* **1980**, *19*, 779–807.

(75) Vaughan, W. R.; Milton, K. M. The Steric Factor in the Diene Reaction: Anthracene with A,β-Unsaturated A,β-Dicarboxylic Acids. I. *The Journal of Organic Chemistry* **1951**, *16*, 1748–1752.

(76) Essers, M.; Mück-Lichtenfeld, C.; Haufe, G. Diastereoselective Diels-Alder Reactions of α-Fluorinated A,β-Unsaturated Carbonyl Compounds: Chemical Consequences of Fluorine Substitution. 2. *J. Org. Chem.* **2002**, *67*, 4715–4721.

(77) Rigaudy, J.; Cuong, N. K.; Godard, J.-Y. Transformations Photochimiques D'endoperoxydes Dérivés D'hydrocarbures Aromatiques Polycycliques V. Cas de L'endoperoxyde de Rubréne: Formation D'un Nouveau Type de Photo-Isomére. *Bulletin de la Societe chimique de France* **1985**, 78–83.

(78) Podzorov, V.; Menard, E.; Borissov, A.; Kiryukhin, V.; Rogers, J. A.; Gershenson, M. E. Intrinsic Charge Transport on the Surface of Organic Semiconductors. *Phys. Rev. Lett.* **2004**, *93*, 86602.

(79) McMasters, D. R.; Wirz, J. Spectroscopy and Reactivity of Kekulé Hydrocarbons with Very Small Singlet−Triplet Gaps. *Journal of the American Chemical Society* **2001**, *123*, 238–246.

(80) Jensen, F.; Foote, C. S. Reaction of 4-Phenyl-1,2,4-Triazoline-3,5-Dione with Substituted Butadienes. A Nonconcerted Diels-Alder Reaction. *Journal of the American Chemical Society* **1987**, *109*, 6376–6385.

(81) Handoo, K. L.; Lu, Y.; Parker, V. D. Resolution of the Non-Steady-State Kinetics of the Two-Step Mechanism for the Diels−Alder Reaction between Anthracene and Tetracyanoethylene in Acetonitrile. *Journal of the American Chemical Society* **2003**, *125*, 9381–9387.

(82) Overney, R. M.; Howald, L.; Frommer, J.; Meyer, E.; Güntherodt, H.-J. Molecular Surface Structure of Tetracene Mapped by the Atomic Force Microscope. *J. Chem. Phys.* **1991**, *94*, 8441–8443.

(83) Meador, M. A. B.; Frimer, A. A.; Johnston, J. C. Reevaluation of Tetrahydrophtalic Anhydride as an End Cap for Improved Oxidation Resistance in Addition Polyimides. *Macromolecules* **2004**, *37*, 1289–1296.

(84) Findlay, N. J.; Park, S. R.; Schoenebeck, F.; Cahard, E.; Zhou, S.-Z.; Berlouis, L. E. A.; Spicer, M. D.; Tuttle, T.; Murphy, J. A. Reductions of Challenging Organic Substrates by a Nickel Complex of a Noninnocent Crown Carbene Ligand. *J. Am. Chem. Soc.* **2010**, *132*, 15462–15464.

(85) Bawa, R. A.; Jones, S. Synthesis and Diels-Alder Reactions of 9-(4-Benzyloxazolin-2-Yl) Anthracene. *Tetrahedron* **2004**, *60*, 2765–2770.

(86) Nelsen, S. F.; Petillo, P. A.; Chang, H.; Frigo, T. B.; Dougherty, D. A.; Kaftory, M. Effects of CNN Bond Angle Restriction in 2,3-Diazabicyclo[2.11]hexane Derivatives on Nitrogen Inversion Barrier, Ease of Oxidation, and Acidity. *J. Org. Chem.* **1991**, *56*, 613–618.

VITA

Brittni A. Qualizza was born in Evanston, Illinois and was raised on the northside of the city and in Skokie. Before attending Loyola University Chicago for her graduate studies, she attended Saint Mary's College of Notre Dame and received a B.Sc. in Chemistry with a minor in mathematics in 2009.

While at Loyola University Chicago, Qualizza was a graduate student organization representative for two years from 2010 to 2012. In 2012, she participated in the Research Mentoring Program (RMP) and demonstrated her research in the Emerging Scientists' Workshop three years in a row from 2011 to 2014. In 2015 she won the Department of Chemistry and Biochemistry Denkewalter Lecture Poster Award for graduate students. For demonstrating an excellence in all aspects of graduate study, Qualizza received the Arthur J. Schmitt Fellowship for graduate studies from 2014-2015, which is intended to provide support to PhD students in the final year of their dissertations at Catholic Universities, and followed that with the 2015-2016 academic year of teaching Honors Physics, Honors Chemistry and AP Chemistry to the students attending Mount Vernon Presbyterian Upper School in Sandy Springs, Georgia.

Currently, Qualizza is searching for new teaching endeavors in the field of chemistry and other physical sciences. She also aims to continue studies of organic electronic materials and self-assembled monolayers.